TOWARD UNDERSTANDING THE FUNCTION OF THE UNIVERSALLY CONSERVED GTPASE HFLX

JEFFREY JAMES FISCHER
B.Sc. University of Lethbridge, 2005
M.Sc. University of Lethbridge, 2007

A Thesis
Submitted to the School of Graduate Studies
of the University of Lethbridge
in Partial Fulfillment of the
Requirements for the Degree

DOCTOR OF PHILOSOPHY

IN

BIOMOLECULAR SCIENCE

Department of Chemistry and Biochemistry
University of Lethbridge
LETHBRIDGE, ALBERTA, CANADA

Abstract

Members of the ubiquitous GTPase superfamily regulate numerous cellular functions. A core group of eight GTPases are present in all domains of life: initiation factor 2, elongation factors Tu and G, protein secretion factors Ffh and FtsY, and the poorly characterized factors YihA, YchF, and HflX. While the first five members have well defined roles in the essential cellular process of protein synthesis, a role for YihA, YchF and HflX in this process has only recently been suggested. Here, a detailed kinetic analysis examining the interaction between HflX and its cellular partners is described. 50S and 70S ribosomal particles function as GTPase activating factors for HflX by stabilizing the nucleotide binding pocket of HflX, inducing a "GTPase activated" state. These data indicates a novel mode of GTPase activation, and suggests a role for HflX in regulating translation.

Acknowledgements

HJ: despite all the mess ups, despite all the struggles, he never gave up on me.

Erin: now my wife, who pushes me to succeed. Without her, there was no way. Funny how a relationship motivates one to excel…….even more with a little one on the way!

My family: pursuing a PhD is a selfish thing, and my family has been unwavering in their support. Mom, Dad, Kris, Elaine, Jared, Jess, Brady, Tante Gitti, Spence, Robyn, Gram, David, Julia, Liam, Tanya…….the list goes on and on.

Mike, Mackenzie, Shey, Harland, Angela, Dustin: I hope that you learned from me just as I learned from you, and had just as much fun doing so as I did.

Ute, Evan, Evey, Marion, Alvin, Fan, Kirsten, Lindsay, Raja, Laura, Jessica, and all the numerous others who helped, encouraged, worked with, debated with, tore apart, built up, and listened to me: Not possible without you all.

Contents

List of Figures

List of Tables

List of Abbreviations

β-mEtOH	β-mercaptoethanol
30S	Small ribosomal subunit (S = Svedberg)
50S	Large ribosomal subunit (S = Svedberg)
70S	Associated ribosome couples (30S + 50S)
aa-tRNA	Aminoacyl-tRNA
ADP	Adenosine-5'-diphosphate
ADPNP/AMPPNP	Adenosine-5'-(β,γ-imido)-triphosphate
apo	Free of a bound cofactor
A-site	Aminoacyl-tRNA binding site
ATP	Adenosine-5'-triphosphate
Azi	Azithromycin
Cam	Chloramphenicol
Clin	Clindamycin
Cryo-EM	Cryo-electron microscopy
DNA	Deoxyribonucleic acid
EF	Elongation factor
E-site	tRNA exit site
Ery	Erythromycin
fMet	Formyl Methionine
FRET	Fluorescence (Förster) Resonance Energy Transfer
Fus	Fusidic acid
GAC	GTPase activating centre
GAP	GTPase activating protein (factor)
GDI	Guanine nucleotide dissociation inhibitor
GDP	Guanosine-5'-diphosphate
GDPNP/GMPPNP	Guanosine-5'-(β,γ-imido)-triphosphate
GMPPCP	Guanosine-5'-(β,γ-methylene)-diphosphate
GEF	Guanine nucleotide exchange factor
GTP	Guanosine-5'-triphosphate
HAS	Hydrophobic amino acid substituted
HflX	High frequency of lysogenation factor X
HygB	Hygromycin B
IC_{50}	50% inhibitory concentration
IF	Initiation factor
IPTG	Isopropyl-β-D-galactopyranoside
Kan	Kanamycin
K_D	Equilibrium dissociation constant
L1-L34	Large ribosomal subunit protein 1,2….34
LB	Luria-Bertani
Linc	Lincomycin
m^7G	Methyl-guanosine
mant	2' (or 3')-*O*-(*N*-methylanthraniloyl)

List of Abbreviations (continued)

MIC	Minimum inhibitory concentration
miRNA	Micro ribonucleic acid
mRNA	Messenger RNA
MWCO	Molecular weight cutoff
MS	Mass spectrometry
Neo	Neomycin
OD_{600}	Optical Density at 600 nm
ORF	Open reading frame
PAGE	Polyacrylamide gel electrophoresis
Par	Paromomycin
PDB ID	Protein data bank identification code
PEP	Phosphoenolpyruvate
PK	Pyruvate kinase
P-loop	Phosphate binding loop
PMSF	Phenylmethylsulfonylfluoride
P-site	Peptidyl-tRNA binding site
PTC	Peptidyl transferase centre
Pur	Puromycin
Rb	Ribosome
RF	Release factor
RNA	Ribonucleic acid
RRF	Ribosome recycling factor
rRNA	Ribosomal ribonucleic acid
S1-S21	Small ribosomal subunit protein 1,2….21
SAXS	Small angle X-ray scattering
SDS	Sodium dodecyl sulfate
Tet	Tetracycline
TNP	2’ (or 3’)-*O*-(2,4,6-trinitrophenyl)
Tob	Tobramycin
TRAFAC	Translation factor class
tRNA	Transfer ribonucleic acid
$tRNA_i$	Initiator transfer ribonucleic acid
SAXS	Small Angle X-ray Scattering
Spec	Spectinomycin
Strp	Streptomycin
X-Gal	5-bromo-4-chloro-3-indolyl- β-D-galactopyranoside

1. Prokaryotic Protein Synthesis

1.1 Overview of the central dogma

The central dogma of molecular biology (Figure 1.1) describes how genetic information, encoded by deoxyribonucleic acid (DNA), functions as a template for the production of proteins. A DNA template (a gene) is read by a DNA-dependent ribonucleic acid (RNA) polymerase, producing a messenger RNA (mRNA) transcript. Following transcription, the mRNA transcript is then read to produce a polypeptide chain (which subsequently folds into its functional three-dimensional structure) in a process called translation (hence, mRNA is a coding RNA). There are few exceptions to this general scheme; RNA sequences can be reverse transcribed through the activity of RNA-dependent DNA polymerase (reverse transcriptase), while some RNA sequences are not translated (and hence are non-coding) but instead play additional structural (such as ribosomal, or rRNA) or functional (such as transfer (tRNA), micro (miRNA), short interfering (siRNA), or ribozymes) roles within the cell. Protein synthesis (translation) is a highly conserved process in all cell types, catalyzed by the ribosome: a megadalton-sized complex consisting of two ribosomal subunits; the 30S subunit, composed of 16S rRNA and 21 proteins (labeled S1-S21) and the 50S subunit, containing two rRNA species (23S rRNA and 5S rRNA) and 34 proteins (labeled L1-L34). This cyclic process consists of four distinct steps: (i) initiation, during which ribosomal subunits, messenger RNA (mRNA), and initiator tRNA (fMet-$tRNA_i^{fMet}$ in bacteria) are brought together; (ii) elongation, during which mRNA is read codon by codon by the ribosome and cognate amino acids are sequentially added to the growing polypeptide chain; (iii) termination, during which a stop codon is read by a release factor, thus

triggering release of the completed polypeptide; and (iv) recycling, during which the ribosomal subunits, bound mRNA, and deacyl-tRNA are dissociated in preparation for the initiation phase. Importantly, these four phases require the activity and precise coordination of multiple protein factors, including members of the P-loop GTPase superfamily, to maintain protein synthesis rates capable of supporting cellular function. The focus of this chapter is to briefly discuss these four phases with respect to the factors involved therein.

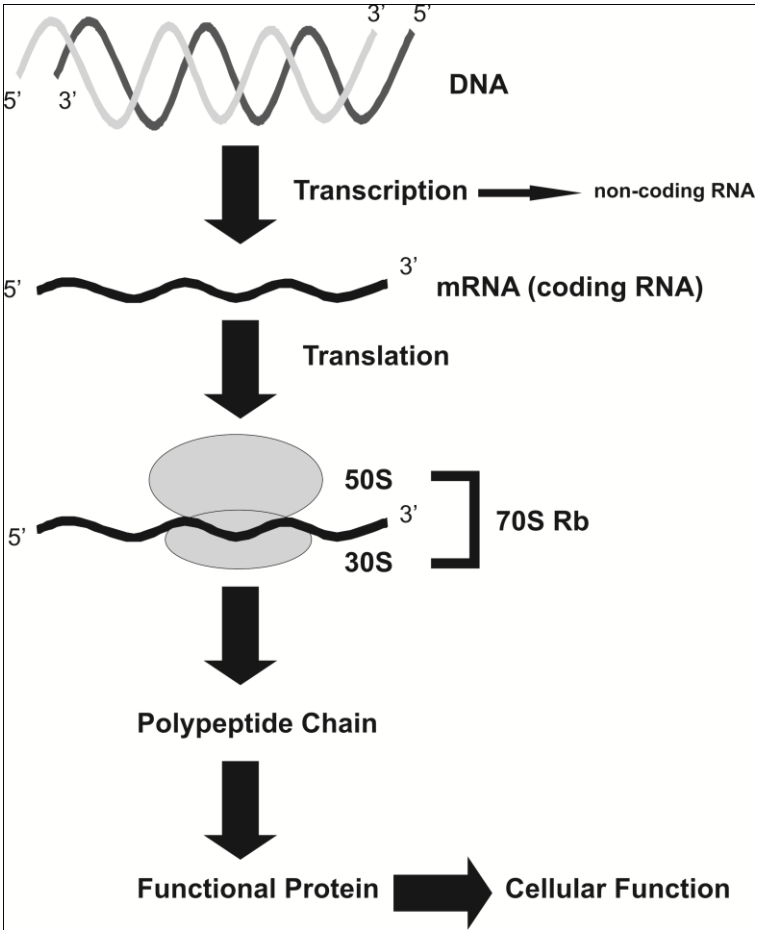

Figure 1.1. The Central Dogma of Molecular Biology

A DNA template is transcribed by DNA-dependent RNA polymerase. RNA can either encode for genetic information (coding RNA, or mRNA) or play a structural role (non-coding RNA). mRNA transcripts are translated in a ribosome catalyzed process, to produce polypeptide chains that can then fold into a three-dimensional structure.

1.2 Initiation

Initiation in prokaryotes (summarized in Figure 1.2, reviewed in references (Kozak, 1999; Laursen et al., 2005)) requires the interaction of 30S and 50S ribosomal subunits, initiator tRNA (fMet-$tRNA_i^{fMet}$), and initiation factors (IFs) 1, 2, and 3. This process is more complex in eukaryotes, which require additional factors for regulation of initiation and recognition of eukaryotic mRNAs. In prokaryotes, the 30S ribosomal subunit with bound IF-3 (from the recycling phase) interacts with an mRNA, correctly positioning the "AGG AGG" Shine-Dalgarno sequence (6-10 nucleotides upstream of the AUG start codon) with the complementary anti-Shine-Dalgarno sequence on the 16S rRNA. As a result, the AUG start codon is positioned in the ribosomal P-site with the aid of a ternary complex consisting of IF-2•GTP•$tRNA_i$. IF-3 stabilizes the interaction between the $tRNA_i$ and the ribosomal P-site. IF-1 binds to the ribosomal A-site, stabilizing the newly formed pre-initiation complex. A conformational change is required for cognate fMet-$tRNA_i^{fMet}$•AUG codon interaction and formation of a stable 30S initiation complex; following this recognition, IF-1 and IF-3 dissociate, allowing IF-2 to promote association of the 50S subunit. IF-2 hydrolyzes GTP (discussed in section 2.1.1), causing release of the $tRNA_i$ into the ribosomal P-site. IF-2•GDP then dissociates from the ribosome, leaving a 70S ribosome with bound mRNA and P-site $tRNA_i$, which can then proceed to the elongation cycle. It is important to note that IF-3 has a ribosome subunit anti-association ability (Hirokawa et al., 2007), which is thought to function as a regulator of translation initiation. IF-3 and IF-1 may also play direct roles in ribosome recycling (Pavlov et al., 2008; Singh et al., 2005b; Varshney and Seshadri, 2006) (Section 1.5). Displacement of IF-3 may be induced by ribosome stabilizing agents such as the antibiotic paromomycin (Hirokawa et al., 2007).

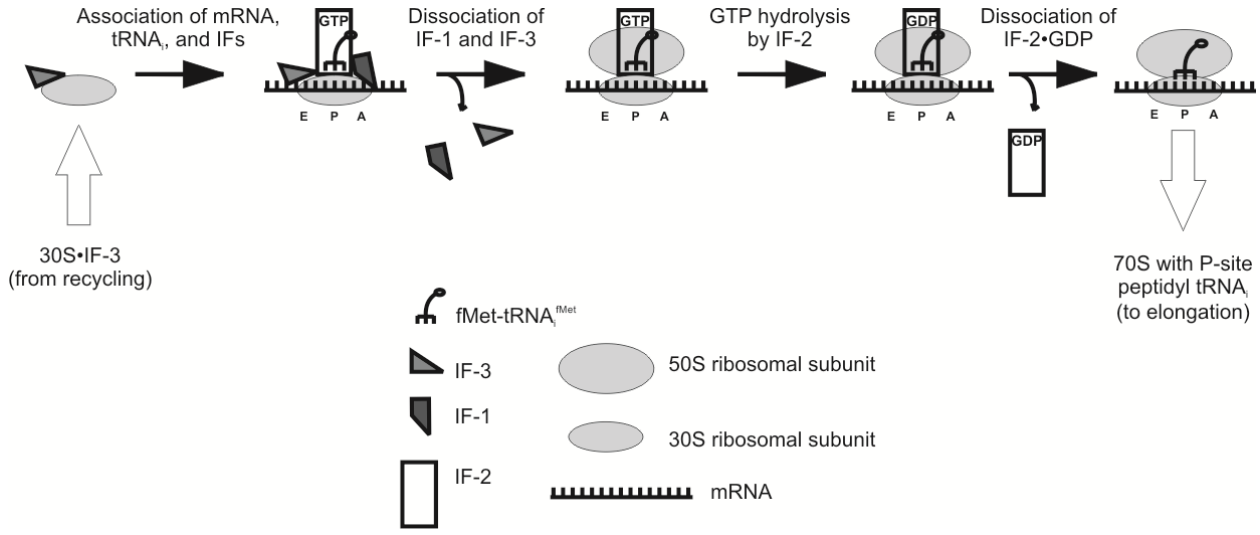

Figure 1.2. Prokaryotic Initiation

The 30S ribosomal subunit in complex with IF-3 (from the recycling phase) associates with mRNA, IF-1, and the IF-2•GTP•tRNA$_i$ ternary complex. IF-1 and 3 stabilize binding of the ternary complex to the 30S subunit and aid in correctly positioning the tRNA$_i$ on the AUG start codon. Once IF-1 and IF-3 dissociate, 50S subunit binding is facilitated by IF-2. GTP is hydrolyzed, IF-2•GDP dissociated, and the newly formed 70S complex with peptidyl-tRNA in the ribosomal P-site is ready for entering the elongation cycle.

It is worth noting that additional factors, present in eukaryotes but not prokaryotes, are responsible for recognizing different elements of eukaryotic mRNA. For example, the 5' methyl-guanosine cap (m^7G) is recognized by eukaryotic initiation factor 4E (eIF-4E), while the 3' poly(A) tail is recognized by the poly(A) binding protein, as well as eIF-4A.

1.3 Elongation

The elongation cycle of translation (Figure 1.3) is well characterized in the literature. The roles of EF-Tu and EF-G during the elongation cycle are described (Pape et al., 1998a; Rodnina et al., 2000; Wieden et al., 2002). Translocation is reviewed in (Shoji et al., 2009). The elongation cycle consists of the sequential addition of amino acids to the growing polypeptide chain in a codon-dependent manner. Once a functional ribosome has been assembled, consisting of the 70S ribosome with bound mRNA and $tRNA_i$ in the ribosomal P-site, the aminoacyl-tRNA (aa-tRNA) is delivered to the ribosomal A-site as a ternary complex consisting of aa-tRNA, elongation factor (EF) Tu, and GTP. This complex binds to the ribosomal A-site, and upon cognate codon-anticodon recognition, GTP is hydrolyzed, and the aminoacyl-tRNA is fully accommodated. EF-Tu with bound GDP then dissociates following release of inorganic phosphate (P_i). The inactive EF-Tu•GDP binary complex is recycled by the guanine nucleotide exchange factor (GEF) EF-Ts, which catalyzes the efficient release of GDP and thus facilitates rebinding of GTP, allowing EF-Tu•GTP to bind aa-tRNA for another round. At the ribosome, rRNA catalyzes the formation of a peptide bond between the P-site and the A-site aa-tRNAs (Figure 1.5). Following peptide bond formation, EF-G•GTP associates with the ribosome and hydrolyzes its bound nucleotide. Release of P_i from EF-G and translocation of peptidyl-tRNA in the A-site and deacyl-tRNA in the P-site occurs simultaneously with mRNA translocation (Peske et al., 2004). This results in formation of the post-translocation complex, consisting of deacyl-tRNA in the ribosomal E-site and peptidyl-tRNA in the ribosomal E-site. EF-G•GDP then dissociates from the ribosome following a conformational change in the protein. E-site deacyl-

tRNA then dissociates from the ribosome, allowing for another round of elongation to occur. EF-Tu and EF-G, and their role in protein synthesis, are discussed in greater detail in Chapter 2.

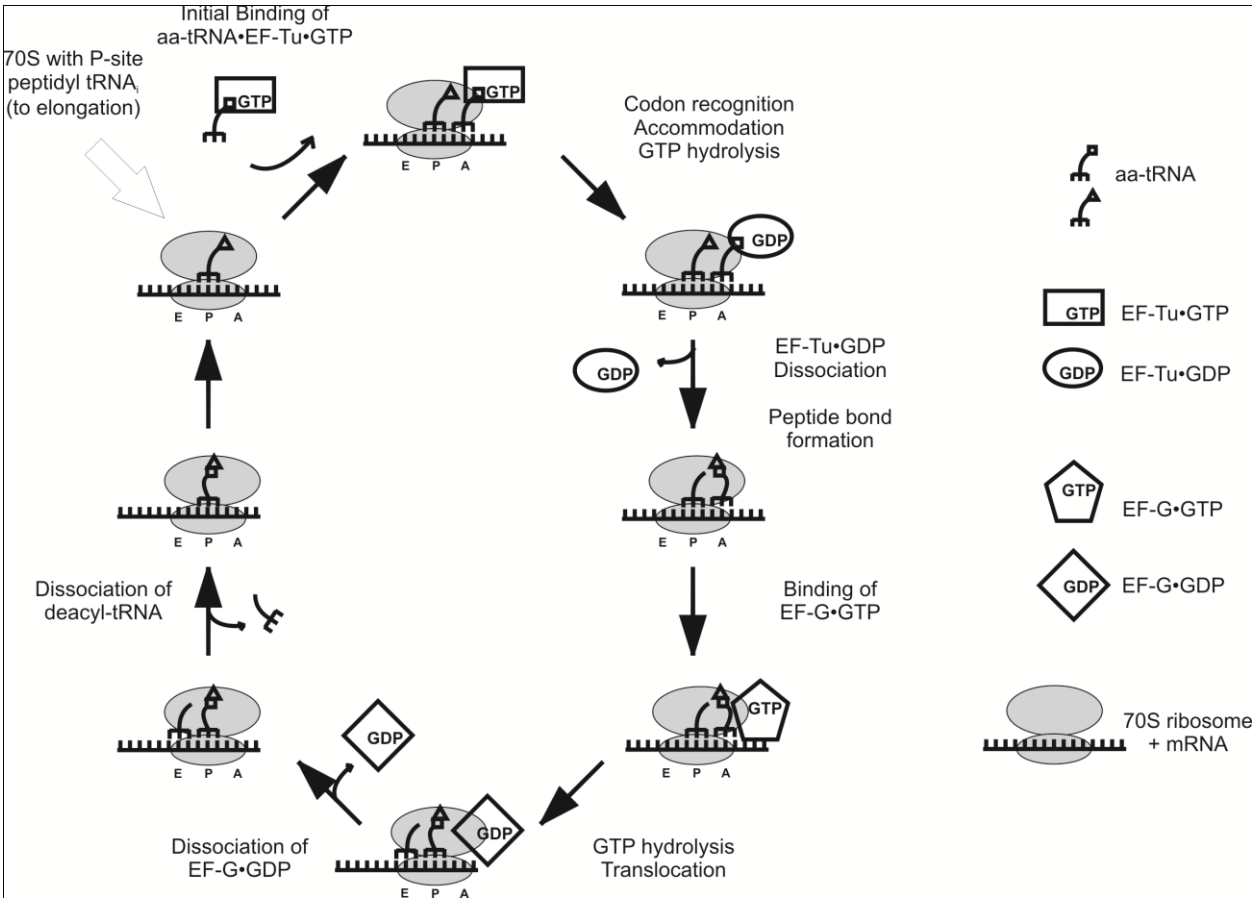

Figure 1.3. The Prokaryotic Elongation Cycle

Once the ribosome enters the elongation cycle from the initiation phase, aa-tRNA is delivered to the 70S ribosome as a ternary complex consisting of EF-Tu•GTP•aa-tRNA. Upon cognate codon-anticodon recognition, GTP is hydrolyzed and the aa-tRNA is fully accommodated into the A-site. The EF-Tu•GDP binary complex then dissociates; simultaneously, peptide bond formation is catalyzed by rRNA residues in the peptidyl transferase centre. With A-site peptidyl-tRNA and P-site deacyl-tRNA bound, EF-G•GTP binds to the A-site, and hydrolyzes GTP. Following release of P_i, the A- and P-site tRNAs, along with the mRNA, are translocated by one codon. EF-G•GDP and E-site deacyl-tRNA dissociate, and the cycle continues with another delivery of aa-tRNA. This continues until the A-site reaches a stop codon, at which point termination can occur.

1.4 Termination

Termination of protein synthesis (Figure 1.4) occurs once the elongating ribosome reaches a stop codon, which is then read by a release factor (RF). In prokaryotes, two class I release factors are present with overlapping specificity: RF-1 recognizes the UAA and UAG stop codons, while RF-2 recognizes UAA and UGA codons. Hydroxyl radical protection mapping of rRNA at the decoding centre of 16S rRNA and in nearby regions of the 23S rRNA indicate a conformational change in the ribosome occurs upon binding of release factors to the ribosomal A-site (He and Green, 2010; Youngman et al., 2007). This conformational change allows catalysis of peptide release through a nucleophillic attack by a water molecule on the aminoacyl ester linkage of the P-site peptidyl-tRNA (Brunelle et al., 2008; Youngman et al., 2007). During this process, the GTP-dependent class II release factor RF-3 stabilizes the interaction between the class I factor and the ribosome, perhaps aiding in this conformational change. The mechanism of peptide release is similar to peptide bond formation during the elongation phase, where the primary amine of the aminoacyl-tRNA in the A-site acts as a nucleophile (Figure 1.5). Interestingly, mutation of key nucleotides (A2451, U2506, U2585, and A2602) in the peptidyl transferase centre has little impact on peptidyl transferase activity, but a show substantial defects in peptide release (Youngman et al., 2004). Upon hydrolysis, the free polypeptide dissociates from the ribosome, leaving behind a post-termination complex consisting of a 70S ribosome with a P-site deacyl-tRNA and an mRNA with an A-site stop codon that then progresses into the recycling phase.

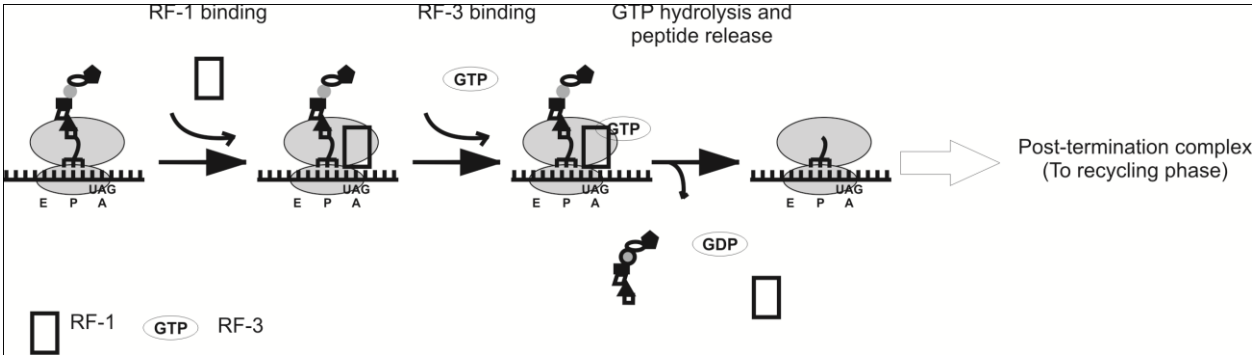

Figure 1.4. Prokaryotic Termination

Upon encountering a stop codon, class I release factors recognize the stop codon and associate to the ribosomal A-site. This interaction is stabilized by the class II release factor RF-3. GTP is hydrolyzed and following a nucleophilic attack by a water molecule the produced polypeptide, class I RF factor, and RF-3•GDP dissociate. The resulting post-termination complex proceeds to the recycling phase.

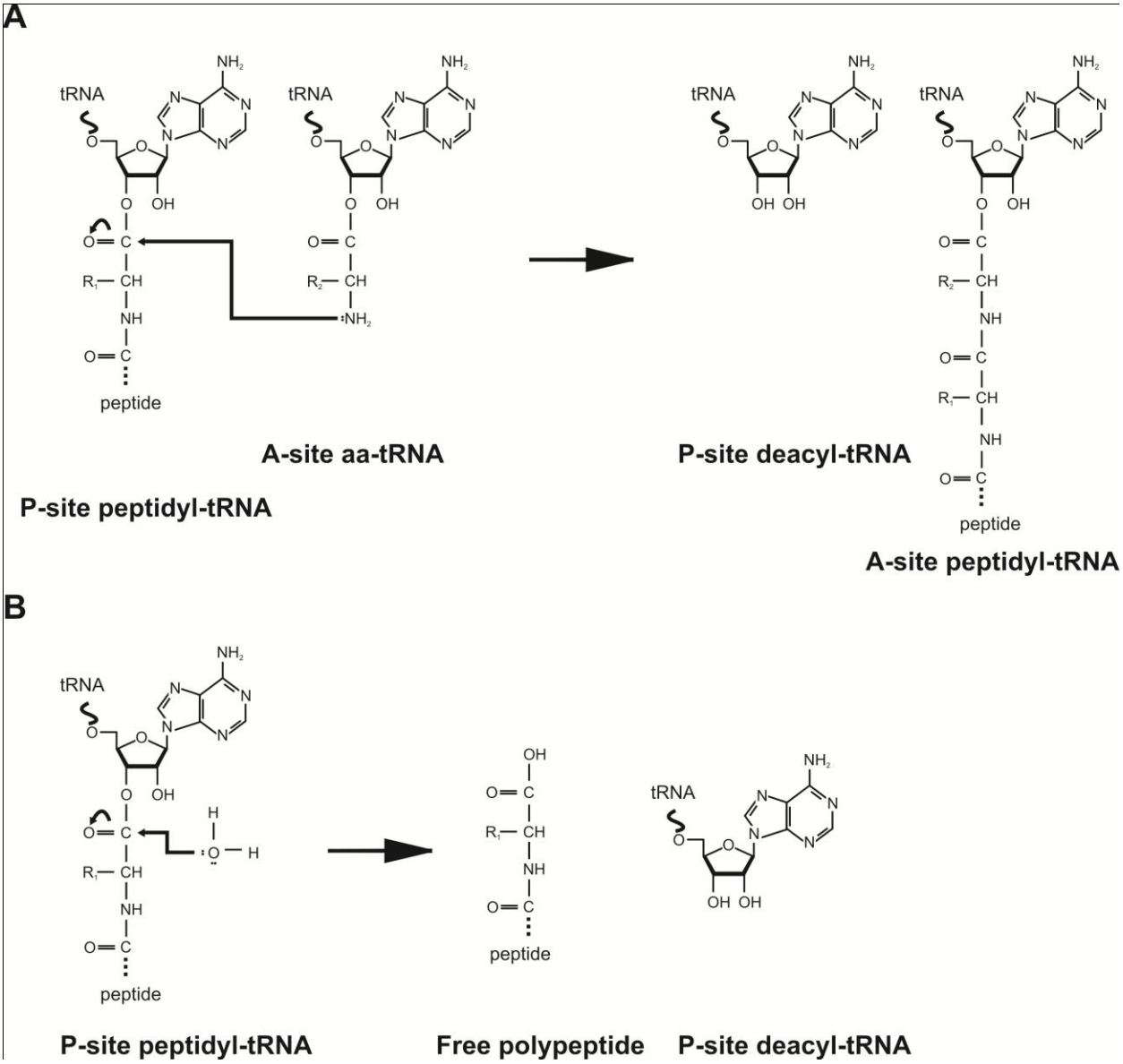

Figure 1.5. Peptidyl Transferase and Polypeptide Release

A) Peptidyl transfer: the amine of the A-site aa-tRNA acts as a nucleophile, attacking the aminoacyl ester linkage between the P-site amino acid and the terminal adenosine of the P-site peptidyl-tRNA. The result is a P-site deacyl-tRNA and an A-site peptidyl-tRNA, elongated by one amino acid. B) Peptide release: in analogy to peptidyl transfer, a water molecule acts as the nucleophile and attacks the peptidyl-tRNA in the ribosomal P-site. The result is a free polypeptide and a post-termination complex, which can then proceed to the recycling phase. Adapted from Brunelle *et al.* (Brunelle et al., 2008).

1.5 Recycling

Unlike initiation, elongation, and termination, there is no consensus model for ribosome recycling. Following termination and subsequent release of the produced polypeptide, the post-termination complex is recycled into its components: 30S and 50S subunits, along with mRNA and deacyl-tRNA. These components can then be used for subsequent rounds of protein synthesis, and enter the cycle at the initiation phase. Only recently has ribosome recycling been recognized as a distinct step during protein synthesis (Barat et al., 2007). As such, the molecular mechanism and roles of the various factors remains unclear. Pioneering work by Akira Kaji initially revealed the requirement for a GTPase and an additional factor in 1968 (Kuriki and Kaji, 1968); the GTPase was identified as EF-G (Hirashima and Kaji, 1972). The additional factor, called ribosome releasing factor (RR; (Hirashima and Kaji, 1972)), was later named ribosome recycling factor (RRF) and is encoded for by the *frr* gene in *E. coli* (Janosi et al., 1994). Initially, cryo-electron microscopy results suggested that translocation of RRF in a GTP-dependent manner was required for splitting of ribosomal subunits (Agrawal et al., 2004); however, it has been observed that EF-G mutants active in GTPase activity but inactive in translocation activity fully activate RRF activity (Fujiwara et al., 2004). The current consensus (based on available crystal and cryo-EM structures of RRF bound to ribosomal particles) is that movement of RRF through the ribosome, catalyzed by EF-G, disrupts intersubunit bridges, destabilizing the 70S ribosome and allowing subunit dissociation (Barat et al., 2007; Pai et al., 2008).

To further complicate defining a mechanism for ribosome recycling, distinct roles for IF-1 and IF-3 have been suggested: Using a combination of genetic techniques (demonstrating that IF-3 overexpression in a temperature-sensitive phenotype with mutated RRF can rescue the

phenotype) and biochemical approaches (showing IF-3 facilitates both *in vivo* and *in vitro* ribosome recycling), a role for IF-3 has been suggested (Singh et al., 2005a). This model suggests that EF-G and RRF induce a transient separation of the 70S ribosomes which is stabilized by IF-3 binding to the 30S subunit (Singh et al., 2005a), thereby preventing subunit reassociation until the 30S•IF-3 complex enters the initiation phase. However, this model does not fully explain how mRNA and deacyl-tRNA dissociates from the split ribosome; three additional models have been proposed (Varshney and Seshadri, 2006). In the first model, EF-G-induced translocation of RRF causes release of deacyl-tRNA, the subunits dissociate, and mRNA spontaneously dissociates (IF-3 prevents reassociation). In the second model, EF-G•GDP binds to the post-termination like complex, exchanges GDP for GTP, which causes a conformational change in RRF. Subunit dissociation occurs, and IF-3 binds to the 30S complex, aiding in tRNA and mRNA release from the 30S subunit. In the third model, a conformational change induced by EF-G and RRF allows IF-3 to associate to the transiently dissociated ribosome, which then actively induces full subunit dissociation and remains bound to the 30S subunit.

In the event of a ribosome being incorrectly assembled during translation initiation, Pavlov *et al.* (Pavlov et al., 2008) suggested that there are two mechanisms by which 70S ribosome complexes may be recycled. Ribosomes containing a strong Shine-Dalgarno sequence are preferentially split by the concerted efforts of IF-1 and IF-3 (Pavlov et al., 2008). This may be useful in dissociating incorrectly assembled ribosomes, which are not cellular targets for RRF and EF-G. By contrast, post-termination like complexes are inefficiently dissociated by IF-1 and IF-3 but rapidly dissociated by RRF and EF-G (Pavlov et al., 2008). This suggests that incorrectly assembled ribosomes are recycled by IF-1 and IF-3, whereas post-termination

complexes are dissociated by RRF and EF-G. This study also contradicted the role of IF-3 in preventing subunit re-association after splitting by EF-G and RRF (Pavlov et al., 2008).

Two common features of ribosome recycling are that ribosome recycling requires the activity of both EF-G and RRF and that IF-3 plays a role in this process, either directly by promoting subunit dissociation (in conjunction with RRF and EF-G) or indirectly by preventing subunit reassociation. The presence of IF-3 in these models provides a basis for progression of the 30S subunit from the recycling to the initiation phases. The various models presented by Seshadri and Varshney (Varshney and Seshadri, 2006) are summarized (Figure 1.6). Recent kinetic data, based on fluorescence techniques using differentially labeled subunits, mRNA, and tRNA, indicates that GTP hydrolysis by EF-G does not induce translocation of RRF through the ribosome, and that IF-3 indeed stimulates release of deacyl-tRNA from the post-termination complex (Peske et al., 2005). The bound mRNA then rapidly dissociates from the 30S•IF-3 complex. This data is thus consistent with the model presented in Figure 1.6B.

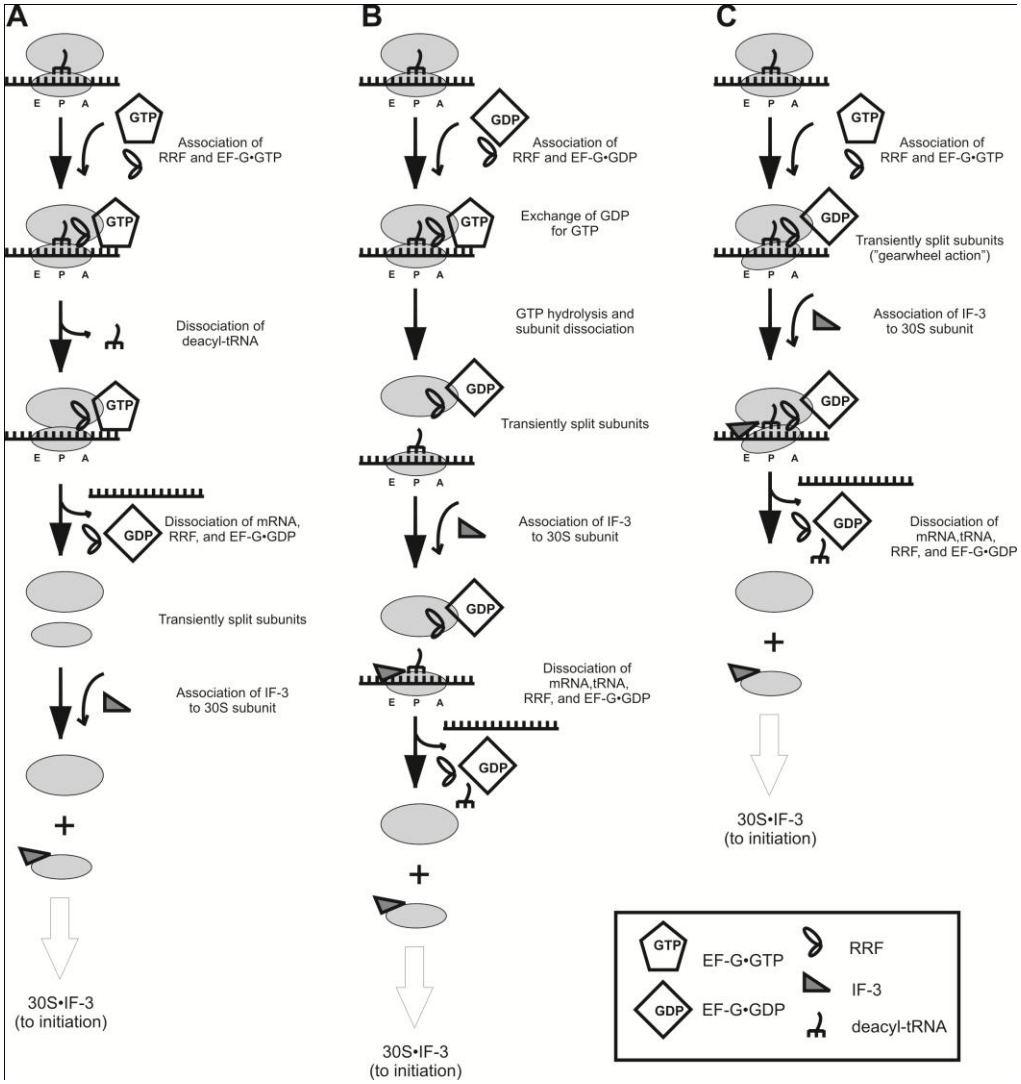

Figure 1.6. Models for Prokaryotic Ribosome Recycling

A) Passive role for IF-3 in recycling. Upon association of RRF and EF-G•GTP to the post-termination complex, RRF moves into the ribosome, causing deacyl-tRNA dissociation. Following GTP hydrolysis, subunits are dissociated and mRNA, RRF, EF-G•GDP dissociate. IF-3 association to the 30S subunit prevents subunit reassociation and allows progression into the initiation phase. B) IF-3 functions in releasing mRNA and tRNA. Upon binding of RRF and EF-G•GDP to the post-termination complex, GDP is exchanged for GTP. Subunit dissociation follows GTP hydrolysis; IF-3 association to the 30S subunit prevents reassociation and aids in mRNA/tRNA release from the 30S subunit. The 30S•IF-3 complex can proceed to the initiation phase. C) An active role for IF-3 in ribosome recycling. Association of RRF and EF-G•GTP to the post-termination complex, results in GTP hydrolysis and a "gearwheel" action between RRF and EF-G, exposing the IF-3 binding site. IF-3 association leads to dissociation of all components; the 30S•IF-3 complex can proceed to the initiation phase. Adapted from (Varshney and Seshadri, 2006).

2. Guanine Nucleotide Binding Proteins

The guanine nucleotide triphosphatases (GTPases) are a ubiquitous family of molecular switches that function in a wide variety of cellular processes such as signal transduction, tRNA modification, DNA replication, and protein synthesis (Bourne et al., 1991; Brown, 2005; Caldon and March, 2003). GTPases exist in three different conformations. The transient *apo* state can bind to either GTP or GDP under cellular concentrations of guanine nucleotides. Binding to GTP causes the protein to adopt a functional GTP-bound "active" state (Bourne et al., 1991). Upon hydrolysis of GTP, the protein reverts to its "inactive", GDP-bound state. GDP then dissociates, and the cycle continues. The conversions between these states are often catalyzed by regulatory proteins, which affect the kinetics of the interaction between the GTPase and guanine nucleotides. These regulators include guanine nucleotide exchange factors (GEFs), which catalyze the release of bound GDP, which in turn promotes GTP binding. GTPase activating proteins or factors (GAPs or GAFs) stimulate the low intrinsic GTPase activity of the protein. Guanine nucleotide dissociation inhibitors (GDIs), decrease the rate of GDP dissociation in eukaryotes, and regulate factors such as Rab and Rho (Dovas and Couchman, 2005; Seabra and Wasmeier, 2004; Siderovski and Willard, 2005). An overview of the GTPase cycle is presented in Figure 2.1.

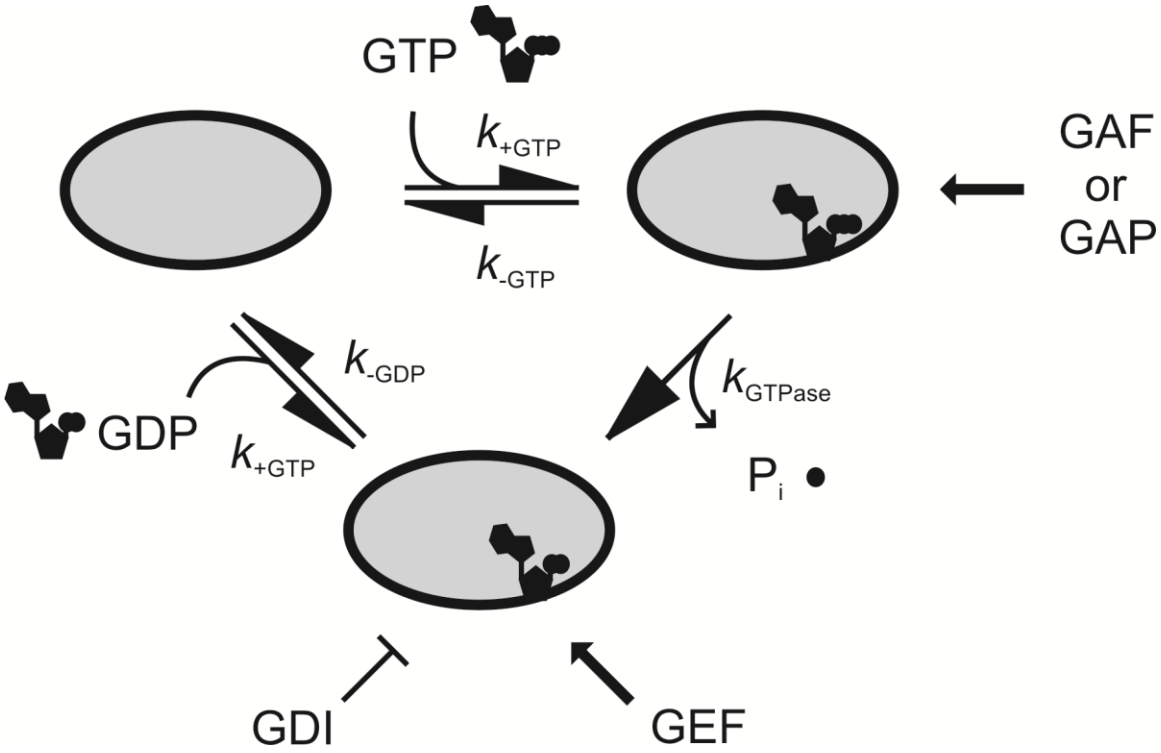

Figure 2.1. Overview of the GTPase Cycle

The *apo* state can interact with GTP or GDP. Interaction with GTP causes the factor to adopt an active, GTP-bound conformation. Hydrolysis of GTP, often induced by GTPase activating factors or proteins (GAF/GAP), causes the protein to adopt an inactive, GDP-bound conformation. The rate of GDP dissociation can either be accelerated by a guanine nucleotide exchange factor (GEF), or repressed by a guanine nucleotide dissociation inhibitor (GDI).

Structurally, these proteins contain a conserved α/β G-domain, consisting of the G1, (P-loop; consensus $GX_4GK(S/T)$), G2 (effector loop, or switch I; DX_nT), G3, (switch II; DX_2G), and G4 (NKXD) motifs responsible for interaction with the guanine nucleotide. A core group of 8 universally conserved GTPases present in all domains of life has been identified (Caldon and March, 2003). These GTPases include elongation factors (EFs) Tu and G (eEF-1α and eEF-2 in eukaryotes), initiation factor (IF) 2, protein secretion factors Ffh and FtsY, and the relatively poorly characterized proteins YihA, YchF, and HflX (Caldon and March, 2003). Additional GTPases, conserved in prokaryotes and eukaryotes but not archaea, include Obg, EngA, and Era

(Caldon and March, 2003). Factors such as members of the septin, Ras, Rho, and Rab families perform essential functions in eukaryotes, but lack homologs in bacteria or archaea (Figure 2.2). A unifying principle in the study of these GTPases is that understanding their function requires detailed knowledge of their interaction partners, kinetic parameters, and structural features. Thus, determining the properties of an unknown GTPase using techniques established for studying factors whose function has been elucidated will provide critical information for determining both the cellular role of a novel GTPase and the mechanism by which it carries out this function. The objective of this chapter is to briefly outline the known structural and functional features of the 8 universally conserved GTPases, and describe their regulators and interaction partners.

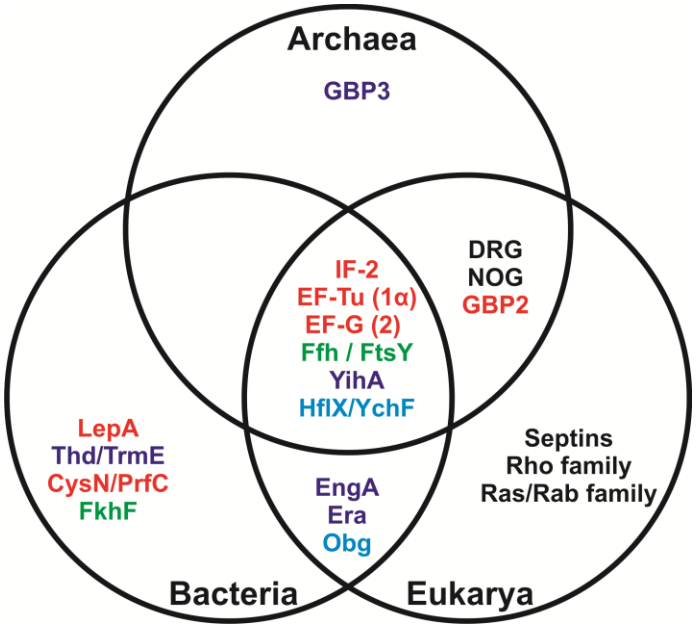

Figure 2.2. Conservation of the GTPase Superfamily

Red, elongation factor group; Green, protein secretion factors; Purple, Era-like GTPases; blue, oligonucleotide binding GTPases (Obg) group. The eight universally conserved GTPases are: initiation factor (IF) 2, elongation factors (EFs) Tu and G (1α and 2 in eukaryotes, respectively), Ffh, FtsY, YihA, HflX, and YchF.

2.1 Five universally conserved GTPases of known function

2.1.1 Initiation Factor 2

Initiation factor 2 (IF-2) functions in delivering initiator tRNA ($tRNA_i$; $fMet\text{-}tRNA_i^{fMet}$ in prokaryotes and $Met\text{-}tRNA_i^{Met}$ in eukaryotes) to the 30S ribosomal subunit (reviewed along with EF-Tu and EF-G in (Rodnina et al., 2000)). During initiation of protein synthesis in prokaryotes, the 30S and 50S subunits, initiator tRNA, and initiation factors 1, 2, and 3 function to assemble a 70S ribosome, with an AUG start codon and aminoacyl-tRNA in the ribosomal P-site. In archaea and eukaryotes, this factor is a heterotrimer (α, β, and γ subunits), while in prokaryotes IF-2 is a single five domain protein homologous to members of the eukaryotic and archaeal complexes,

eIF-2α and aIF-5b. This suggests a difference in the regulation of translation initiation by IF-2 in prokaryotes compared to eukaryotes and archaea.

Structurally, the N-terminal domain is poorly conserved among bacterial species, and is required for translation initiation (Gualerzi et al., 1991; Marzi et al., 2003). The next domain (GI) is highly conserved and contains structural elements required for GTP binding and hydrolysis. The GII domain is predicted to be a β-barrel domain similar to the corresponding domain II of EF-G and EF-Tu. Following the GII domain is the C-terminal domains CI and CII, which are essential for binding $tRNA_i$ (Marzi et al., 2003). The structures of the GI and GII domains are widely predicted to be similar to their counterparts in EF-G and EF-Tu. While the X-ray crystal structure of the full prokaryotic protein has not yet been solved, small angle X-ray scattering (SAXS) has revealed that the four C-terminal domains of the *E. coli* factor roughly adopt a chalice-like structure similar to EF-G (Rasmussen et al., 2008). Nuclear magnetic resonance (NMR) experiments have revealed that the CI subdomain of *Bacillus stearothermophilus* consists of a four-stranded β-sheet flanked by 3 α-helices (Wienk et al., 2005). Cryo-electron microscopy (Cryo-EM) experiments support this data, and also have provided the structure of the IF-2•GTP•$tRNA_i$•30S•mRNA complex (Simonetti et al., 2008).

The affinity of IF-2 for interacting with either GTP or GDP have been reported as approximately 140 and 13 μM respectively using ^{1}H NMR and isothermal titration calorimetry (ITC) (Hauryliuk et al., 2009; Pon et al., 1985b). The thermodynamic parameters of nucleotide binding suggest that IF-2 adopts different conformations in the switch I and switch II regions of the protein, depending on the bound nucleotide (Hauryliuk et al., 2009). The pre-steady state kinetics of IF-2 interacting with either mant-GDP or mant-GTP have also been studied using

fluorescence resonance energy transfer from the intrinsic tryptophan residues of IF-2 to the mant group of fluorescently labeled nucleotides (Milon et al., 2006). Interestingly, IF-2 also interacts (with a similar affinity compared to GTP and GDP) with the alarmone guanosine 3',5'-(bis) diphosphate (ppGpp), indicating that IF-2 is modulated by the so-called stress response (Milon et al., 2006). IF-2 also interacts with all ribosomal particles, with a preference for 30S>70S>50S, an interaction that does not depend on the nucleotide bound to IF-2 (Pon et al., 1985b).

Based on the determined nucleotide and ribosome binding affinities, IF-2 was determined to be predominantly found on the 30S subunit, almost exclusively in the GTP-bound form (Milon et al., 2006). Interestingly, recent kinetic studies suggest that IF-2 in complex with the 30S subunit (as a preinitiation complex) is responsible for recruitment of $tRNA_i$ to this complex rather than delivery as a ternary complex (analogous to the function of EF-Tu (Milon et al., 2010)). Unlike EF-Tu and EF-G, the activation of GTPase activity is not stimulated by the presence of L7/L12 (Huang et al., 2010b). However, similar to EF-Tu and EF-G, IF-2 is stimulated by the GTPase activating centre of the ribosome (Simonetti et al., 2008), a conserved region of 23S rRNA responsible for coordinating a conserved His residue of translational GTPases in a catalytically active position for nucleotide hydrolysis (Voorhees et al., 2010a). Thus while the function of IF-2 is to promote accurate initiation through recruitment of $tRNA_i$ and the 50S subunit to the 30S preinitiation complex, the role of GTP hydrolysis during this process remains unclear (Rodnina et al., 2000).

2.1.2 Elongation Factor Tu

Elongation factor (EF) Tu (Thermo unstable) is responsible for the delivery of aminoacyl-tRNA to the translating ribosome during the elongation phase of protein synthesis, and is essential for maintaining translational fidelity by ensuring delivery of the correct aminoacyl-tRNA to the elongating ribosome (Pape et al., 1998b). In the GTP bound conformation (Figure 2.3), EF-Tu has a high affinity for aa-tRNA, while the GDP bound form has a significantly decreased affinity for aa-tRNA (Yokosawa et al., 1975). The crystal structures of EF-Tu from multiple organisms, bound to the non-hydrolyzable GTP analog GDPNP, show a major structural rearrangement in the switch I and II regions of domain I (the G domain), causing a reorientation of domains II and III by ~ 90 º relative to domain I (Figure 2.3) and thus accounts for the altered affinity of EF-Tu binding to aa-tRNA, which binds in a cleft between domains I and II. This rearrangement of the domains, induced by GTP hydrolysis and subsequent P_i release, is essential for the binding and release of aa-tRNA, as well as the dissociation of the EF-Tu•GDP binary complex from the 70S ribosome. Domains II and III are also required for contact with the 70S ribosome and EF-Ts (elongation factor thermo stable) respectively (Gromadski et al., 2002).

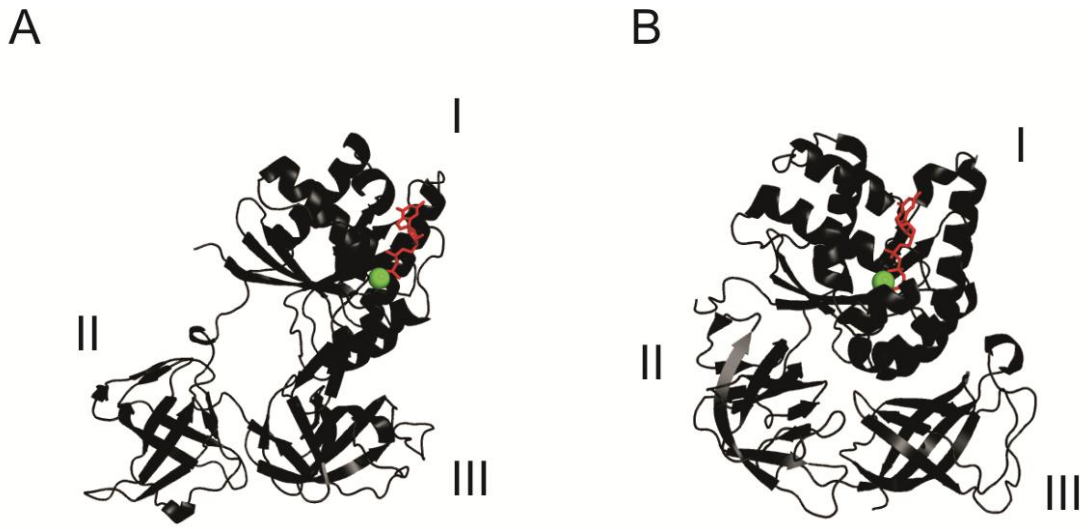

Figure 2.3. Structures of EF-Tu•GDP and EF-Tu•GDPNP

Cartoon representation of the structure of EF-Tu A) from *E. coli* in complex with GDP (PDB 1EFC) and B) *Thermus thermophilus* EF-Tu in complex with the non-hydrolyzable GTP analog GDPNP (PDB 1EXM). Domains I, II, and III are indicated. The nucleotide is shown as a red stick model, and a Mg^{2+} responsible for coordinating the β-phosphate of the bound nucleotide is shown as a green sphere.

During the elongation cycle, a ternary complex of EF-Tu•GTP•aa-tRNA initially binds to a ribosome (with peptidyl-tRNA in the P-site and an empty A-site) in a codon-independent manner. The kinetic mechanism of this process has been examined (Pape et al., 1998b), and is outlined in Figure 2.4. Ribosomal protein L7/L12 (4 copies in *E. coli*) is required for recruitment (via the C-terminus of L7/L12) of the ternary complex to the elongating ribosomal A-site, and is essential for GTPase activation of EF-Tu (Diaconu et al., 2005; Kothe et al., 2004) as shown by examining the GTPase activity of EF-Tu in the presence of 70S ribosomes depleted of L7/L12 (Kothe et al., 2004; Savelsbergh et al., 2000). After initial binding, codon recognition occurs. Upon cognate codon-anticodon interaction, the GTPase activating centre, through a proposed

network of interactions between the decoding centre at the ribosomal A-site and the G domain of EF-Tu, causes a conformational change in EF-Tu that induces GTP hydrolysis (Voorhees et al., 2010a). Thus, in analogy to the GTPase cycle in Figure 2.1, the 70S ribosome acts as a GAP for the EF-Tu•GTP•aa-tRNA ternary complex upon the cognate codon-anticodon interaction (specifically, the GTPase activating centre and ribosomal proteins L7/L12). Following GTP hydrolysis, P_i is released (Rodnina et al., 2005; Rodnina et al., 2000), leaving the EF-Tu•GDP binary complex, which then dissociates from the ribosome. A cognate codon-anticodon interaction is required for efficient GTPase activation, which causes the aa-tRNA to be fully accepted into the ribosomal A-site and a peptide bond to be formed (Rodnina et al., 2005). Alternatively, a non-cognate codon-anticodon interaction occurs, causing the rejection of the aa-tRNA (and the ternary complex dissociates from the ribosome). With P-site deacyl-tRNA and A-site aminoacyl-tRNA, the ribosome can then undergo EF-G mediated translocation (Pape et al., 1998b). At this point, one of two possibilities can occur: if a non-cognate interaction was rejected, the aa-tRNA and EF-Tu•GDP dissociate. If a cognate interaction occurs and aa-tRNA is accommodated into the ribosomal A-site, then the EF-Tu•GDP dissociates.

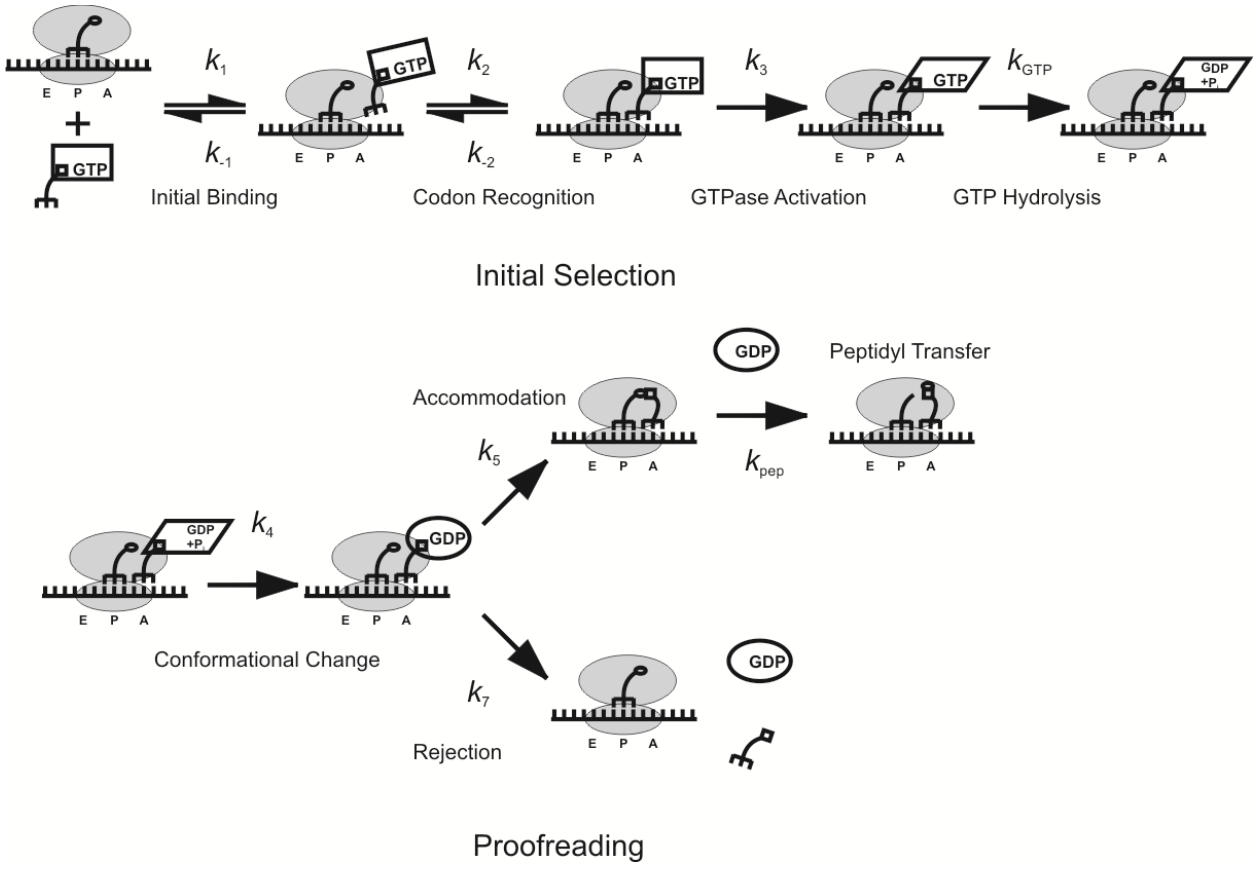

Figure 2.4. Kinetic Mechanism of aminoacyl-tRNA Binding to the Ribosome

EF-Tu•GTP•aa-tRNA associates with the 70S ribosome (with P-site peptidyl-tRNA) in a codon-independent initial binding step (k_1, k_{-1}). Upon cognate codon-anticodon recognition (k_2, k_{-2}), the GTPase activity of EF-Tu is activated (k_3) and GTP is hydrolyzed (k_{GTP}). A conformational change in EF-Tu (k_4) upon release of P_i causes EF-Tu to adopt the GDP-bound conformation. Non-cognate aa-tRNA is rejected (k_7) and dissociates along with EF-Tu•GDP, or cognate aa-tRNA is fully accommodated (k_5) into the ribosomal A-site and EF-Tu•GDP dissociates. Peptide bond formation occurs (k_{pep}), leaving the ribosome with P-site deacyl-tRNA and A-site peptidyl-tRNA. Adapted from (Rodnina et al., 2005).

Upon dissociation, the EF-Tu•GDP binary complex interacts with EF-Ts to promote the dissociation of bound GDP and promote binding of GTP. This is required as the affinity of EF-Tu for GDP is significantly higher compared to GTP (1 nM and 60 nM respectively, (Gromadski et al., 2002)). The kinetic scheme of EF-Tu interacting with GTP, GDP, and EF-Ts was studied

by fluorescence techniques such as FRET by Gromadski *et al* (Gromadski et al., 2002), and is described in Figure 2.5 below. The rate of GDP dissociation from EF-Tu is relatively slow (k_{-1} = 0.002 s^{-1}), thereby preventing EF-Tu from adopting the active, GTP-bound conformation. Interaction with EF-Ts increases the rate of GDP dissociation from EF-Tu by 62 500 fold (k_{-4} = 125 s^{-1}), thus facilitating GTP binding to EF-Tu (Gromadski et al., 2002). This is also reflected in a change in the nucleotide binding affinities from 1 nM for GDP in the absence of EF-Ts to ~ 10 µM in the presence of EF-Ts. Thus, the cellular partitioning of EF-Tu is shifted toward the GTP-bound state, which binds to aa-tRNA (Pingoud et al., 1977)and can thus promote protein synthesis rates of ~ 10 peptide bonds formed s^{-1} (Gromadski et al., 2002). Mutation of amino acid residues along the intermolecular contact surface in EF-Tu significantly affect both the kinetics of EF-Tu interacting with other factors such as L7/L12 and with guanine nucleotides (Dahl et al., 2006; Daviter et al., 2003; Kothe et al., 2004; Wieden et al., 2010). The information gleaned from structural studies as well as examining the kinetics of both aa-tRNA delivery and guanine nucleotide exchange has led to a detailed understanding of the role of EF-Tu and its interaction partners during protein synthesis.

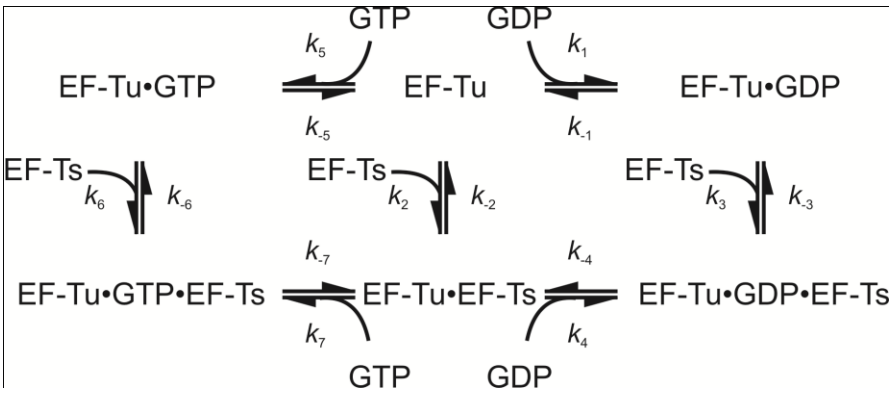

Figure 2.5. Kinetic Mechanism of Nucleotide Exchange in EF-Tu

EF-Tu can associate with GDP (k_1, k_{-1}), GTP (k_5, k_{-5}), or EF-Ts (k_2, k_{-2}). Likewise, the EF-Tu•GDP and EF-Tu•GTP bound forms can also interact with EF-Ts (k_3, k_{-3} and k_6, k_{-6} respectively). Upon interaction with EF-Ts, the rate of GDP dissociation from the EF-Tu•GDP•EF-Ts complex (k_{-4}) is increased significantly, thereby facilitating association of EF-Tu to GTP. Based on the kinetic scheme described in (Gromadski et al., 2002).

2.1.3 Elongation Factor G

Elongation factor G catalyzes the GTP-dependent translocation of ribosome-bound mRNA, P-site deacyl-tRNA, and A-site peptidyl-tRNA. After delivery of aa-tRNA to the ribosomal A-site by EF-Tu and subsequent peptide bond formation, the ribosome exists in a so-called pre-translocation complex (P-site deacyl-tRNA and A-site peptidyl-tRNA). The binary complex of EF-G•GTP then associates with the ribosomal pre-complex. Following GTP hydrolysis, P_i is released from EF-G, which is followed by translocation, leaving an empty A-site, peptidyl-tRNA in the P-site, and deacyl-tRNA in the E-site. The EF-G•GDP complex then dissociates from the ribosome, now in the post-translocation state, allowing for delivery of another aa-tRNA to the A-site. EF-G also functions during the ribosome recycling phase, utilizing GTP hydrolysis to drive RRF-mediated ribosome dissociation (Outlined in Figure 1.6).

The X-ray crystal structure of EF-G•GDP from *Thermus thermophilus*, solved by Czworkowski *et al.* (Czworkowski et al., 1994), reveals that EF-G consists of five domains resembling a "tadpole" shape: an N-terminal G domain contains an extension termed the G' domain not found in EF-Tu; domain II is structurally similar to its counterpart in EF-Tu (a β sandwich domain) despite dissimilar primary sequences. Domains III, IV, and V are all α-β domains. Domain IV represents the "tail" of EF-G, and domain V closely resembles domain III of EF-Tu. Indeed, structural comparison of the EF-Tu•GTP•aa-tRNA ternary complex with EF-G•GDP reveals the two factors are quite similar (Clark and Nyborg, 1997; Nyborg, 1998), which suggests similar modes of binding to the ribosome (Gao et al., 2009a). Unlike EF-Tu, the GDP and GDPNP bound forms of EF-G do not significantly differ (Figure 2.6 (Hansson et al., 2005)). Cryo-electron micrscopy studies have indicated that binding to the ribosome significantly alters the conformation of EF-G (Datta et al., 2005; Gao et al., 2004; Stark et al., 2000), which has been confirmed by X-ray crystal structures of EF-G bound to the ribosome in the post-translocation state (Gao et al., 2009b). Binding of EF-G to the ribosome and GTP hydrolysis is thought to induce a "ratchet-like" motion, unlocking the subunits relative to each other and allowing movement of bound mRNA and tRNAs (reviewed in (Schmeing and Ramakrishnan, 2009) from a structure-based perspective).

The conserved structural features of EF-G, revealed by X-ray crystallography, are shared with the ribosomal protection protein Tet(O) (Connell et al., 2003; Thakor et al., 2008), the ribosomal back-translocase LepA (Evans et al., 2008), and the stress response factor BipA (DeLivron et al., 2009). These factors share a common G domain (though lack a significant G' insert), as well as domains II and III. The remaining two domains (IV and V, or the C-terminal domain) can be spatially superimposed, yet are structurally distinct from one another in terms of

secondary structure. Indeed, it is currently hypothesized that the unique C-terminus of LepA is responsible for allowing retro-translocation of ribosome-bound aminoacyl-tRNA (Evans et al., 2008), and for GTPase activation (E. DeLaurentiis, Personal Communication); a similar C-terminal domain is required for GTPase activation of BipA (DeLivron et al., 2009). These common structural features and a common binding site suggest a common mode of GTPase activation, which in EF-G (similar to EF-Tu) is through the recognition of a specific ribosomal complex (pre-translocation) and subsequent binding and interaction with the GTPase activating centre and L7/L12 (Datta et al., 2005; Diaconu et al., 2005; Savelsbergh et al., 2005b; Savelsbergh et al., 2000).

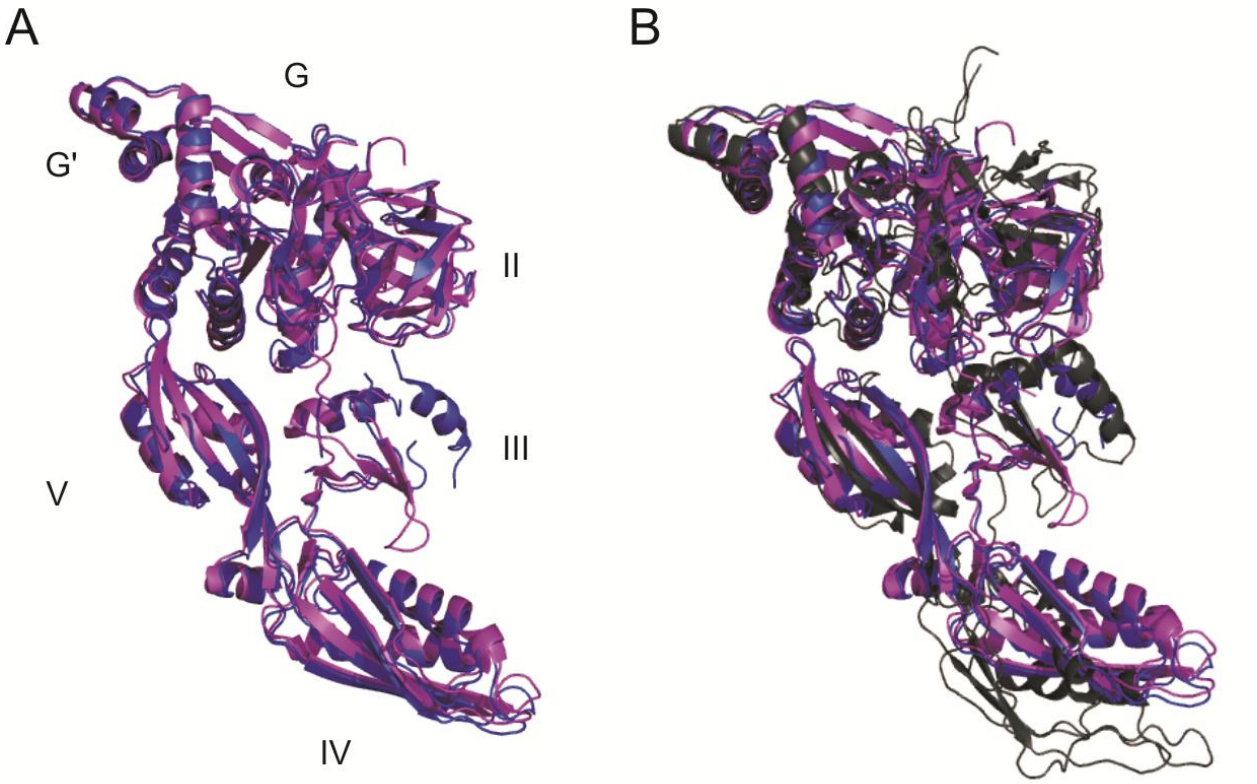

Figure 2.6. Structure of EF-G in complex with GDP, GDPNP, and bound to the Post-translocation Ribosome.

A) Superimposition of EF-G•GDP from *Thermus thermophilus* (PDB ID 2EFG, blue) and EF-G•GDPNP from the same organism (PDB ID 2BV3, purple). Structures are shown as cartoon representations. Domains I (G domain), G', II, III, IV, and V are indicated. B) Superimposition of EF-G•GDP (also *T. thermophilus)* in the ribosome-bound posttranslocational state (grey) upon structures shown in A).

Structural data on EF-G is complemented by kinetic studies of nucleotide binding by EF-G, which reveal that the binding of mant-GDPNP is stabilized 30 000-fold when EF-G is bound to the 70S ribosome by reducing the nucleotide dissociation rate (Wilden et al., 2006a). This is supported by structural probing studies using limited trypsinolysis, which demonstrates that the switch I region of EF-G is protected from proteolysis by the ribosome in different nucleotide bound states (Ticu et al., 2009). GTP hydrolysis by EF-G (stimulated by the pre-translocation

ribosome) has been shown to drive a conformational change of the ribosome, unlocking the 30S relative to the 50S in a "ratchet-like" motion (Savelsbergh et al., 2003). P_i release, an important step in EF-G turnover (Savelsbergh et al., 2005b), and translocation of bound mRNA and tRNA occur rapidly, allowing EF-G•GDP to dissociate (Savelsbergh et al., 2003). This leaves the ribosome in a post-translocation state, from which deacyl-tRNA dissociates from the ribosomal E-site and and allows for another round of elongation to occur (Savelsbergh et al., 2003). Again, this data clearly demonstrates regulation of EF-G via the ribosome through stabilization of the nucleotide binding pocket to increase the affinity for GTP, thereby facilitating the progression of the ribosome through the elongation cycle.

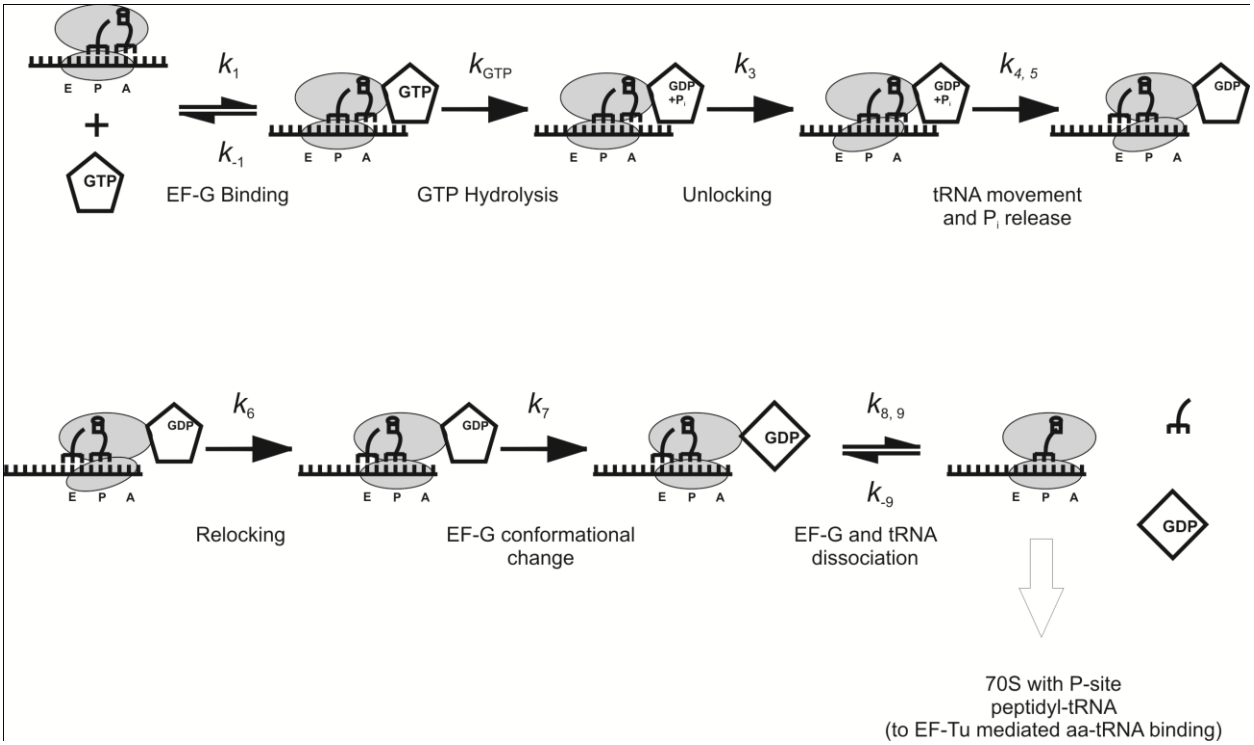

Figure 2.7. Kinetic Scheme of EF-G Mediated Translocation.

After binding of EF-G•GTP to the ribosome, GTP hydrolysis induces an "unlocking" of the 30S subunit relative to the 50S. Following rapid P_i release and mRNA/tRNA translocation, the ribosome and EF-G undergo conformational changes, "relocking" the ribosome. EF-G•GDP and deacyl-tRNA then dissociate from the post-translocation ribosome. Adapted from references (Savelsbergh et al., 2003; Savelsbergh et al., 2005b).

2.1.4 Protein secretion factors Ffh and FtsY

The conserved GTPases Ffh (Fifty four homolog, a conserved component of the signal recognition particle) and FtsY make up key members of the co-translational protein secretion pathway in all living cells (reviewed in (Walter and Johnson, 19964)). Proteins that require either insertion into or translocation across plasma membranes are synthesized with an N-terminal 13-36 amino acid signal sequence, usually with a high proportion of positively charged residues. The signal peptide contains an approximately 6-15 amino acid hydrophobic core, flanked by

hydrophilic residues; the N-terminus is characterized by a basic amino acid sequence (Zheng and Gierasch, 1996). Once the ribosome has synthesized a chain of ~ 40 amino acids, the signal sequence protrudes from the polypeptide exit channel. The signal recognition particle (SRP) recognizes the signal sequence and binds to the ribosome and signal peptide. The SRP consists of multiple proteins (including the SRP54 protein, homolog of Ffh) associated to a 7S RNA in eukaryotes, but a single protein, Ffh, bound to a 4.5S RNA molecule in prokaryotes. Structurally, Ffh consists of three domains; an N-terminal domain of unknown function, a central G domain, and the methionine-rich (M) domain that interacts with the 4.5S RNA at the C-terminus. Once associated, Ffh exchanges its bound GDP for GTP; thus, the elongating ribosome with the protruding signal sequence acts as a guanine nucleotide exchange factor in analogy to the GTPase cycle (Figure 2.1). GTP locks the SRP onto the ribosome, causing an arrest of the elongation cycle. The SRP•GTP•Ribosome complex diffuses to the plasma membrane, where it associates to a SRP receptor (SR) in complex with the translocon. The prokaryotic SR is the GTPase FtsY, a 497 amino acid protein. In eukaryotes, the SR consists of the GTPases SRα and SRβ. The translocon consists of the SecYEG heterotrimer which forms a pore in the plasma membrane via a predicted 10 helix transmembrane span.

Association of the SRP•GTP•Ribosome complex to the SR results in exchange of GDP for GTP by the SR (again, acting as a GEF in analogy to Figure 2.1). Fluorescence experiments examining the association of GTP to the SRP and FtsY suggest a binding and subsequent conformational change (Jagath et al., 2000). The SRP and SR mutually induce GTP hydrolysis, for which the 4.5S RNA is required (Ataide et al., 2011; Peluso et al., 2001), resulting in further conformational changes that cause dissociation from each other. The resulting ribosome•translocon complex can then resume elongation. The signal peptide passes through the

translocon, the nascent polypeptide begins folding into its native conformation. Once termination of translation occurs, the ribosome dissociates from the translocon and is recycled, thereby entering the translation cycle again. Proteins are either secreted through the translocaon (for example, β-lactamase) or remain associated to the plasma membrane via C-terminal hydrophobic anchors that remain in the plasma membrane (such as extracellular receptors).

Cryo-electron microscopy studies have provided structural information on the SR•SRP•Ribosome complex (Estrozi et al., 2011). Additionally, the crystal structure of the SRP•SR complex has been solved, and reveals that the GTP bound forms of SRP and SR (bound to the non-hydrolyzable GTP analog GMPPCP) localize to the distal end of the associated 4.5S RNA and form a head-to tail dimer between Ffh and FtsY (Ataide et al., 2011). The 4.5S RNA, which is responsible for GTPase activation upon binding of the SRP to the SR, acts as a GAP; truncation of a core region resulted in abolishment of GTPase stimulation (Ataide et al., 2011).

2.2 Three universally conserved GTPases of unknown function

2.2.1 YihA/YsxC

The *yihA* gene, encoding for the 210 amino acid YihA protein, is essential in *E. coli*, *Bacillus subtilis,* and *Staphylococcus aureus* (Arigoni et al., 1998; Cooper et al., 2009; Schaefer et al., 2006). Recombinant expression of *E. coli* YihA as a soluble, 23.4 kDa N-terminally 6X-His tagged protein has been reported (Lehoux et al., 2003). FRET-based titrations, using the intrinsic tryptophan residues of YihA and the mant moiety of mant-GDP/GTP as FRET donor and acceptor fluorophores respectively, have revealed K_D values of ~ 2 and 30 μM for GDP and GTP respectively, independent of magnesium concentration (Lehoux et al., 2003). Hydrolysis of

GTP was not detected using a malachite green detection of inorganic phosphate (Lehoux et al., 2003). The 195 amino acid *B. subtilis* homolog, YsxC (also known as EngB) is 35.4% identical and shows 51.3% sequence similarity to *E. coli* YihA, and has been linked to ribosome biogenesis (Cooper et al., 2009). Based on the observation that multiple additional GTPases, such as RbgA, Era, Obg, and YjeQ may be involved in ribosome assembly or function, Schaefer *et al.* examined a potential role for YsxC and YphC (*B. subtilis* homolog of *E. coli* EngA) in ribosome biogenesis (Schaefer et al., 2006). Sucrose density ultracentrifugation of ribosomal particles from *ysxC*-depleted cells revealed the presence of a 45S intermediate that was also examined by this group (Schaefer et al., 2006). Analysis of ribosomal protein content of ribosomes purified from the depleted strain revealed a lack of proteins L16, L27, and L36, indicating a role for YsxC in 50S assembly (Schaefer et al., 2006). Purified YsxC was also found to interact directly with 50S subunits; stability of this complex is enhanced when GDPNP is present. Further research into purified samples of YsxC revealed co-purification with a high molecular mass material, likely rRNA. Addition proteins that co-purified with YsxC were analyzed by mass spectrometry and revealed that the factor associates with proteins L6, L10, L7/L12, L23, and L27 (Wicker-Planquart et al., 2008). Association between *B. subtilis* YsxC and L1, L6, and L7/L12 could be reconstituted *in vitro* (Wicker-Planquart et al., 2008) and *S. aureus* YsxC was also found to associate with ribosomal proteins S2, S10, and L17 (Cooper et al., 2009).

The crystal structures of *B. subtilis* YsxC in the *apo,* GDP, and GDPNP bound states (Figure 2.8) were determined in 2004 by Ruzheinikov *et al.* (Ruzheinikov et al., 2004). Similar to other translational GTPases, large scale conformational changes were observed between the various states; in particular, in the switch I and switch II regions (the G2 and G3 motifs

respectively) (Ruzheinikov et al., 2004). Notably, the G1 motif undergoes a conformational change from an α-helix in the *apo* state to a loop structure in the GDP and GDPNP bound forms (Figure 2.8). Additionally, the region between the G1 and G2 motifs is not resolved in the GDP or *apo* structures, but is resolved in the GDPNP bound form; the loop adjacent to the G3 motif also changes its conformation compared to the *apo* and GDP bound forms. An electrostatic surface potential map generated using PYMOL (DeLano, 2006) reveals a highly electropositive face and a highly electronegative face, which may interact with rRNA and basic ribosomal proteins respectively. *In silico* molecular dynamics simulations of *S. aureus* YsxC, aimed at identifying potential residues involved in binding to ribosomal proteins have also been performed, leading to the development of a model for ribosomal subunit assembly. In this model, GTP hydrolysis induces binding to L17 to the 50S, followed by association of S2, and S10 to the 30S subunit (Goyal et al., 2011). The GTPase activity of YsxC has not been examined, nor have any regulators of GTPase activity/nucleotide binding been identified. Thus, while YihA functions during ribosome biogenesis (Cooper et al., 2009), the role of GTP hydrolysis by this factor is unknown. It would be of great interest to determine if the ribosome acts as a regulator of GTP hydrolysis by YihA, or if this interaction modulates the structural features of YihA.

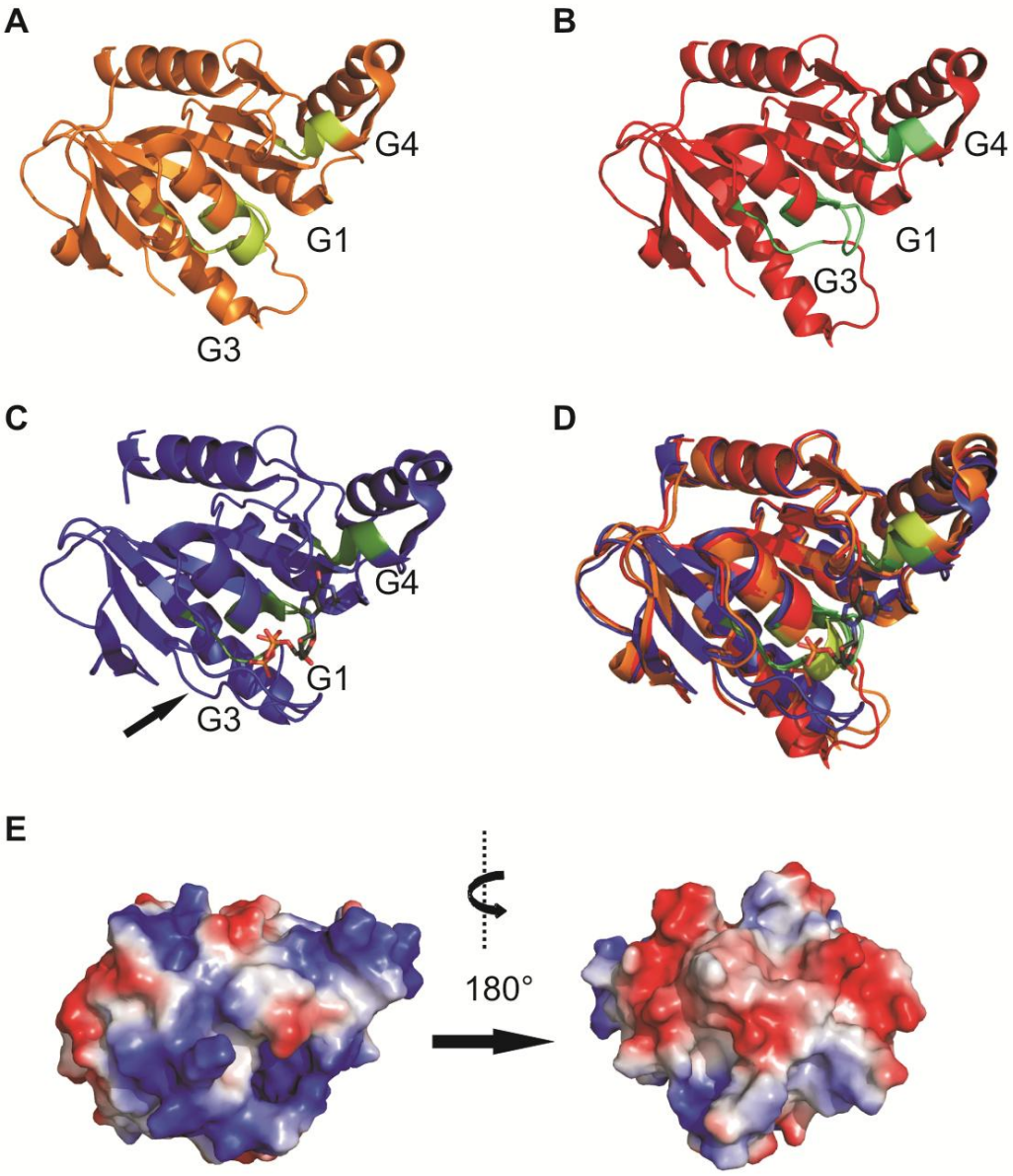

Figure 2.8. Structure of YihA/YsxC.

Cartoon representation of the structures of A) *apo*, B) GDP-bound (nucleotide omitted for visualization of G1 helix to loop conformational change), and C) GDPNP bound state. The G1, G3, and G4 motifs are labeled and shown in shades of green (light green for the *apo* state, darker for the GDP-bound state, and darkest for the GDPNP bound state). The arrow indicates a resolved loop present in the GDPNP bound state but not observed in the GDP or *apo* states. D) superimposition of the three states. E) Electrostatic surface potential map of YihA. Left, same orientation as in A)-D); right, 180 degree rotation. PDB IDs are 1SUL, 1SVI, and 1SVW for the *apo,* GDP, and GDPNP structures respectively (Ruzheinikov et al., 2004).

2.2.2 YchF

The crystal structure of YchF from *Haemophilus influenzae* was reported in 2003 by Teplyakov *et al.* (Teplyakov et al., 2003), and that of the human YchF homolog, hOLA1 (*h*uman *O*bg-*l*ike *A*TPase 1) in 2007 (Koller-Eichhorn et al., 2007). These structures reveal a three domain protein with a "claw-like" structure. The electrostatic surface potential map of the interior of the "claw" reveals a highly electropositive region, which was suggested to interact with the negatively charged phosphate backbone of a nucleic acid strand (Teplyakov et al., 2003). Indeed, upon incubation with double stranded DNA (dsDNA) the intrinsic tryptophan fluorescence of YchF was reported to be quenched (Teplyakov et al., 2003).

Structurally, YchF consists of an N-terminal G domain, interrupted by a central α-helical A domain, and C-terminal TGS (Threonyl-tRNA synthetase, GTPase, SpoT-like) domain (Figure 2.9), forming the "claw-like" structure. While the roles of the A and TGS domains are unknown, ability of YchF to bind and hydrolyze purine nucleotide triphosphates has been examined. Addition of 2'-(or 3')-*O*-(2,4,6-trinitrophenyl)-GTP (TNP-GTP) to YchF caused an increase in TNP fluorescence, indicating that the factor binds to GTP (Teplyakov et al., 2003); similarly, addition of mant-GTP and mant-ATP to hOLA1 showed a similar increase in mant polarization (mant-ATP to a greater extent (Koller-Eichhorn et al., 2007)). Perhaps due to the non-canonical G4 motif NV(L)NE in YchF/hOLA1 (Normally NKxD), both hOLA1 and *Trypanosoma cruzi* YchF hydrolyze ATP more efficiently than GTP (Gradia et al., 2009; Koller-Eichhorn et al., 2007; Teplyakov et al., 2003). A recent publication by Tomar *et al.* (Tomar et al., 2011) indicates that potassium is required for hydrolysis of ATP by YchF. This makes YchF the first potassium-dependent ATPase described in the literature (Tomar et al., 2011).

The strongest evidence that YchF plays a role during protein synthesis is that YchF interacts with polysomes in *T. cruzi* (Gradia et al., 2009). Recently, Tomar *et al.* indicated that YchF associates with 50S and 70S ribosomal particles in a nucleotide-independent manner (Tomar et al., 2011). Additionally, *Oryza sativa* YchF was shown to interact with the large ribosomal subunit (Cheung et al., 2010). Further evidence for a role of YchF in protein synthesis lies in the fact that in the presence of 70S ribosomes, the rate of ATP hydrolysis is in fact stimulated ~ 4 fold (M. Becker, K. Rosler, A. Altamirano; personal communication). Similar NTPase stimulation of *O. sativa* YchF was also recently reported by the GTPase activating protein OsGAP1, which stimulated both the ATPase and GTPase activity by 3-4 fold (Cheung et al., 2010). Since no bacterial homologs of OsGAP1 have been identified, it is likely that interaction partners in addition to the ribosome may be responsible for regulation of YchF.

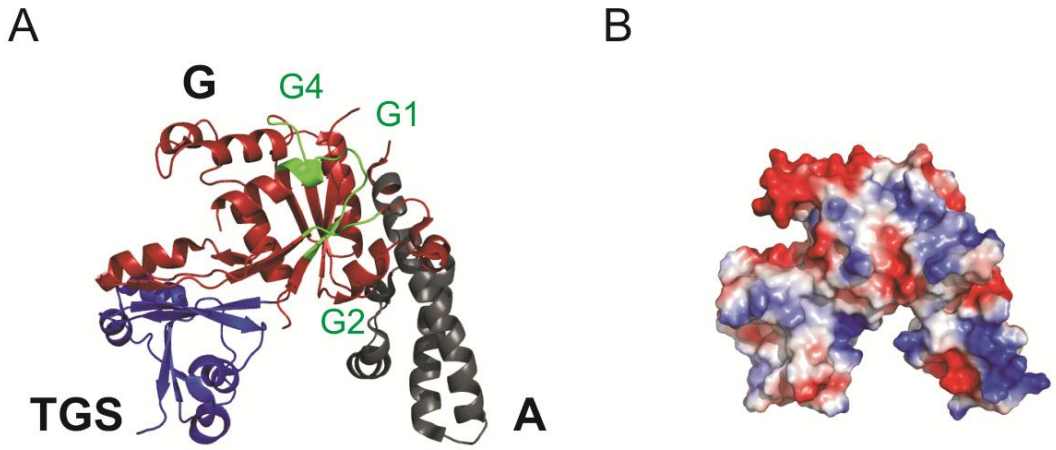

Figure 2.9. *Haemophilus influenzae* YchF.

A) Crystal structure of *Haemophilus influenzae* YchF (PDB ID 1JAL, (Teplyakov et al., 2003)). The G domain is shown in red; A domain in dark grey, and TGS domain in blue. The G1, G3, and G4 motifs are shown in green. B) Electrostatic surface potential map of *Haemophilus influenzae* YchF.

2.2.3 HflX

The *hflX* open reading frame was initially identified as a part of the *hflA* locus, consisting of the open reading frames *hflC, hflK*, and *hflX*, which encode for 37, 46, and 50 kDa proteins respectively (Banuett and Herskowitz, 1987). These factors were identified as governing the lysis/lysogeny decision of bacteriophage λ upon infection of cells (summarized in Figure 2.10). In situations where nutrients are abundant, *E. coli* cells rapidly grow and divide, thus provide additional host cells for viral propagation (lytic cycle). However, under stress conditions, the host cells are more sparse and weak, thus providing a poor base for viral propagation, and the viral genome incorporates into the host genome (lysogeny) until more optimal conditions trigger viral protein expression (Banuett and Herskowitz, 1987; Herskowitz and Hagen, 1980). *E. coli* defective in the *hflA* locus were shown to have a high frequency of lysogenation (hence *hfl*), thus implicating this locus in regulating viral protein expression. This increased lysogenation efficiency was linked to increase concentrations of the viral cII protein, which in turn stimulates viral integrase expression, a required factor for genome integration (Herskowitz and Hagen, 1980). The *hflA* locus was later discovered to encode for a three-polypeptide protease, HflA, that cleaved the cII protein (Cheng et al., 1988). HflA, upon cleaving cII, would therefore induce lysis over lysogeny. Interestingly, experiments performed by Cheng *et al.* did not show expression of the 50 kDa polypeptide corresponding to HflX; rather, proteins HflK, HflK', and HflC were copurified and resulted in proteolysis of cII (Cheng et al., 1988). In 1993, Noble *et al.* determined the nucleotide sequence of much of the *hflA* locus, and determined that the corresponding amino acid sequence of *hflX* contained three sequence motifs (the P-loop, GxxD, and the NKxD specificity motif) associated with the GTPase superfamily (Noble et al., 1993).

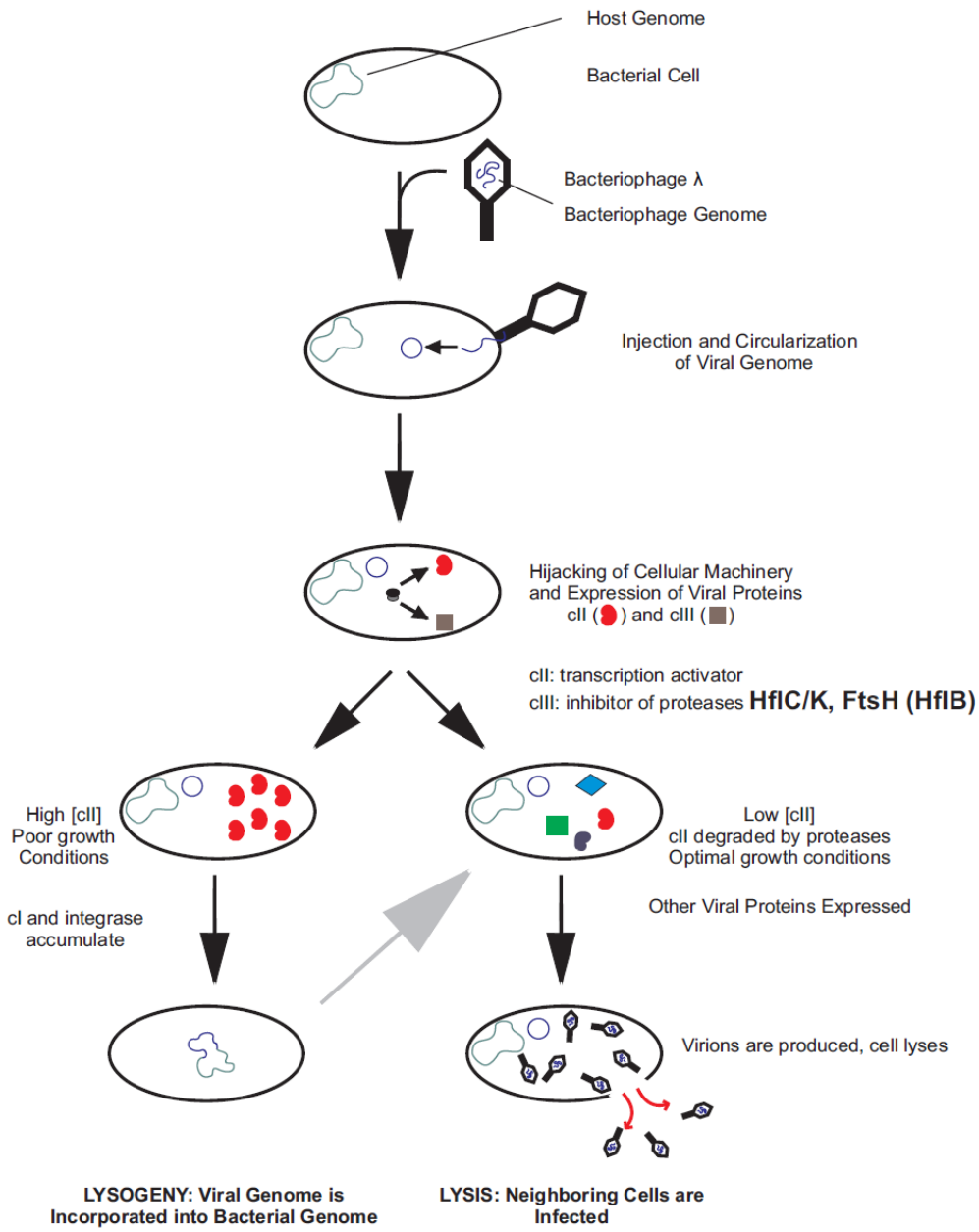

Figure 2.10. Lysis/lysogeny Decision of Bacteriophage λ upon Infection of a Bacterial Cell.

After injection and circularization of the viral genome, viral proteins are expressed upon transcription of viral mRNA using the host cell machinery. Under optimal conditions, viral protein cII is degraded by HflC/K, resulting in expression of viral proteins, virion production, and lysis. Under suboptimal conditions, cII is not degraded; cI and viral integrase accumulate, and the viral genome is integrated into the host genome. Viral gene expression remains dormant until the host cell encounters more favourable conditions. Adapted from reference (Herskowitz and Hagen, 1980).

Not until 2008, when Polkinghorne *et al.* published results implicating HflX as a 50S ribosomal subunit associated factor was HflX linked to protein synthesis (Polkinghorne et al., 2008). *C. pneumonia* HflX heterologously expressed in *E. coli* was shown to exhibit a slow intrinsic GTPase activity that was inhibited by mutations to the P-loop, G2, and G4 motifs, thus confirming HflX as a GTPase (Polkinghorne et al., 2008). Competition assays with adenine, uridine, and cytidine nucleotides showed no inhibition of GTPase activity whereas incubation with non-radioactively labeled guanine nucleotides strongly inhibited GTP hydrolysis; thus, HflX was deemed to be guanine nucleotide-specific (Polkinghorne *et al.*). Co-localization experiments demonstrated that HflX co-localized with Chlamydial membranes in infected eukaryotic cells (Polkinghorne et al., 2008). Ultracentrifugation assays demonstrated that HflX associated with 50S ribosomal subunits, and that the full length protein was required for specificity, as N- or C-terminal truncations were unable to associate with ribosomal particles (Polkinghorne et al., 2008).

E. coli HflX was recently found to copurify with RNA species similar in size to 1S and 23S rRNA, an interaction that could be reconstituted independent of nucleotide phosphorylation state (Jain et al., 2009). Furthermore, *E. coli* HflX was found to associate with the 50S ribosomal subunit, confirming the study by Polkinghorne *et al* (Jain et al., 2009). This interaction was found to occur in the presence of purine nucleotides though not in the *apo* state of HflX, though this interaction required the full length protein (Jain et al., 2009). HflX from *E. coli*, in contrast to the *C. pneumonia*, counterpart, possessed ATPase activity in addition to GTPase activity, and showed an 8-fold stimulation in GTPase activity in the presence of 50S ribosomal subunits (Dutta et al., 2009; Jain et al., 2009). However, HflX was found not to associate with either of

the HflC or HflK proteins, nor did it have any effect on lysis and lysogeny, contradicting previous research (Dutta et al., 2009).

Whereas the G-domain of HflX bears significant similarity to other canonical G-domains, the structure of the unique N-terminal domain remained unknown until the structure of HflX from the hyperthermophillic archaeon *Solfalobus solfataricus* was elucidated in 2009 (Wu et al., 2010). This unique, glycine-rich "HflX domain" was found to consist of two subdomains: a four-stranded parallel β-sheet flanked by a pair of α-helices, followed by an anti-parallel coiled coil consisting of two longer α-helices connected to the G-domain (20 amino acids linking the two helices are unstructured; another 12 linker amino acids remain disordered in the solved *apo* and GDP-bound structures linking the "HflX" and G-domains). Interestingly, the full-length was found to have a lower GTPase activity compared to the truncated G-domain alone, suggesting that the "HflX domain" functions as a negative regulator of the G-domain (Huang et al., 2010a; Wu et al., 2010).

In early 2011, a further study by Blombach *et al.* (Blombach et al., 2011) on *S. solfataricus* HflX indicated that, based on ultracentrifugation assays, HflX interacts only with the 50S subunit, in the nucleotide free *apo* state. This interaction was proposed to be weaker than either the GDP or the GDPNP bound forms; a heteronuclear ^{15}N-^{1}H NMR experiment revealed that the NMR spectra of isotopically labeled HflX broadened significantly in the presence of 50S subunits and GTP, which was not observed in the absence of nucleotide (Blombach et al., 2011). This study also indicated that a number of additional resonances, likely from ribosomal protein L12, arose upon binding of isotopically labeled HflX (Blombach et al., 2011). However, experiments along the same lines with EF-G indicated that resonances from L12 are broadened

beyond detection, suggesting a different interaction surface for the two factors (Blombach et al., 2011; Christodoulou et al., 2004).

3. Nucleotide Binding and Hydrolysis Properties of HflX

Reprinted with permission from

"Toward Understanding the Function of the Universally Conserved GTPase HflX from *Escherichia coli*: A Kinetic Approach"

Michael J. Shields[†], Jeffrey J. Fischer[†], and Hans-Joachim Wieden

Biochemistry 2009; 48 (45): 10793-10802

[†] Authors contributed equally to this work.

3.1 Introduction

The GTPases of the P-loop family are highly conserved proteins that function as molecular switches, modulating a wide variety of cellular processes in response to conformational changes induced by hydrolysis of GTP. Structurally, these proteins contain the α/β G-domain, consisting of the following conserved sequence motifs (Figure 3.1): the G1 motif (or P-loop), consensus $GX_4GK(S/T)$, which is responsible for interacting with the α- and β-phosphates of nucleotide di- and tri-phosphates; the G2 variable effector loop (DX_nT); the G3 motif (DX_2G), which interacts with the γ-phosphate of nucleotide tri-phosphates; and the G4 motif (NKXD), which conveys specificity for guanine nucleotides through hydrogen bonding to the base (Bourne et al., 1991).

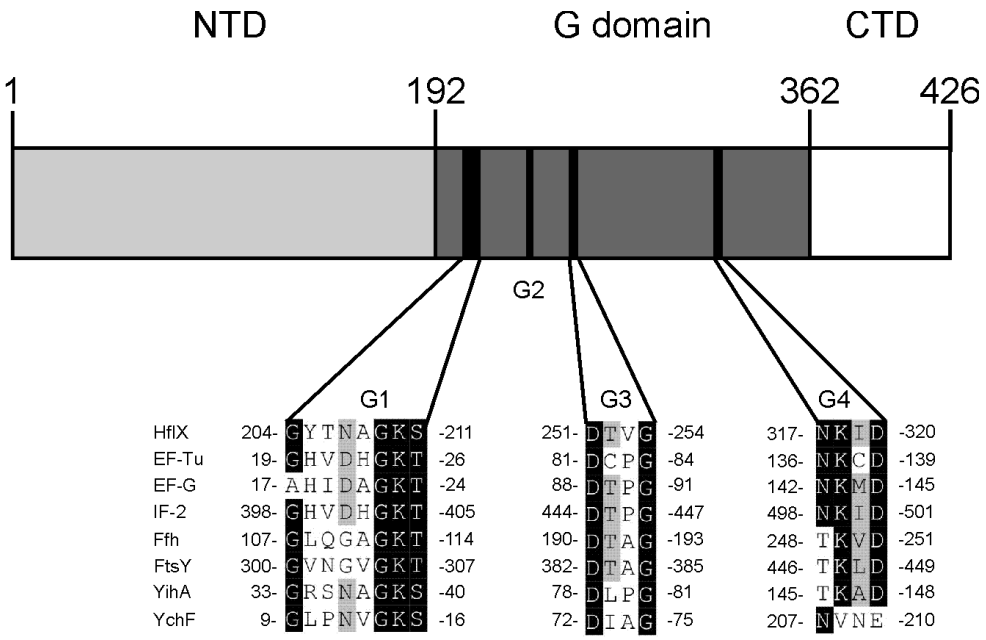

Figure 3.1. Structural Features of HflX.

The protein consists of 3 domains; an N-terminal domain (light grey), a central G domain (dark grey), and a short C-terminal domain (white). The G1, G3, and G4 motifs are conserved with other members of the universally conserved GTPases (black).

Guanine nucleotide binding proteins exist in three different conformations: the transient *apo* state can bind to either GTP or GDP under cellular concentrations of guanine nucleotides. Binding to GTP causes the protein to adopt a functional GTP-bound "active" state (Bourne et al., 1991). Upon hydrolysis of GTP, the protein reverts to its "inactive", GDP-bound state. GDP then dissociates, and the cycle continues. The conversions between these states are often catalyzed by regulatory proteins, which affect the kinetics of the interaction between the GTPase and guanine nucleotides. These regulators include guanine nucleotide exchange factors (GEFs), which catalyze the release of bound GDP, which in turn promotes GTP binding; GTPase activating proteins (GAPs), which stimulate the low intrinsic GTPase activity of the protein; and guanine nucleotide dissociation inhibitors (GDIs), associated with regulating members of the small G-protein superfamily, such as Rab and Rho in eukaryotes (Dovas and Couchman, 2005; Seabra

and Wasmeier, 2004; Siderovski and Willard, 2005), which inhibit nucleotide dissociation as a regulatory mechanism.

A core group of 8 universally conserved GTPases found in all domains of life has been identified and includes elongation factors (EFs) Tu and G, initiation factor (IF) 2, protein secretion factors Ffh and FtsY, and the relatively poorly characterized proteins YihA, YchF, and HflX (Caldon and March, 2003). Additional GTPases, conserved in prokaryotes and eukaryotes but not archaea, include Obg, EngA, and Era (Caldon and March, 2003). HflX, a member of the Obg-HflX superfamily, was initially linked to a role in determining the lysis-lysogeny decision of bacteria infected with bacteriophage lambda (Banuett and Herskowitz, 1987; Noble et al., 1993). However, recent data has shown that HflX from *Chlamydophila pneumonia* possesses a slow intrinsic GTPase activity and co-fractionates with *Escherichia coli* 50S ribosomal subunits, suggesting the protein may have a role in protein synthesis (Polkinghorne et al., 2008). *E. coli* HflX has been shown to possess both GTPase and ATPase activity; surprisingly, only the GTPase activity was shown to be stimulated by the 50S ribosomal subunit (Jain et al., 2009). Thus, HflX represents the second member of the Obg-HflX superfamily after YchF which demonstrates both GTPase and ATPase activity (Gradia et al., 2009; Koller-Eichhorn et al., 2007), despite the presence of the G4 specificity motif. Additionally, HflX interacts with both 16S and 23S rRNA in a nucleotide-dependent manner, as shown by gel shift assays (Jain et al., 2009). Recently, Dutta and colleagues confirmed that HflX binds and hydrolyzes both purine nucleotides, and also discounted suggested roles for HflX in the bacterial lysis/lysogeny decision and transposition (Dutta et al., 2009). However, no detailed information about the kinetic parameters governing these interactions is available to date, information pivotal to unraveling the functional mechanism of HflX action.

In this chapter, the detailed analysis of the purine nucleotide binding properties of HflX as studied by equilibrium and pre-steady state fluorescence techniques are reported for the first time. This confirms that HflX can bind to both adenine and guanine nucleotides, with a preference for guanine nucleotides. Using fluorescent analogs of guanine nucleotides (mant-GDP and mant-GTP), the elemental rate constants governing the interaction between HflX and the respective mant-guanine nucleotides were determined using the stopped-flow technique. Based on this data, appropriate conditions to study the NTPase activity of HflX were established. Under these optimized conditions, the NTPase activity of HflX is not only stimulated by 50S ribosomal subunits, but also to a similar extent by empty 70S ribosomes as well as ribosome complexes containing the synthetic mRNA analog poly(U) and deacylated $tRNA^{Phe}$ in the ribosomal P-site. Although an interaction between 16S / 23S rRNA and HflX has been reported by Jain and colleagues (Jain et al., 2009), the NTPase activity of HflX is not significantly stimulated by 30S ribosomal subunits. Based on this pre-steady state analysis and nucleotide hydrolysis data, a minimal kinetic scheme for HflX, with respect to the GTPase cycle as described by Bourne and colleagues (Bourne et al., 1991), is presented. Furthermore, the 70S ribosome stimulated GTPase activity is inhibited by the antibiotic chloramphenicol, but not by kanamycin. Chloramphenicol binds to the 50S ribosomal subunit at 23S rRNA bases A2451 and A2452, near the peptidyl transferase centre (Schlunzen et al., 2001), while kanamycin interacts at a site common to aminoglycoside antibiotics on the 30S ribosomal subunit at 16S rRNA bases A1408, G1419, and G1494, near the mRNA decoding centre on the 70S ribosome (Jerinic and Joseph, 2000; Moazed and Noller, 1987; Woodcock et al., 1991).

3.2 Experimental Procedures

3.2.1 Materials

All chemicals were obtained from VWR, Sigma, or Invitrogen, unless otherwise specified. Restriction enzymes were from Fermentas; all other enzymes were purchased as described in the following sections. PCR primers, nucleotides, and mant-nucleotides were purchased from Invitrogen (mant-nucleotides ≥ 94% purity based on manufacturers specifications). Radiochemicals were purchased from Perkin-Elmer. Small-scale plasmid preparations were performed according to the manufacturer's specifications (EZ spin column plasmid DNA kit, BioBasic). Antibiotics were from BioBasic.

3.2.2 Molecular Biology

Open reading frame *hflX* was PCR amplified from *E. coli* genomic DNA in a reaction catalyzed by Phusion polymerase (Finnzymes) using primers 5'- CTA TTT AAG AGG GGT TAT ACA TAT GTT - 3' and 5' - AAG CTT CGC CGT TAG ATC AGG TA - 3', where underlined nucleotides respectively denote *Nde*I and *Hind*III restriction sites engineered into the primers. 1.3 kb PCR product was ligated (T4 DNA ligase, Invitrogen) into *Sma*I digested pUC19. The resulting ligation mixture was transformed into sub-cloning efficiency *E. coli* DH5α cells (Invitrogen), which were then grown at 37°C on LB-agar plates supplemented with 50 μg/mL ampicillin and 50 μg/mL X-gal (Rose Scientific). Based on blue-white selection, and restriction analysis, cells containing recombinant plasmids were further propagated for plasmid isolation. The open reading frame was excised from pUC*hflX* using *Nde*I and *Hind*III restriction endonucleases and ligated into similarly digested pET28a to create plasmid pET*hflX*. *E. coli* strain DH5α was used for propagation. All recombinant plasmids were characterized by DNA

sequencing (Macrogen DNA Sequencing Services) to confirm sequence, gene orientation, and reading frame.

3.2.3 Expression and Detection

The plasmid pET*hflX* was transformed into *E. coli* strain BL21-DE3 (Invitrogen) for expression of recombinant His-tagged HflX. Cells were grown at 37 °C in LB media supplemented with 50 μg/mL kanamycin and induced at an OD_{600} ~ 0.6 with IPTG (final concentration of 1 mM). Cells were grown for an additional 3 h until the late logarithmic growth phase was reached, and harvested by centrifugation at 5 000 xg. Cells were flash frozen and stored at -80 °C prior to use.

To monitor protein expression levels, small culture samples were taken and lysed in 8 M urea. Cleared cell lysates were then analyzed using 12% SDS-PAGE at 200 V for 55 min. Gels were stained with Coomassie blue; all other SDS-PAGEs were performed in a similar manner.

3.2.4 Protein purification

Cells were resuspended in 7 mL/g cells buffer A (50 mM Tris-Cl pH 8.0 at 4 °C, 60 mM NH_4Cl, 300 mM KCl, 7 mM $MgCl_2$, 7 mM β-mercaptoethanol, 10 mM imidazole, 15% v/v glycerol, 50 μM GDP, 1 mM PMSF) and opened by incubation on ice with lysozyme (1 mg/mL final concentration) for 30 min. Sodium deoxycholate (12.5 mg/g cells) was added, followed by incubation on ice until the viscosity of the solution increased. The solution was then sonicated until the viscosity of the solution decreased again. The solution was centrifuged for 30 min at 3 000 xg (4 °C) to remove cell debris. The supernatant was further centrifuged for 45 min at 30 000 xg (4 °C) to obtain cleared cell lysate.

The resulting cleared lysate was applied to a 10 mL Ni^{2+} sepharose column (GE Healthcare). The column was washed with 50 column volumes buffer A, followed by a similar wash with

buffer B (buffer A with 20 mM imidazole, lacking GDP). Recombinant His-tagged HflX was eluted from the column in several steps (90% column volume each) using buffer E (buffer A with 300 mM imidazole, lacking GDP). Fractions containing HflX were pooled and concentrated using a Vivaspin 20 (10 000 MWCO, Sartorius). The protein was further purified by size exclusion chromatography using Superdex-75 (XK26/100 column, GE Healthcare) equilibrated in buffer C (50 mM Tris-Cl pH 7.5 at 4 °C, 70 mM NH_4Cl, 300 mM KCl, 7 mM $MgCl_2$). Fractions containing pure HflX were pooled and concentrated; protein concentration was determined photometrically at 280 nm using a molar extinction coefficient of 32 555 $M^{-1}cm^{-1}$ (calculated using the software ProtParam (Gasteiger et al., 2005)) and using the BioRad microassay. Protein samples were aliquoted, flash frozen, and stored at -80 °C prior to use.

3.2.5 Purification of ribosomes and complex formation

Vacant ribosomes were purified from *E. coli* MRE600 cells essentially as described in (Rodnina et al., 1994), but using a Ti 45 rotor rather than a Ti 50.2 rotor. Ribosomal complexes were programmed with poly(U) mRNA and P-site $tRNA^{Phe}$ (both from Sigma) similarly to previous literature (Watanabe, 1972). Briefly, complexes were formed by incubating 70S ribosomes (60 pmol) with 1.3 molar excess of $tRNA^{Phe}$ and 1 mg/mL poly(U) (determined by absorbance at 260 nm) in buffer $TAKM_7$ (50 mM Tris-Cl pH 7.5 at room temperature, 70 mM NH_4Cl, 30 mM KCl, 7 mM $MgCl_2$) at 37 °C for 15 min.

3.2.6 Fluorescence techniques

To determine nucleotide binding affinities, fluorescence measurements were performed using a Varian Cary Eclipse Fluorescence Spectrophotometer. The intrinsic tryptophan fluorescence of HflX (4 residues) was excited at 280 nm in a 0.3 x 0.3 cm quartz cuvette (Starna) at room temperature. Fluorescence measurements were carried out using 1 μM HflX in buffer $TAKM_7$

and increasing amounts of the respective nucleotide were added. Fluorescence was monitored from 305-450 nm through 5 nm slits for titrations with adenine and guanine nucleotides, and from 305-605 nm for titrations with respective mant-nucleotides. Changes in fluorescence were corrected for dilution and plotted as a function of nucleotide concentration at 338 nm for nucleotide and mant-nucleotide titrations. Fluorescence signals due to the presence of protein and nucleotide individually were subtracted from the overall fluorescence of the system. Fluorescence changes (ΔFl) plotted against nucleotide concentration ([nt]) were fitted to a quadratic function (Equation 1), with respect to the initial (Fl_0) and maximum (Fl_{max}) fluorescence to determine the dissociation constant (K_D) for each nucleotide or fluorescent derivative using the software TableCurve (Jandel Scientific). Additional variables for total protein concentration ([P]) and signal amplitude ($B = Fl_{max} - Fl_0$) were accounted for (Wilden et al., 2006b). Fluorescence signals were normalized prior to fitting.

$$\Delta Fl = 0.5(B/[P])(K_D + [P] + [nt] - ((K_D + [P] + [nt]^2 - 4[P][nt])^{1/2}) \quad \text{(Eq. 1)}$$

The pre-steady state kinetics of mant-nucleotide dissociation and association were determined using a KinTek SF-2004 Stopped-flow apparatus. Rate constants for the bimolecular association of mant-GTP and mant-GDP (k_1 and k_3) were determined by rapidly mixing 25 μL HflX (2 μM, nucleotide free) with 25 μL of varying concentrations of mant-nucleotides at 20 °C in $TAKM_7$. Tryptophan residues were excited at 280 nm and fluorescence emission from the mant group was monitored through LG-400-F cutoff filters (NewPort). As only single-exponential time courses were observed, the data were treated on the basis of a one-step binding model, HflX + mant-nt ↔ HflX•mant-nt, and analyzed by exponential fitting (equation 2; with the characteristic

apparent rate constant k_{app}, A for signal amplitude, Fl for the fluorescence at time t, and Fl_∞ for the final fluorescence signal) to determine the value of k_{app} for each titration point.

$$Fl = Fl_\infty + A\exp(-k_{app}t) \quad \text{(Eq. 2)}$$

The obtained apparent rate constants were plotted as a function of nucleotide concentration; the slope of this function provided the association rate constants (k_1 and k_3). The y-axis intercept provided estimated k_{-1} and k_{-3} for mant-GTP and mant-GDP dissociation respectively.

To determine the rate constants for dissociation of mant-GTP and mant-GTP (k_{-1} and k_{-3} respectively), 1 μM HflX was incubated with 30 μM mant-nucleotide for 15 min at 37 °C (in $TAKM_7$). Experiments were then performed by rapidly mixing 25 μL of HflX•mant-nucleotide with 25 μL of 300 μM nucleotide (no fluorescent label) at 20 °C in $TAKM_7$. Again, only single-exponential fluorescence time courses were observed and the resulting fluorescence signal was therefore fitted with an exponential decay function (Equation 2, with the characteristic apparent rate constant k_{app} corresponding to the rate of nucleotide dissociation). Rate constants for mant-nucleotide dissociation from HflX were also calculated from the respective K_D values and k_1/k_3 rate constants for comparison. Similar experiments were performed for mant-adenine nucleotides.

3.2.7 Nucleotide hydrolysis assays

Hydrolysis of GTP and ATP by HflX was monitored by determining the release of $^{32}P_i$ from [γ-^{32}P]GTP and [γ-^{32}P]ATP. Nucleotide charging solution (radioactive nucleotide at ~ 100 dpm/pmol, 0.25 μg/μL pyruvate kinase (PK), 3 mM phosphoenolpyruvate (PEP)) and HflX-charging solution (15 μM HflX, 0.25 μg/μL PK, 3 mM PEP) were incubated at 37 ºC for 15 min to catalyze nucleotide triphosphate formation from the diphosphate form. To ensure nucleotide di-phosphate inhibition of multiple turnover experiments was negligible, radioactive nucleotide

was diluted with non-labeled nucleotide tri-phosphates (final amounts of nucleotide, 7500 pmol) Hydrolysis assays were carried out in buffer $TAKM_7$. Reaction volumes were 60 μL and contained 1 μM HflX, 125 μM radiolabeled nucleotide solution, and 1 μM 70S ribosomes, 50S subunits, or 0.5 μM 30S ribosomal subunits. For antibiotic titrations, the appropriate concentration of antibiotic was also added. 5 μL samples were removed at different time points and quenched in 50 μL 1M $HClO_4$ with 3 mM K_2HPO_4.

Following the addition of 300 μL 20 mM Na_2MoO_4 and 400 μL isopropyl acetate, samples were mixed for ~30 s and centrifuged at 15 800 xg for 5 min. $^{32}P_i$ was extracted as a phosphate-molybdate complex in the organic phase, added to 2 mL of EcoLite scintillation cocktail (EcoLite, MP Biomedical), and counted in a Perkin-Elmer Tri-Carb 2800TR liquid scintillation analyzer. Background radioactivity due to NTP hydrolysis by ribosomes or self hydrolysis was subtracted; concentration of $^{32}P_i$ released was calculated and plotted. In the presence of antibiotics, the final GTPase activity was normalized to 100 % after 90 min.

The apparent rate of nucleotide hydrolysis by HflX, alone or in the presence of ribosomes and antibiotics, was calculated from fitting the initial linear phase of multiple turnover experiments to a linear equation, where the slope of the fit is the apparent rate of nucleotide hydrolysis, k_{app}.

3.3 Results

3.3.1 Equilibrium analysis of HflX interacting with nucleotides

The overexpression of HflX and the final purified protein preparation are shown in Figure 3.2. The final purity of HflX after Ni^{2+} sepharose chromatography and size exclusion chromatography is estimated as greater than 99% based on SDS-PAGE analysis.

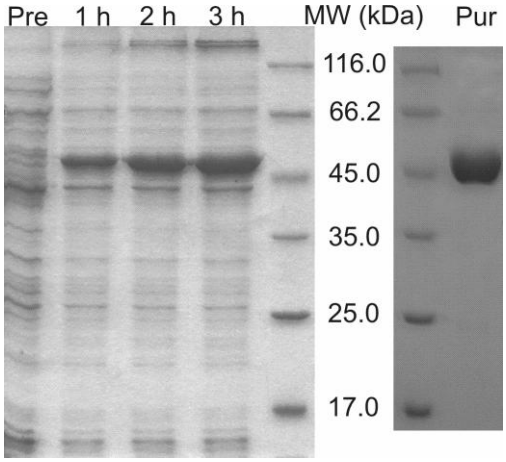

Figure 3.2. Overexpression and Purification of HflX.

Samples were taken pre and 1-3 h post IPTG induction. A final sample of purified HflX (Pur) is shown, with purity estimated as greater than 99%. Molecular masses (MW) are indicated.

Jain and colleagues generated truncations of HflX at the proposed domain junctions based on analysis of the proteins primary sequence, and demonstrated that all three domains are required for association with the 50S ribosomal subunit (Jain et al., 2009). Within the G domain, the essential elements required for nucleotide binding and specificity are indeed conserved among the universally conserved GTPases, with the exception of the G4 motif of YchF. Despite the conservation of these motifs, previous studies on HflX's purine nucleotide specificity are contradictary. Results reported by Polkinghorne *et al.* based on competition assays support the annotation that HflX from *C. pneumoniae* is specific for guanine nucleotides (Polkinghorne et al., 2008) while results by Jain *et al.* and Dutta *et al.* indicate that HflX from *E. coli* binds and hydrolyzes ATP and GTP (Dutta et al., 2009; Jain et al., 2009). Since the experimental approaches used in these previous studies did not take into account a wide range of affinities for the different nucleotides, they might not have been sensitive enough to detect the interaction. Therefore, a quantitative kinetic description of the interaction with the two purine nucleotides is

crucial for understanding their functional importance. Equilibrium fluorescence spectroscopy measurements were utilized to study the nucleotide binding properties of purified *E. coli* HflX (Figure 3.3). Guanine and adenine di- and tri-phosphates were added into HflX protein solutions and changes in tryptophan fluorescence were monitored. The addition of increasing amounts of guanine nucleotides resulted in a decrease in tryptophan fluorescence ($\lambda_{emission,\ max}$ = ~ 338 nm, Figure 3.3A and 3.3B). Similar results were obtained for titrations of the protein with adenine nucleotides (data not shown). From these titrations the equilibrium dissociation constant (K_D) was determined by fitting the concentration dependence of tryptophan fluorescence to a quadratic function (Experimental Procedures). These results not only reveal a preference for nucleotide di-phosphates (K_D values of 3.2 ± 0.4 μM and 12 ± 1 μM for GDP and ADP respectively) compared to nucleotide tri-phosphates (K_D values of 187 ± 7 μM and 362 ± 20 μM for GTP and ATP respectively), but also a slightly higher affinity for guanine nucleotides.

In order to improve the signal-to-noise ratio for the pre-steady state analysis, fluorescence resonance energy transfer (FRET) between the tryptophan residues in HflX and the respective mant-labeled nucleotides was utilized. Prior to a pre-steady state analysis, the equilibrium binding constants of HflX to several mant-nucleotide derivatives, a modification that has previously been successfully used in the pre-steady state analysis of other G-proteins such as EF-Tu (Wieden et al., 2002), were determined. Upon excitation of tryptophan residues in HflX, FRET to the mant group of mant-GTP and GDP was observed, as reflected by a decrease in tryptophan fluorescence (Figure 3.3C and 3.3D) and an increase in mant fluorescence ($\lambda_{emission,\ max}$ = ~ 450 nm). Changes in the relative fluorescence at the tryptophan emission wavelength (338 nm) as a function of mant-nucleotide concentration revealed comparable, but slightly higher, binding affinities for mant-nucleotides when compared to the non-fluorescent nucleotides

(0.8 ± 0.1 μM and 48 ± 4 μM for mant-GDP and mant-GTP respectively). Similar trends were observed for titrations of HflX with mant-adenine nucleotides (8.1 ± 1.9 μM and 87 ± 19 μM for mant-ADP and mant-ATP respectively). However, in these titrations the observed change in mant fluorescence was significantly smaller when compared to the guanine nucleotide derivatives (data not shown). The equilibrium binding constants for the respective nucleotides are summarized in Table 3.1 and are consistent with those reported for the other universally conserved GTPases (Table 3.2).

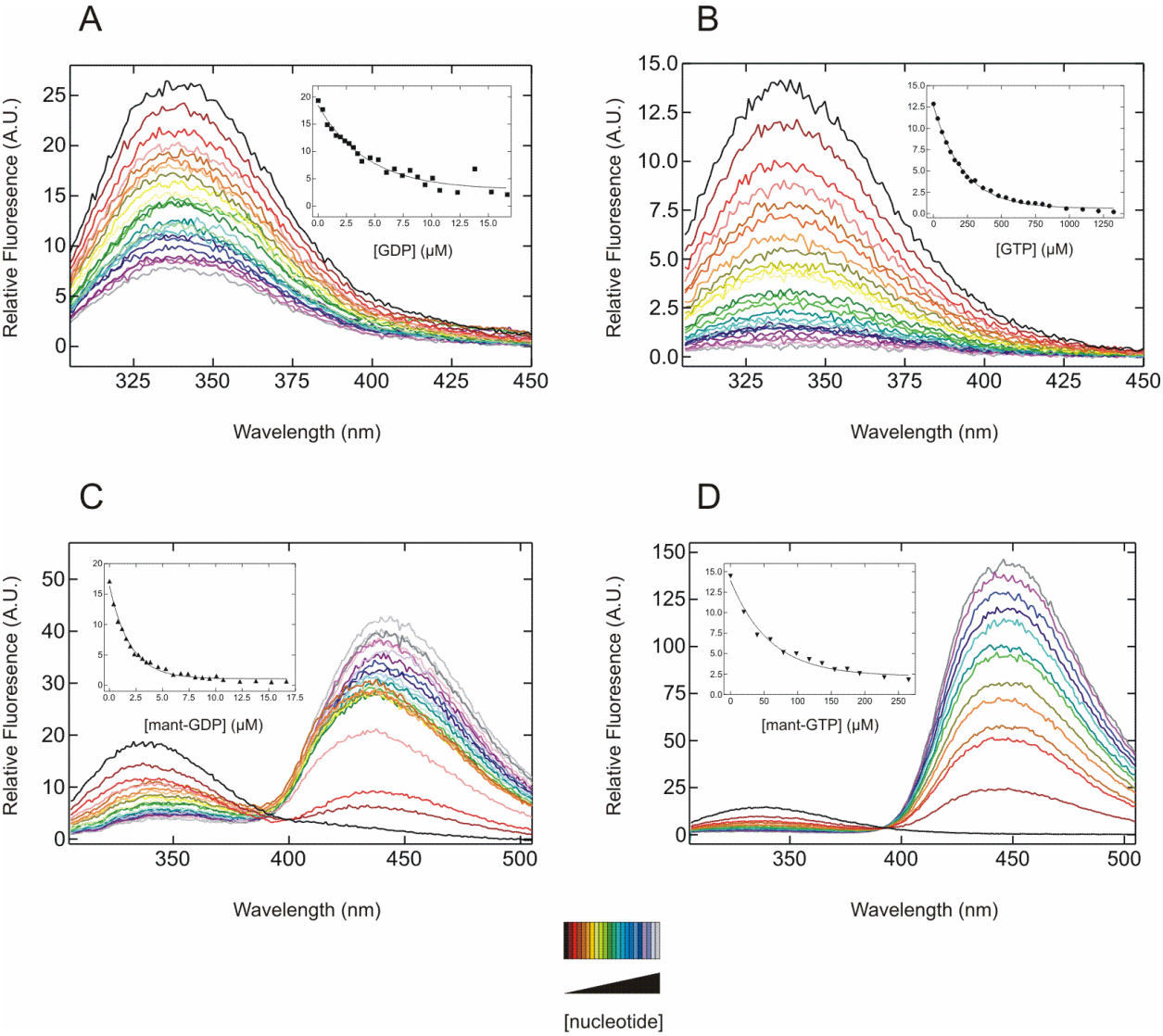

Figure 3.3. Equilibrium Fluorescence Titration of HflX with Guanine Nucleotides.

HflX was titrated with increasing amounts of A) GDP, B) GTP, C) mant-GDP, and D) mant-GTP according to the color scheme provided (bottom). Insets show the nucleotide concentration dependence of the obtained tryptophan fluorescence signal (at 338 nm) used to determine K_D values.

Table 3.1. Equilibrium Dissociation Constants Governing the Interaction between HflX and Purine Nucleotides.

Nucleotide	Parameter, signal	Description	Value
GTP	K_D, HflX intrinsic tryptophan	Dissociation constant	187 ± 7 μM
GDP	K_D, HflX intrinsic tryptophan	Dissociation constant	3.2 ± 0.4 μM
mant-GTP	K_D, HflX intrinsic tryptophan	Dissociation constant	48 ± 4 μM
mant-GTP	K_D, calculated from k_{-1}/ k_1	Comparison to $K_{D\ mant\text{-}GTP}$	30 ± 1 μM
mant-GDP	K_D, HflX intrinsic tryptophan	Dissociation constant	0.8 ± 0.1 μM
mant-GDP	K_D, calculated from k_{-3}/ k_3	Comparison to $K_{D\ mant\text{-}GDP}$	2.7 ± 0.2 μM
ATP	K_D, HflX intrinsic tryptophan	Dissociation constant	362 ± 20 μM
ADP	K_D, HflX intrinsic tryptophan	Dissociation constant	12 ± 1 μM
mant-ATP	K_D, HflX intrinsic tryptophan	Dissociation constant	87 ± 19 μM
mant-ADP	K_D, HflX intrinsic tryptophan	Dissociation constant	8.1 ± 1.9 μM

Table 3.2. Equilibrium Dissociation Constants Governing the Interaction between GTP/GDP and the Universally Conserved GTPases.

Classification	Protein	K_D, GTP	K_D, GDP	Ratio	Reference
Translation Factors	EF-Tu	60 nM	1 nM	60	(Gromadski et al., 2002)
	EF-G	7 μM	17 μM	0.41	(Wilden et al., 2006b)
	IF-2	140 μM	13 μM	11	(Pon et al., 1985b)
Protein Secretion Factors	FtsY	14 μM	26 μM	0.54	(Peluso et al., 2001)
	FfH	0.3 μM	0.2 μM	1.5	(Peluso et al., 2001)
Era Group	YihA	3 μM	27 μM	0.11	(Lehoux et al., 2003)
Obg Group	YchF	5 μM	~ 15 μM *	0.33	(Teplyakov et al., 2003)
	HflX	187 μM	3.2 μM	58	This study

* A. Altamirano, Personal Communication

3.3.2 Pre-steady state kinetic analysis of HflX interacting with mant-nucleotides

Based on the GTPase cycle outlined by Bourne (Bourne et al., 1991), and the observation that HflX seems to have a preference for guanine nucleotides, a minimal kinetic scheme for the interaction of HflX with guanine nucleotides is presented (Figure 3.4). To study the mechanism of nucleotide interaction with HflX, a rapid kinetics analysis using the stopped-flow technique observing FRET between HflX tryptophan residues and the mant group of mant-nucleotides over time was performed. This approach has been successfully used previously to study nucleotide binding properties of a variety of other GTPases such as EF-Tu and IF-2 (Gromadski et al., 2002; Milon et al., 2006; Wieden et al., 2002). Upon rapid mixing of varying concentrations of mant-GDP with HflX, a fast increase in fluorescence of the mant group due to FRET, reflecting the binding of mant-GDP, was observed that was dependent on the nucleotide concentration (Figure

3.5A). As only single exponential time courses were observed, these data were treated as a one-step binding model, similar to that of EF-Tu binding to mant nucleotides (Wieden et al., 2002). The bimolecular association constant for binding of mant-GDP to HflX (k_3) was obtained from the slope of the linear concentration dependence of k_{app} (Figure 3.5B), and was determined to be $9.7 \pm 0.6 \times 10^5$ $M^{-1}s^{-1}$. A similar experiment examining the interaction between mant-GTP and HflX yielded a value of $k_1 = 6.4 \pm 0.3 \times 10^4$ $M^{-1}s^{-1}$.

To measure the rate of nucleotide dissociation (k_{-3}), HflX was incubated with a 30 fold excess of mant-GDP; the HflX•mant-GDP complex was then rapidly mixed with an excess of non-fluorescent GDP (300-fold excess). The change in fluorescence reflecting the mant-GDP dissociation was monitored (Figure 3.5C) and k_{-3} was determined by fitting the observed fluorescence change to a single-phase exponential function. The value for k_{-3} was determined to be 2.6 ± 0.2 s^{-1}. This value is in agreement with the y-axis intercept of the concentration dependence of the association rate (k_{app}) used to determine k_3 ($k_{-3} = 2.2 \pm 0.3$ s^{-1}). Due to the low intrinsic NTPase activity of HflX, k_{-1} was determined in a similar fashion. Values for k_{-1} were determined as 2.1 ± 0.1 s^{-1} from dissociation experiments and 1.9 ± 0.1 s^{-1} from the plot of k_{app} dependence of k_1. A summary of all determined rate constants is given in Table 3.3.

Interestingly, when similar experiments were performed with mant-derivatives of adenine nucleotides, no changes in the mant fluorescence signal were observed (data not shown). This was surprising since binding data demonstrated FRET between the intrinsic tryptophan residues of HflX and the mant group of mant-adenine nucleotides. However, the mant-fluorescence signal was significantly smaller for the mant-adenine nucleotide titrations compared to the respective mant-guanine nucleotide titrations, and possibly too small to be detected in stopped-flow assays. Since FRET is very sensitive to variations in distance between the fluorescence donor and

acceptor dyes, these observations might reflect a slightly different position of the guanine compared to the adenine nucleotides relative to the donor tryptophan.

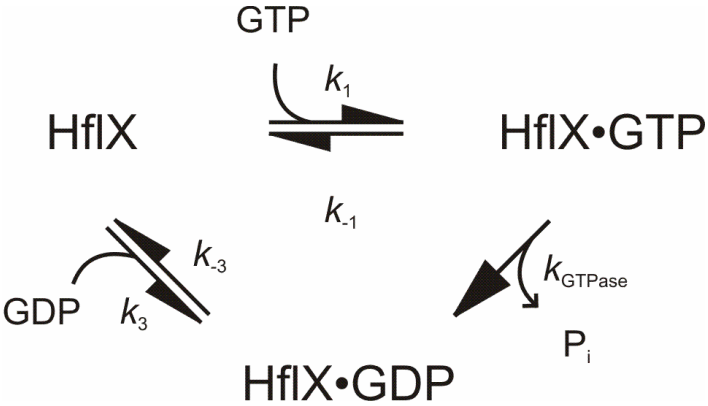

Figure 3.4. Minimal Kinetic Model for HflX.

A minimal proposed kinetic mechanism of the interaction between HflX and guanine nucleotides.

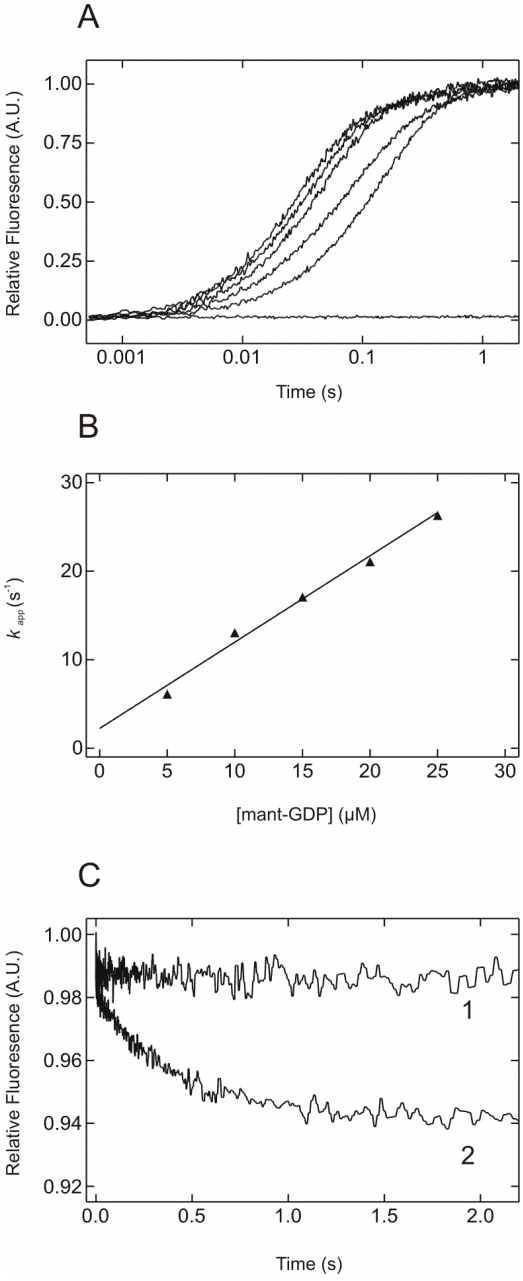

Figure 3.5. Rapid Kinetic Analysis of the Interaction of mant-GDP with HflX.

A) Time courses of mant-GDP binding to HflX measured by FRET. From *right to left*: 5, 10, 15, 20, and 25 μM mant-GDP, baseline (control without nucleotide). B) Concentration dependence of k_{app}. Values of k_{app} were calculated as described in experimental procedures; standard deviations range from 1.4% to 3.2%. From the slope of this plot, the association rate constant k_3 ($9.7 \pm 0.6 \times 10^5$ $M^{-1}s^{-1}$) was calculated. The y intercept corresponds to k_{-3} (2.2 ± 0.3 s^{-1}). C) Determination of the rate constant of mant-GDP dissociation k_{-3} from HflX. (1) Nucleotide free control and (2) dissociation of mant-GDP from HflX. All traces were normalized with respect to the initial fluorescence of the system.

Table 3.3. Pre-steady State Kinetics of mant-guanine Nucleotides Associating to and Dissociating from HflX.

Nucleotide	Parameter, signal	Description	Value
mant-GTP	k_1, FRET to mant group	mant-GTP association	$6.4 \pm 0.3 \times 10^4$ M^{-1} s^{-1}
mant-GTP	k_{-1}, FRET to mant group	mant-GTP dissociation	2.1 ± 0.1 s^{-1}
mant-GTP	k_{-1}, from k_{app} vs [mant-GTP] plots	mant-GTP dissociation	1.9 ± 0.1 s^{-1}
mant-GDP	k_3, FRET to mant group	mant-GDP association	$9.7 \pm 0.6 \times 10^5$ M^{-1} s^{-1}
mant-GDP	k_{-3}, FRET to mant group	mant-GDP dissociation	2.6 ± 0.2 s^{-1}
mant-GDP	k_{-3}, from k_{app} vs [mant-GTP] plots	mant-GDP dissociation	2.2 ± 0.3 s^{-1}

3.3.3 NTPase activity of HflX in the presence of ribosomes and ribosomal subunits

The GTPase activity of HflX was recently reported to be specifically stimulated by 50S ribosomal subunits (Jain et al., 2009). Here it is demonstrated that the intrinsic GTPase activity of HflX (Figure 3.6A) is very slow ($k_{GTPase} = 8.4 \pm 1.0 \times 10^{-4}$ μM s^{-1}) and can be stimulated ~ 1000 fold by 50S ribosomal subunits ($k_{GTPase,\ 50S} = 0.19 \pm 0.01$ μM s^{-1}) as well as by empty 70S ribosomal complexes ($k_{GTPase,\ 70S}$ 0.24 ± 0.01 μM s^{-1}). In an effort to elucidate the functional state in which HflX interacts with the ribosome, the GTPase activity of HflX was examined in the presence of ribosome complexes containing poly(U) as the message and $tRNA^{Phe}$ in the P site. Programming and P-site occupancy had little effect on the ribosome-stimulated GTPase activity of HflX (Figure 3.6, $k_{GTPase,\ p(U)\ 70S} = 0.17 \pm 0.01$ μM s^{-1}).

Surprisingly, previous studies indicate that although *E. coli* HflX is able to bind both purine nucleotides, only the GTP hydrolysis activity but not the ATP hydrolysis activity could be stimulated by 50S ribosomal subunits (Jain et al., 2009). This might be explained by the

significantly different affinities for the nucleotide di-phosphates and tri-phosphates (between 30 and 58 fold difference) determined in this study, i.e. the experimental conditions might favor binding of the di-phosphate being formed in the first round of catalysis, thereby preventing binding and hydrolysis of further tri-phosphates. To overcome this, pyruvate kinase and phosphoenolpyruvate were used to convert all nucleotide present into the tri-phosphate form. Based on the equilibrium dissociation constant of GTP (around 190 μM), the hydrolysis experiments were performed in the presence of 125 μM radiolabeled nucleotide, ensuring efficient binding to the enzyme. Using this optimized assay condition, both the HflX GTP and ATP hydrolysis activity can be stimulated by both 70S ribosomes and 50S ribosomal subunits. The observed stimulated multiple turnover ATP hydrolysis rates (Figure 3.6: $k_{ATPase,\ 70S}$ = 1.4 ± 0.4 x 10^{-2} μM s^{-1}; $k_{ATPase,\ 50S}$ = 2.3 ± 0.4 x 10^{-2} μM s^{-1}) are significantly slower compared to the respective GTPase activity ($k_{GTPase,\ 70S}$ 0.24 ± 0.01 μM s^{-1}; $k_{GTPase,\ 50S}$ = 0.19 ± 0.01 μM s^{-1}) of HflX, which is consistent with the lower affinity of HflX for ATP (2-3 times lower than GTP, Table 3.4).

3.3.4 Effect of translation-inhibiting antibiotics on the ribosome stimulated GTPase activity of HflX

In order to address the question, does HflX specifically interact with the 50S ribosomal subunit, the effect of two antibiotics that inhibit protein synthesis by binding to different subunits of the ribosome on the rate of ribosome stimulated GTP hydrolysis was examined. To this effect, the apparent rate of ribosome stimulated GTP hydrolysis by HflX was determined in the presence of increasing concentrations of chloramphenicol and kanamycin, which interact specifically with the 50S and 30S ribosomal subunit respectively. While kanamycin did not show any effect on the rate of GTP hydrolysis (Figure 3.7A), in the presence of chloramphenicol the

apparent rate of ribosome stimulated GTP hydrolysis by HflX decreased significantly with increasing concentration of the antibiotic (Figures 3.7B and 3.7C). Based on this effect, 50% inhibitory concentrations (IC_{50}) of chloramphenicol were calculated as 200 μM for both 70S ribosomes and 50S ribosomal subunits.

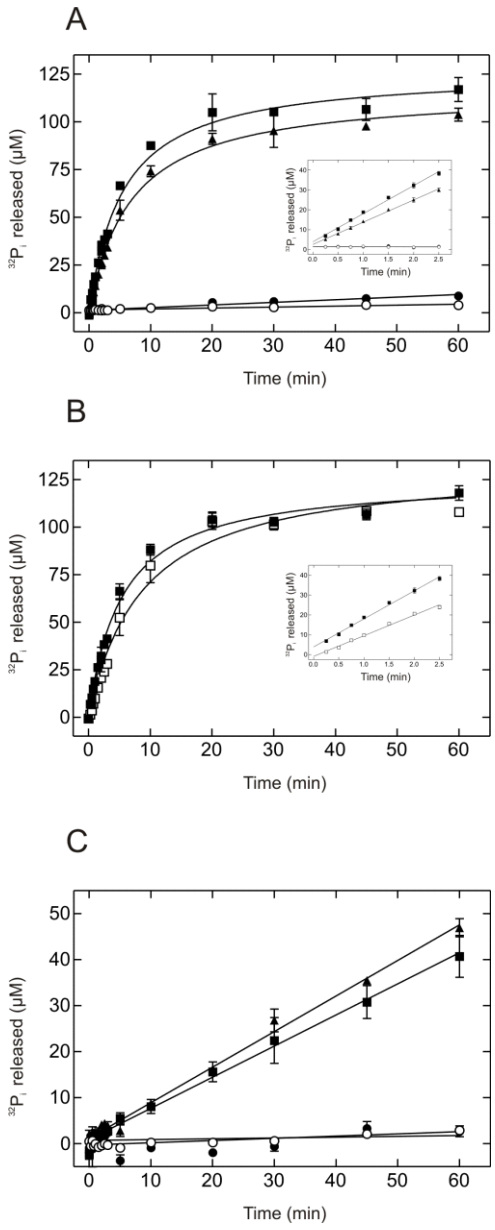

Figure 3.6. Ribosome-stimulated NTPase Activity of HflX.

(A) Time courses of GTP hydrolysis by HflX were obtained by extracting liberated $^{32}P_i$ and scintillation counting. The reaction was followed in the absence of ribosomes (open circles) or in the presence of 70S ribosomes (closed squares), 50S ribosomal subunits (closed triangles), and 30S ribosomal subunits (closed circles). The insert shows the initial hydrolysis of GTP. (B) Time courses of GTP hydrolysis by HflX in the presence of empty 70S ribosomes (closed squares) as well as ribosomes programmed with poly(U) as a mRNA message and the P-site occupied with $tRNA^{Phe}$ (open squares). Insert, same as in (A). (C) Time courses of ATP hydrolysis by HflX in the absence of ribosomes (open circles) or in the presence of 70S ribosomes (closed squares), 50S ribosomal subunits (closed triangles), and 30S ribosomal subunits (closed circles).

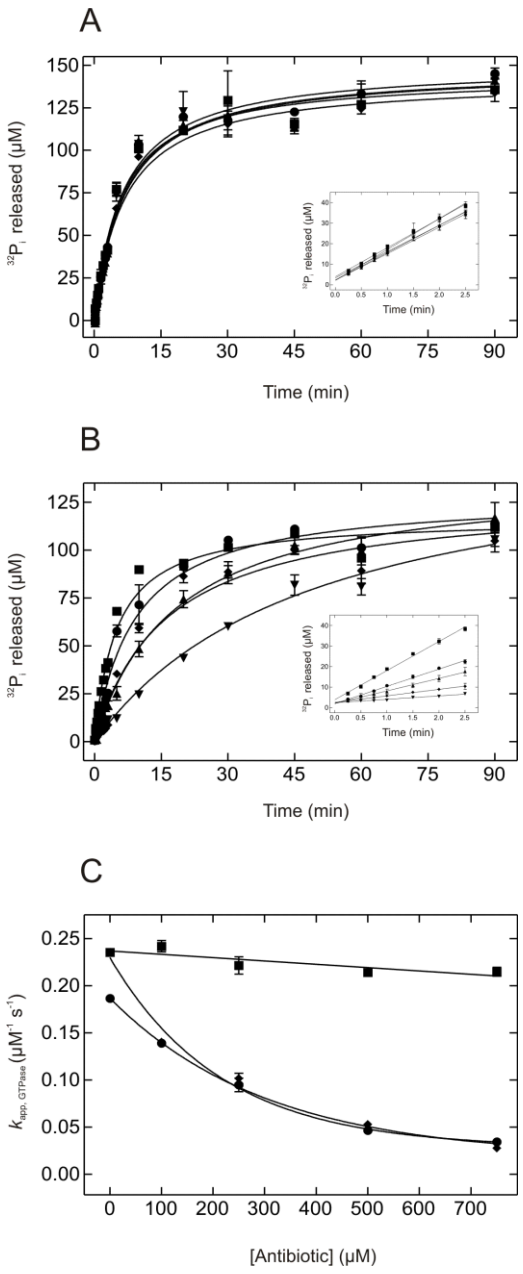

Figure 3.7 Inhibition of the Ribosome-stimulated GTPase Activity of HflX by Chloramphenicol.

Time courses of GTP hydrolysis in the presence of increasing amounts of kanamycin (A) and chloramphenicol (B). Inserts, the initial hydrolysis of GTP. Antibiotic concentrations: 0 μM, closed squares; 100 μM, closed circles; 250 μM, closed triangles; 500 μM, closed diamonds; 750 μM, reversed closed triangles. (C) Dependence of the apparent rate constant of GTP hydrolysis (k_{GTPase}) on the concentration of kanamycin (closed squares) and chloramphenicol (closed diamonds, 70S ribosomes; closed circles, 50S ribosomal subunits).

Table 3.4. Purine Nucleotide Hydrolysis Rates of HflX in the Presence of Ribosomal Particles.

Nucleotide	Parameter, signal	Description	Value ($\mu M\ s^{-1}$)
GTP	k_{GTPase}, hydrolysis of [γ-^{32}P]GTP	GTP hydrolysis	$8.4 \pm 0.1 \times 10^{-4}$
GTP	k_{GTPase}, hydrolysis of [γ-^{32}P]GTP	GTP hydrolysis + 70S	0.24 ± 0.01
GTP	k_{GTPase}, hydrolysis of [γ-^{32}P]GTP	GTP hydrolysis + programmed 70S	0.17 ± 0.01
GTP	k_{GTPase}, hydrolysis of [γ-^{32}P]GTP	GTP hydrolysis + 50S	0.19 ± 0.01
GTP	k_{GTPase}, hydrolysis of [γ-^{32}P]GTP	GTP hydrolysis + 30S	$2.3 \pm 0.2 \times 10^{-3}$
ATP	k_{ATPase}, hydrolysis of [γ-^{32}P]ATP	ATP hydrolysis	$8.0 \pm 1.6 \times 10^{-4}$
ATP	k_{ATPase}, hydrolysis of [γ-^{32}P]ATP	ATP hydrolysis + 70S	$1.4 \pm 0.4 \times 10^{-2}$
ATP	k_{ATPase}, hydrolysis of [γ-^{32}P]ATP	ATP hydrolysis + 50S	$2.3 \pm 0.4 \times 10^{-2}$
ATP	k_{ATPase}, hydrolysis of [γ-^{32}P]ATP	ATP hydrolysis + 30S	$3.8 \pm 3.2 \times 10^{-4}$

3.4 Discussion

HflX is a member of the Obg-HflX superfamily of conserved TRAFAC GTPases (Leipe et al., 2002). The members of this superfamily include Obg (also CtgA or YhbZ), YchF, and HflX (Caldon and March, 2003), and have been implicated in ribosome biogenesis and regulation of

translation. For example, Obg from *E. coli* and *Vibrio harveyi* has been shown to associate with the 50S ribosomal subunit, and has an essential role in its maturation (Jiang et al., 2006; Sikora et al., 2006). On the basis of the kinetic parameters reported in this study we are now making progress toward a detailed understanding of the molecular mechanism of HflX's function, one of the eight universally conserved GTPases found in all domains of life. HflX is particularly interesting since it represents the second member of these conserved GTPases, after YchF, that binds both purine nucleotides (Koller-Eichhorn et al., 2007). This is surprising, since the G4 motif (NKID) found in HflX from *E. coli* corresponds well with the consensus sequence NKXD motif determining nucleotide specificity in P-loop GTPases. In contrast, YchF from *E. coli* preferentially binds adenine nucleotides and contains an altered G4 sequence (NVNE), which, supported by the available X-ray structures, is likely to be responsible for the observed change in specificity. The equilibrium binding constants for GTP and ATP (187 μM and 362 μM respectively) reported here for HflX support the previously observed lack of purine nucleotide specificity (Dutta et al., 2009; Jain et al., 2009), but also show a slight preference for guanine nucleotides. Adenine nucleotides are in ~ 3 fold excess over guanine nucleotides *in vivo* and cellular concentrations of purine nucleotides are ~ 10 to 20 fold higher for the tri-phosphate form compared to the di-phosphate form (GTP = 0.9 – 1.7 mM / GDP = 0.1 – 0.2 mM and ATP = 2.5 – 3.6 mM / ADP = 0.13 – 0.25 mM) (Buckstein et al., 2008; Neuhard and Nygaard, 1987). Therefore, approximately 19% of HflX will be bound to the tri-phosphates (roughly equal amounts to GTP and ATP), 80% to the di-phosphates (70% to GDP and 10% to ADP) and only 1% in the nucleotide free form. This in turn also indicates that almost 80% of the cellular HflX will be found in the guanine nucleotide bound form, suggesting that HflX functions as a guanine nucleotide dependent enzyme *in vivo*. The observation that HflX is non-essential under optimal

growth conditions, based on the growth pattern of a *hflX* knockout strain (Baba et al., 2006), suggests to us a role for HflX under stress conditions instead, probably by regulating either ribosome biogenesis or protein synthesis. Determining the affinity of HflX for 70S ribosomal complexes and the 50S subunit with respect to its nucleotide bound state will provide valuable information on the association of the protein with the ribosome under *in vivo* conditions.

The presented pre-steady state kinetic analysis of HflX has revealed that the association rate constants for GTP and GDP binding (k_1 = 6.4 x 10^4 $M^{-1}s^{-1}$ and k_3 = 9.7 x 10^5 $M^{-1}s^{-1}$, respectively) are ~ 20 fold different. However, the dissociation rate constants of GTP and GDP dissociation are of the same order of magnitude (k_{-1} = 1.9 ± 0.1 s^{-1} and k_{-3}= 2.6 ± 0.2 s^{-1}), resulting in an approximately 20 fold lower affinity for the purine nucleotide tri-phosphate compared to the respective di-phosphate. These rapid nucleotide dissociation rates are also observed in Obg from *Caulobacter crescentus* (1.4 s^{-1} and 1.5 s^{-1} for mant-GDP and mant-GTP respectively (Lin et al., 1999)) and *E. coli* (1.1 s^{-1} and 0.57 s^{-1} for mant-GDP and mant-GTP respectively (Wout et al., 2004)). The relatively fast dissociation of both nucleotides from the complex will ensure the rapid turnover of the bound nucleotide, and thus no guanine nucleotide exchange factor (GEF) will be required for HflX's function. This is in contrast to the dissociation rate constants of for example EF-Tu (k_{-GDP} = 0.002 s^{-1} and k_{-GTP} = 0.03 s^{-1} (Wilden et al., 2006b)), which requires EF-Ts as the GEF, but consistent with EF-G (k_{-GDP} = 300 s^{-1} and k_{-GTP} = 7 s^{-1} (Wilden et al., 2006b)) which does not require a GEF for its cellular function. The kinetic data also suggests that HflX is in a constant state of nucleotide exchange in the cell similar to EF-G but opposed to EF-Tu (Gromadski et al., 2002; Wieden et al., 2002). However, the rates of nucleotide dissociation from HflX are one order of magnitude lower than for the EF-Ts catalyzed nucleotide dissociation in EF-Tu (125 s^{-1} and 85 s^{-1} for GDP and GTP respectively (Gromadski et al., 2002)). Furthermore,

the rate constants governing the interaction between GTP and IF-2 (k_{-GTP} = 15 s^{-1} and k_{+GTP} = 4 x 10^5 $M^{-1}s^{-1}$ (Milon et al., 2006)) are very similar to HflX (Table 3.3). It is however astonishing that, different from EF-Tu and EF-G, the rates of nucleotide dissociation from both the GDP- and GTP-bound HflX complexes are very similar suggesting a common structure for the two complexes. Together with the different association rates for the di- and tri-nucleotides this suggests a model where the nucleotides interact with the nucleotide free form of HflX and induce structural rearrangements that will result in the formation of the nucleotide bound form of the enzyme that is structurally similar for both, the di- and tri-nucleotide bound state. Different structures might however exist in the ribosome bound forms of HflX.

The role of the ATP/ADP bound forms versus the GTP/GDP forms of the enzyme, if any exists, remains unclear since previous studies on the *E. coli* and the *C. pneumoniae* factor are not consistent with respect to a potential inhibition of the intrinsic GTPase by excess adenine nucleotides and vice versa (Jain et al., 2009; Polkinghorne et al., 2008). The observation that FRET from the tryptophans in HflX to the mant-group of mant-adenine nucleotides is less efficient than to the respective guanine nucleotides (as observed in both the equilibrium binding studies and pre-steady state experiments) may be explained by either extremely slow association or dissociation rates, or an increased distance between the donor fluorophore (intrinsic tryptophan residues in HflX) and the acceptor fluorophore (mant-group) for the adenine compared to the guanine nucleotides. This would support the idea that the adenine-nucleotide bound state differs structurally from the guanine-nucleotide bound state, and may be part of a regulatory mechanism (Jain et al., 2009). However, based on the equilibrium dissociation constants reported here the majority of HflX will be bound to guanine nucleotides *in vivo*.

In this study, the use of a highly purified reconstituted translation system revealed for the first time that the GTPase activity of HflX is dramatically increased in the presence of 70S and poly(U)-programmed ribosomes and not only by 50S ribosomal subunits as previously reported (Jain et al., 2009). This finding suggests a functional interaction of HflX with the intact 70S ribosome, raising the question to what the functional role of HflX is and with which functional state of the ribosome it preferentially interacts. Previously, *E. coli* 70S ribosomes were not reported to interact with HflX nor to stimulate the GTPase activity of the protein (Jain et al., 2009). This may be explained by a lower affinity of *C. pneumonia* HflX for the *E. coli* 70S ribosomes used in the heterologous system or by the experimental conditions, e.g. Mg^{2+} concentrations, which are not mimicking the cellular conditions. More importantly, the ribosome preparations used by Jain *et al*. are only partially purified and may still contain other factors such as mRNA, tRNA and translations factors which could influence the functional state of the ribosome and hence the interaction with HflX, hinting at the fact that HflX indeed competes with translation factors for the interaction with the ribosome. However, our own data using poly(U)-programmed, highly purified ribosomes with $tRNA^{Phe}$ in the ribosomal P site provided the same level of stimulation as observed for purified, empty ribosomes (Figure 3.6B). This demonstrates that the empty ribosome is not the only target of HflX, since the termination-like complex (70S-poly(U)-$tRNA^{Phe}$) is also recognized.

Chloramphenicol or the aminoglycoside kanamycin effectively inhibit protein synthesis (Brock, 1961; Hobbie et al., 2005; Jerinic and Joseph, 2000; Moazed and Noller, 1987; Woodcock et al., 1991). To explore a potential role of HflX during protein synthesis, we have examined the effect of these two antibiotics on the ribosome-stimulated GTPase activity of HflX. Chloramphenicol is a 50S subunit specific antibiotic with two binding sites on the prokaryotic

ribosome: a high affinity (K_D = 2 μM) site near the ribosomal A site, which hampers binding of tRNA to the A site (Schlunzen et al., 2001), and a lower affinity (K_D = 200 μM) site that binds to the peptide exit tunnel, which may inhibit nascent polypeptides leaving the tunnel (Long and Porse, 2003). Chloramphenicol is toxic to prokaryotes but has little effect on eukaryotes, due to the lack of the higher affinity site (Hansen et al., 2003; Hobbie et al., 2005; Long and Porse, 2003). However, it has been suggested that both sites are physiologically important in bacteria, which further explains its potent antimicrobial activity (Hansen et al., 2003). Our own data show an IC_{50} = 200 μM for the ribosome-stimulated GTPase activity of HflX. However, as the chloramphenicol binding sites on the 50S subunit and 70S ribosome are buried, this suggests the inhibition effect observed may be due to a conformational change near the chloramphenicol binding site affecting the HflX binding region, which in turn may influence the activity of the protein. This may hint at a previously unknown mechanism of antibiotic action through inhibition of the ribosome-associated activity of HflX. Kanamycin, in contrast, protects bases A1408, G1419, and G1494 on the 16S rRNA of the 30S subunit near the mRNA decoding centre on the 70S ribosome (Jerinic and Joseph, 2000; Moazed and Noller, 1987; Woodcock et al., 1991) and does not show any effect on HflX's ribosome-dependent GTPase activity. Preliminary data suggests that hygromycin B, another aminoglycoside that binds close to the decoding center on the ribosomal 30S subunit, also shows no effect on the ribosome-stimulated GTPase activity of HflX. Altogether this supports a model where HflX interacts with the 50S subunit of the ribosome which serves as a GTPase activating factor (GAP in analogy to the GTPase cycle) that is specifically inhibited by chloramphenicol.

In summary, this work represents the first detailed kinetic analysis of the nucleotide binding properties for the universally conserved GTPase HflX. Based on this, it was possible to show

that HflX exhibits a ribosome-stimulated GTPase activity, a feature also observed in several other ribosome-associated protein factors, including the canonical translation factors EF-Tu and EF-G. The use of a highly purified *E. coli in vitro* translation system also allowed for an examination of the ATPase activity of HflX, which is also stimulated by ribosomes. As a non-essential protein under optimal growth conditions, this factor may however have a role in protein synthesis or ribosome biogenesis under stress conditions. Data on the antibiotic-dependent inhibition of the ribosome-stimulated GTPase activity point toward a role for HflX during protein synthesis, and suggests that the HflX-ribosome interaction may be a potential target for other antibiotics such as anisomycin, sparsomycin, blasticidin S, and virginiamycin M, which bind at the peptidyl transferase centre of the 50S ribosomal subunit (Hansen et al., 2003). Further kinetic analysis regarding the influence of ribosomal particles is presented in the following chapter.

4. Ribosomal Particles Regulate the Structural and Functional Dynamics of HflX

Based on
"The Ribosome Modulates the Structural Dynamics of the Conserved GTPase HflX and Triggers Tight Nucleotide Binding"

Jeffrey J. Fischer, Mackenzie L. Coatham, Shey Eagle Bear, Harland E. Brandon, Evelina I. DeLaurentiis, Michael J. Shields, and Hans-Joachim Wieden

Submitted to *RNA*, August 2011

4.1 Introduction

Members of the P-loop family of GTPases are ubiquitous throughout all domains of life. These essential proteins function as nucleotide-dependent molecular switches, and modulate processes such as signal transduction, DNA replication, and protein synthesis (Brown, 2005; Caldon and March, 2003). The functional cycle of GTPases is regulated by the phosphorylation state of the bound nucleotide; the *apo* and GDP bound states represent an inactive form, while upon binding to GTP, the protein adopts a functionally active state. GTP hydrolysis triggers a conformational change in the enzyme, reverting the protein back to its inactive, GDP-bound form. This GTPase cycle can be modulated by a variety of factors within the cell: guanine nucleotide exchange factors (GEFs) catalyze the release of bound GDP, thus facilitating binding of GTP; GTPase activating proteins or factors (GAPs) stimulate the intrinsic GTPase activity of the enzyme, and guanine nucleotide dissociation inhibitors (GDIs) regulate the release of GDP, providing an additional temporal regulation of the enzyme.

Of the family of P-loop GTPases, only eight members are universally conserved, which can be subdivided into two groups. The first group contains the well characterized GTPases, whose functions have been elucidated, include translation elongation factors (EFs) Tu and G, initiation factor (IF) 2, and the protein secretion factors Ffh and FtsY (Caldon and March, 2003). The

second group, whose function remains unclear, consist of the proteins YihA, YchF, and HflX (Caldon and March, 2003), and have also been implicated in protein synthesis. YchF associates with ribosomal subunits and polysomes in *Trypanosoma cruzi* (Gradia et al., 2009). In *Bacillus subtilis*, YihA (YsxC) interacts with the 50S subunit; YihA-depleted cells accumulate a 44.5S large subunit intermediate lacking ribosomal proteins L16 and L36, indicating a role for the factor in ribosome biogenesis (Schaefer et al., 2006). HflX associates with 50S ribosomal subunits in both *Chlamydophila pneumoniae* and *Escherichia coli* (Jain et al., 2009; Polkinghorne et al., 2008), and its intrinsic GTPase activity is significantly stimulated by 70S and 50S ribosomal particles, but partially inhibited by the antibiotic chloramphenicol (Shields et al., 2009).

Previous work by Jain *et al.* and Polkinghorne *et al.* revealed that HflX interacts with the 50S subunit in either GDP or GDPNP bound states based on co-fractionation experiments (Jain et al., 2009; Polkinghorne et al., 2006), and that HflX also co-purifies with an RNA species similar in size to 16S rRNA (Jain et al., 2009). Recent work by Blombach *et al.* on HflX from *Sulfolobus solfataricus* indicated that association with the 50S subunit is nucleotide independent, though may be stabilized by guanine nucleotides (Blombach et al., 2011). In this work, we clarify based on microfiltration and ultracentrifugation experiments that *E. coli* HflX interacts with the 30S particles in addition to 50S subunits and 70S ribosomes in a nucleotide independent manner. Contrary to previous results on the *E. coli* protein, we find that association to ribosomal particles occurs in the *apo* state as well, similar to the homologous factor from *S. solfataricus*. Furthermore, the antibiotic chloramphenicol which specifically binds to the 50S subunit of the ribosome and inhibits ribosome stimulated GTPase hydrolysis by HflX, does not interfere with binding.

Based on this data, we performed a detailed fluorescence resonance energy transfer (FRET)-based pre-steady state analysis of HflX interacting with mant-guanine nucleotides in the presence of ribosomal particles. We find that the 50S and 70S particles regulate the interaction between HflX and mant-GDPNP by slowing nucleotide dissociation rates, resulting in an approximate 250 and 70 000 fold increased binding stability based on calculated equilibrium dissociation constants (K_D's) for 70S and 50S complexes respectively. This is similar to the translational GTPase EF-G, where mant-GDPNP binding to EF-G is stabilized ~ 30 000 fold in the presence of vacant ribosomes (Wilden et al., 2006b).

Using limited trypsinolysis we have probed the structural dynamics of HflX in various nucleotide- and ribosome-bound states. Together with our detailed rapid kinetics analysis data, our probing study revealed for the first time the existence of two distinct HflX conformations and that HflX, similar to EF-G, may adopt a "GTPase-activated" form in the presence of 50S or 70S particles. Our findings therefore provide the first steps towards identifying the functional cycle of HflX and suggests that the ribosome modulates the structural dynamics of HflX. Through efficient tuning of the GTP binding properties of HflX the interaction with the ribosome *in vivo* will enable HflX to overcome the surprisingly low GTP binding affinity observed for the free protein (Shields et al., 2009).

4.2 Experimental Procedures

4.2.1 Materials

Chemicals were obtained from VWR, Sigma, or Invitrogen, unless otherwise specified. Nucleotides and mant-nucleotide derivatives were purchased from Invitrogen or Medicorp (mant nucleotides ≥ 94% purity based on manufacturers specifications). Recombinant 6X His-tagged

HflX was purified as previously reported (Shields et al., 2009). Vacant ribosomes and ribosomal subunits were purified from *E. coli* MRE600 cells essentially as described in (Rodnina et al., 1994), but using a Ti 45 rotor rather than a Ti 50.2 rotor. As HflX rapidly hydrolyzes GTP in the presence of 70S ribosomes or 50S ribosomal subunits, the non-hydrolyzable GTP analog GDPNP (or mant derivatives) was utilized in binding studies where ribosomal particles were present. Protein mass spectrometry was performed at the Institute for Biomolecular Design at the University of Alberta.

4.2.2 Microfiltration

HflX•ribosome complexes were formed by incubating HflX (5 μM) with ribosomal particles (1 μM) in the presence of nucleotides (1 mM), and when indicated with chloramphenicol (1 mM), in 20 μL $TAKM_7$ buffer (50 mM Tris-Cl pH 7.5, 70 mM NH_4Cl, 30 mM KCl, 7 mM $MgCl_2$) at 37 °C for 15 min. Following incubation on ice for 5 min, 480 μL $TAKM_7$ was added. Samples were centrifuged in Vivaspin-500 (100 000 MWCO) columns at 10 000 xg to 20 μL final volume, diluted to 500 μL, refiltered, and analyzed using a 12% SDS-PAGE run at 200 V for 1 h and stained with Coomassie blue. The ratio of HflX to ribosomal particle was determined using ImageJ by comparing the band intensity of 6X His-tagged HflX (50.5 kDa) to that of ribosomal proteins S1, S2, L1, and L2 (61.2, 26.8, 26.7, and 30.0 kDa respectively).

4.2.3 Ultracentrifugation

HflX•ribosome complexes were formed by mixing HflX (1 μM), ribosomes or ribosomal subunits (0.1 μM), and nucleotides (1 mM) in 400 μL $TAKM_7$ buffer at 37 °C for 10 min. Complexes were loaded on a 1770 μL sucrose cushion (20 mM Tris-Cl pH 7.5 at 4 °C, 60 mM NH_4Cl, 5.25 mM $Mg(OAc)_2$, 0.25 mM EDTA, 10% (w/v) sucrose; nucleotide present in appropriate experiments) and centrifuged at 65 000 xg for 24 h in a Beckman Coulter TLX

ultracentrifuge using a TLA-100.3 rotor. The resulting pellet was resuspended in 30 µL $TAKM_7$ and analyzed by SDS-PAGE as above.

4.2.4 Pre-steady state kinetics

Rate constants for HflX interacting with mant-GDPNP / mant-GDP were determined via FRET between the intrinsic tryptophan residues in HflX and the mant group as previously reported (Shields et al., 2009) using a KinTek SF-2004 stopped-flow apparatus. Tryptophan residues were excited at 280 nm and the fluorescence emission from the mant group was monitored through LG-400-F cutoff filters (NewPort). The resulting fluorescence traces were initially fit according to one or two exponential functions (equations 1 and 2), where k_{app} is the characteristic apparent rate constant, A is the signal amplitude, Fl is the fluorescence at time t, and Fl_∞ is the final fluorescence signal. Fluorescence data was then normalized with respect to the initial fit, averaged (5-10 traces typically), and refit with the appropriate equation. Kinetic constants are expressed as the final data fit, ± 95% confidence interval. For association experiments, the k_{app} concentration dependence was fit with a linear function; the slope represents the bimolecular association rate constant. All experiments were performed in $TAKM_7$ at 20 °C.

$$Fl = Fl_\infty + A\exp(-k_{app}t) \quad \text{(Eq. 1)}$$

$$Fl = Fl_\infty + A_1\exp(-k_{app1}t) + A_2\exp(-k_{app2}t) \quad \text{(Eq. 2)}$$

The association of mant-nucleotides to HflX•ribosome complexes were determined by preforming complexes (2 µM HflX and ribosomal particle) by incubation at 20 ºC for 15 min prior to use. Complexes were then rapidly mixed with 25 µL of various concentrations (5 to 25 µM final concentration) of mant nucleotides at 20 ºC in $TAKM_7$. The resulting fluorescence

traces were then analyzed according to either equation 1 or 2, depending on the quality of the obtained fit.

To determine the rates of dissociation of mant nucleotides from HflX•mant-nucleotide•ribosome complexes, complexes were formed by incubating 30 μM mant-nucleotide with 2 μM each HflX and ribosomal particles. Experiments were then performed by rapidly mixing 25 μL of HflX•mant-nucleotide•ribosome complex with 25 μL of 300 μM unlabeled nucleotide at 20 °C in $TAKM_7$. Fluorescence traces were fit according to equations 1 or 2. When monitoring nucleotide dissociation from HflX•mant-GDPNP•50S and HflX•mant-GDPNP•70S complexes, these samples were rapidly mixed with similar complexes containing 300 μM unlabeled GDPNP.

Kinetic data was initially fit using TableCurve (Jandel Scientific). As an additional evaluation method, fluorescence traces from each nucleotide association experiment were also analyzed by global fitting using Scientist software (MicroMath). Reported values for each association rate constant were obtained by averaging values obtained from both calculation methods. Values for nucleotide dissociation rate constants were obtained from direct measurements. The *y*-axis intercepts obtained from the nucleotide association experiments provided an accurate estimate for the nucleotide dissociation rates as previously reported (Shields et al., 2009). Global fitting provided accurate estimates for mant-GDPNP dissociation from HflX•50S and HflX•70S complexes, consistent with a very slow nucleotide dissociation rate. Reported standard deviations represent the largest deviation obtained. From the obtained rate constants, the equilibrium dissociation constants (K_D) were calculated based on $K_D = k_{-1}/k_1$ for single-step binding and $K_D = (k_{-1}k_{-2})/(k_1k_2)$ for a two-step binding mechanism. The current analysis was performed along the lines of Pisareva *et al.* (Pisareva et al., 2006).

4.2.5 Limited Trypsinolysis

The structural dynamics of EF-G has previously been studied using limited trypsinolysis to probe the conformation of EF-G bound to the ribosome in various states (Ticu et al., 2009). In order to probe potential nucleotide-dependent conformational changes of free HflX (in 100 μL reactions), the protein (2 μM) was incubated for 10 min at 20 °C in the presence of nucleotides (1 mM). Trypsin (4.5 μg/mL final concentration) was added and samples were further incubated at 20 °C. At various time points, 20 μL aliquots were removed, mixed with SDS-PAGE loading dye, heat denatured (95 °C for 5 min), and analyzed by SDS-PAGE. To probe the ribosome-bound states of HflX, the protein was incubated with 70S ribosomes or subunits (0.5 μM) in the presence of 1 mM nucleotide prior to limited trypsinolysis. Proteolytic fragments generated were identified by mass spectrometry. Based on these mass spectrometry data, combined with theoretical trypsinolysis sites predicted by PeptideCutter (Gasteiger et al., 2005), likely cleavage sites were identified. The amount of remaining HflX was calculated based on the initial SDS-PAGE band intensity (ImageJ) compared to the band intensity at time points after exposure to trypsin. To compare the sensitivity of HflX to proteolysis, $\ln(c_t/c_o)$ was calculated and plotted over time, where the slope indicates the rate of trypsinolysis of HflX, c_t is the amount (%) of HflX at time t and c_o is the initial amount of HflX present. Error bars reflect standard deviations (n = 3).

4.2.6 Structural modeling of *E. coli* HflX

The structure of HflX from *S. solfataricus* was solved in the *apo* and GDP-bound states (PDB IDs 2QTF and 2QTH respectively (Wu et al., 2010)). The structure 2QTH was used as templates to generated a homology model of *E. coli* HflX using the protein modeling server

SWISS-MODEL (Arnold et al., 2006; Guex and Peitsch, 1997; Kiefer et al., 2009; Peitsch, 1995; Schwede et al., 2003) based on the fact that HflX from *S. solfataricus* and *E. coli* share significant similarity (40.4% similarity, 24.4% identity across the 356 amino acids in the *S. solfataricus* factor). The obtained model is 84% complete with respect to the *E. coli* sequence and only lacks 15 N-terminal and 53 C-terminal residues, which are not present in the sequence from *S. solfataricu*s. A sequence alignment comparing the primary sequence of HflX from *E. coli* to that of *S. solfataricus* was generated using CLUSTALW (Higgins et al., 1996) for use in the alignment mode of SWISS-MODEL. Molecular structures were visualized using PyMOL (DeLano, 2006).

4.3 Results

4.3.1 HflX interacts with ribosomal particles in a nucleotide independent manner.

Many GTPases involved in protein synthesis typically bind only transiently and in a nucleotide-dependent manner to the ribosome. However, studies regarding the interaction of HflX with the ribosome have yielded puzzling results. HflX from *C. pneumoniae* was reported to associate with the *E. coli* 50S subunit, and removal of the N-terminal domain resulted in the loss of specificity for this subunit (Polkinghorne et al., 2006). Jain and colleagues reported that *E. coli* HflX interacts exclusively with the 50S ribosomal subunit regardless of the nucleotide bound (ADP, AMPPNP, GDP, GMPPNP) based on co-sedimentation analysis of purified HflX and ribosomes (Jain et al., 2009). Interestingly, this study also showed that HflX co-purifies with 16S and 23S rRNA, suggesting that HflX might be able to interact with the 30S as well as the 50S subunit or its precursors (Jain et al., 2009). Recently, HflX from *S. solfataricus* was reported to not only interact with 50S subunits in its nucleotide bound state, but also in the *apo* form of the enzyme (Blombach et al., 2011). To clarify the mechanistic details governing the interaction

between *E. coli* HflX and the ribosome, we performed reconstitution assays using purified components. Based on the available biochemical data (Shields et al., 2009) we studied the binding of HflX to the three (30S, 50S and 70S) ribosomal particles in the absence and presence of various guanine nucleotides as well as chloramphenicol using microfiltration (Figure 4.1A) and ultracentrifugation techniques (Figure 4.1B). During microfiltration, free HflX (50.5 kDa) passes through the 100 kDa MWCO filter used (Figure 4.1A 70S lane 2), whereas the respective ribosomal particles will be retained above the membrane (Figure 4.1A 70S, 50S and 30S). Since the molecular mass of HflX differs significantly from the masses of ribosomal proteins, the presence of HflX can be easily detected and quantified by SDS-PAGE (indicated by an arrow, Figure 4.1). When excess HflX (5 µM) was incubated with 70S, 50S, or 30S (1 µM) in the presence (1 mM) or absence of nucleotides (GDP, and GDPNP), HflX was retained together with the ribosomal particles, suggesting that HflX is able to bind to either ribosomal subunit independent of the nucleotide bound state. Although chloramphenicol inhibits the ribosome stimulated GTPase activity of HflX, it did not interfere with the binding of the protein to the respective ribosomal particles either in the presence or the absence of nucleotide. Prominent ribosomal proteins (S1, S2, L1, and L2) were identified by mass spectrometry and used to determine the relative amounts of HflX bound to the respective ribosomal particle using densitometry. This analysis revealed a binding stoichiometry of 1:1 for the HflX•30S and HflX•50S and approximately 1.5:1 for the HflX•70S ribosome complex. Similar results were obtained for ultracentrifugation experiments in which HflX (1 µM) was incubated individually with 30S, 50S and 70S ribosomal particles (0.1 µM) in the absence and presence of 1 mM nucleotides (GDP and GDPNP). Here, free HflX was separated from the ribosomal particles and their respective HflX-bound complexes by centrifugation through a 10% sucrose cushion (Figure

4.1B). Under all conditions HflX was found to migrate with the respective ribosomal particles suggesting that HflX can bind tightly to either 30S, 50S or 70S ribosomes and that this interaction does not depend on the presence of nucleotide.

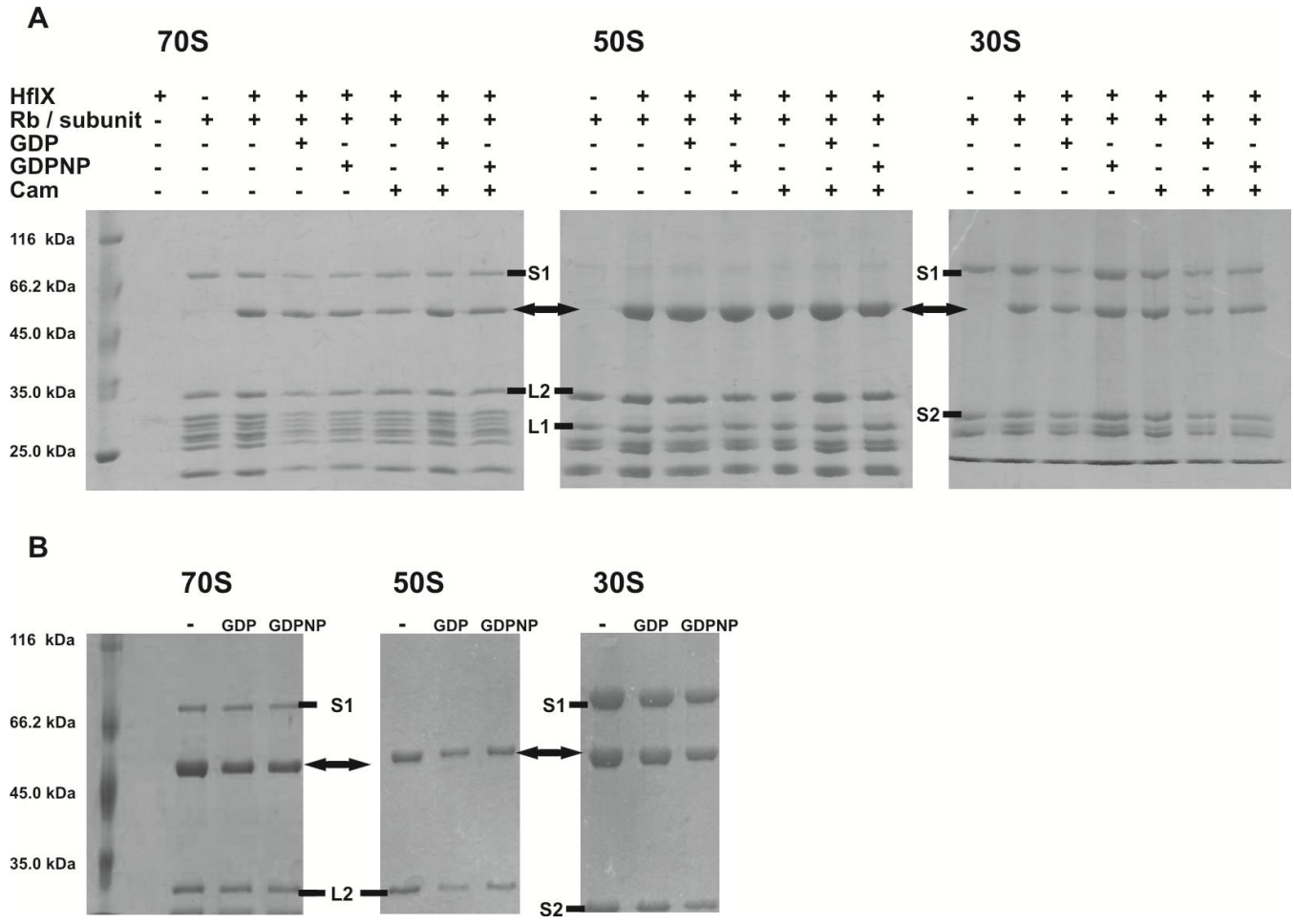

Figure 4.1. HflX Interacts with Ribosomes and Ribosomal Subunits Regardless of Nucleotide or Chloramphenicol.

A) HflX-ribosome complexes were preformed in the absence (*apo*) or presence of nucleotide (GDP, GDPNP) and chloramphenicol (as indicated). Following filtration through 100 kDa MWCO filters, free HflX (50.5 kDa) was found in the flow-through, while ribosome-bound HflX complexes remain in the retentate (12% SDS-PAGE of the various retentates are shown). B) Interaction of HflX with ribosomal particles, independent of nucleotide, was confirmed by ultracentrifugation through a 10% sucrose cushion. The position of HflX is indicated (double-headed arrow) and the Proteins S1, S2, L1, and L2, are labeled as references.

4.3.2 Kinetics of mant-GDP interacting with HflX and its ribosomal complexes.

The kinetic parameters governing the interaction of guanine nucleotides with free HflX have been successfully determined previously using FRET between the intrinsic tryptophan residues of HflX and the mant moiety of mant-GDP and mant-GTP (Shields et al., 2009). Here we wanted to investigate the nucleotide interaction with HflX based on the observation that HflX can form three stable ribosomal complexes (HflX•30S, HflX•50S and HflX•70S, Figure 4.1). In order to address the question if interaction with the ribosomal particles influences the nucleotide binding properties of HflX and to assess the potential of the ribosome as a regulator in the functional cycle of the universally conserved GTPase HflX, we have performed a detailed kinetic analysis of the guanosine di- and tri-phosphate binding properties of free HflX and three different ribosomal complexes (HflX•30S, HflX•50S and HflX•70S) using the stopped-flow technique. All obtained rate constants are summarized in Table 4.1.

The binding kinetics of GDP and HflX was measured using the fluorescent analog mant-GDP. Performing chase experiments by rapid mixing of preformed HflX•mant-GDP complexes with excess GDP resulted in a decrease in mant fluorescence over time consistent with the dissociation of the bound mant-nucleotide (Figure 4.2A). Monitoring the fluorescence change over 120 s revealed a biphasic fluorescence signal decay, suggesting a two-step dissociation mechanism (Scheme 1), best described by a two-exponential time dependence.

$$\text{HflX} + \text{mant-GDP} \underset{k_{-1}}{\overset{k_1}{\leftrightarrow}} \text{HflX•mant-GDP} \underset{k_{-2}}{\overset{k_2}{\leftrightarrow}} \textit{HflX•mant-GDP} \qquad \text{(Scheme 1)}$$

Consistent with this model the obtained fluorescence traces were best fit with a two-exponential equation (Section 4.2) yielding the rate constants $k_{-1,\,GDP} = 2.5 \pm 0.1\ s^{-1}$ and $k_{-2,\,GDP}$ =

$0.040 \pm 0.007\ s^{-1}$. The value reported here for $k_{-1,\ GDP}$ is consistent with our previously reported value of $2.6 \pm 0.2\ s^{-1}$ for mant-GDP dissociation from free HflX (Shields et al., 2009).

When experiments were carried out using mant nucleotides from two different sources as well as several independently prepared batches of HflX, the obtained fluorescence signals showed similar behavior. Thus, the observed two-exponential kinetics reflects a conformational change in HflX preceding nucleotide dissociation and is not due to sample heterogeneity. Furthermore, a conformational change in HflX due to the interaction with the nucleotide is consistent with the observed quenching of tryptophan fluorescence in equilibrium fluorescence titration experiments using unlabeled nucleotides (Shields et al., 2009), where quenching of the tryptophan fluorescence can be attributed to a conformational rearrangement in the proximity of the tryptophan residues upon nucleotide binding.

In addition, association experiments with mant-GDP binding to HflX (Figure 4.2B) also showed a second phase consistent with a two-step binding process (Figure 4.2B, inset) and were therefore fit with a two exponential equation. The apparent rates obtained for the first fast step ($k_{app1,GDP}$) increased with the concentration of mant-GDP, whereas the apparent rate for the second slower step ($k_{app2,GDP}$) was concentration independent, consistent with a conformational rearrangement following the initial binding event. The respective rate constants (k_1 and k_2) were calculated from the slope of the $k_{app1,GDP}$ concentration dependence and the average values of $k_{app2,GDP}$ respectively (Figure 4.2C), and confirmed by global fitting ($k_{1,\ GDP} = 3.5 \pm 0.3 \times 10^5\ M^{-1}s^{-1}$ and $k_{2,\ GDP} = 0.14 \pm 0.02\ s^{-1}$). The value for $k_{1,\ GDP}$ was similar to our previously reported value of $9.7 \pm 0.6 \times 10^5\ M^{-1}s^{-1}$ for mant-GDP association to free HflX (Shields et al., 2009).

We next investigated the influence of ribosomal particles on the kinetics of mant-GDP interaction with HflX. Rapid kinetics measurements were carried out using conditions based on

our initial reconstitution assays, ensuring HflX binding to the respective ribosomal particles. To determine the nucleotide dissociation rate constants, individual HflX•mant-GDP•ribosome complexes (30S, 50S and 70S, respectively) were preformed and rapidly mixed with excess GDP (Figures 4.2D, 4.2G, and 4.2J respectively). Interestingly, only single-exponential fluorescence changes were observed, indicative of one-step dissociation/association kinetics (Scheme 2).

$$\text{HflX + mant-GDP} \underset{k_{-1}}{\overset{k_1}{\leftrightarrow}} \text{HflX•mant-GDP} \qquad \text{(Scheme 2)}$$

The obtained fluorescence time courses were therefore fit with a single-exponential function (Experimental Procedures). Dissociation rate constants for these complexes were $k_{-1,GDP,\ 30S} = 2.4 \pm 0.2\ s^{-1}$, $k_{-1,\ GDP,\ 50S} = 0.53 \pm 0.01\ s^{-1}$, and $k_{-1,\ GDP,\ 70S} = 1.5 \pm 0.1\ s^{-1}$.

To determine the rate constants describing the association of mant-GDP to these HflX•ribosome complexes ($k_{1,\ GDP,\ 30S}$, $k_{1,\ GDP,\ 50S}$, $k_{1,\ GDP,\ 70S}$), the respective preformed complexes were mixed with increasing concentrations of mant-GDP. Only single exponential fluorescence traces were observed, again supporting a one-step binding process (Scheme 2). Fluorescence time courses were fit accordingly with a one exponential equation. The resulting association rate constants were calculated similar to free HflX (as above) from the concentration dependence of the respective calculated k_{app} of association: $k_{1,\ GDP,\ 30S} = 5.1 \pm 0.9 \times 10^5\ M^{-1}s^{-1}$, $k_{1,\ GDP,\ 50S} = 6.7 \pm 0.3 \times 10^5\ M^{-1}s^{-1}$, $k_{1,\ GDP,\ 70S} = 4.9 \pm 1.3 \times 10^5\ M^{-1}s^{-1}$ (Figures 4.2E, 4.2H, and 4.2K respectively; k_{app} plots are found in Figures 4.2F, 4.2I, and 4.2L).

From the obtained rate constants, the equilibrium dissociation constants (K_D) for mant-GDP interacting with HflX, HflX•30S, HflX•50S and HflX•70S complexes were calculated (Experimental Procedures): $K_{D,GDP,HflX} = 2.0 \pm 0.5\ \mu M$ (consistent with our previously reported value (Shields et al., 2009)), $K_{D,\ GDP,HflX•30S} = 4.7 \pm 0.9\ \mu M$, $K_{D,\ GDP,HflX•50S} = 0.79 \pm 0.02\ \mu M$,

and $K_{D,GDP,HflX\bullet 70S}$ = 3.1 ± 0.8 μM (Table 4.2). This indicates that ribosomal particles do not affect binding of mant-GDP to HflX.

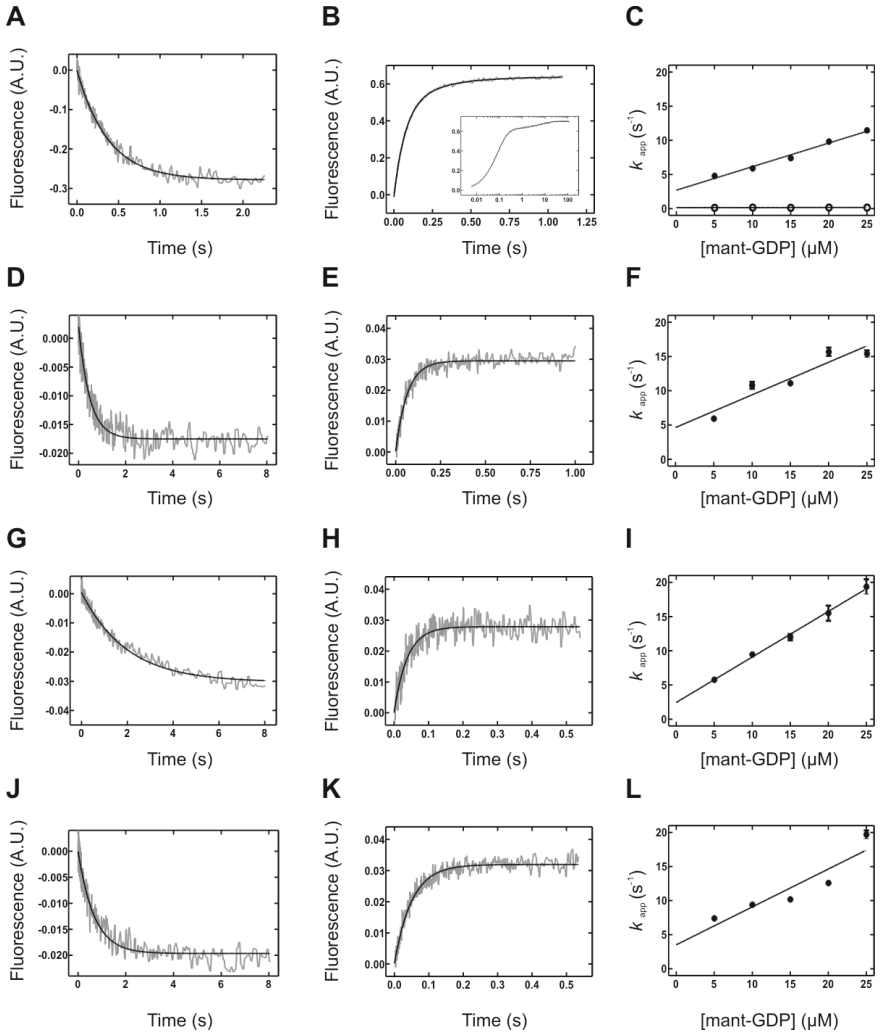

Figure 4.2. Interaction between mant-GDP and HflX•Ribosome Complexes.

Mant fluorescence was excited by FRET from the intrinsic tryptophan residues of HflX (λ_{ex} = 280 nm). All traces (grey) are fit as described in Experimental Procedures; solid black lines represent the resulting fits. All concentrations are given after mixing. A) Time course of the dissociation of mant-GDP from HflX (1 μM HflX, 15 μM mant-GDP) in the presence of GDP (150 μM). B) Association of 25 μM mant-GDP to HflX (1 μM). Inset, long time course of mant-GDP association (log scale). C) Concentration dependence of k_{app} values for mant-GDP association to HflX; closed circles, k_{app1}; open circles, k_{app2}. D) Dissociation of mant-GDP from the HflX•mant-GDP•30S complex (as in A), with 1 μM 30S subunits). E) Association of 25 μM mant-GDP to the HflX•30S complex. F) Concentration dependence of k_{app} values for mant-GDP association to the HflX•30S complex. G) Dissociation of mant-GDP from the HflX•mant-GDP•50S complex, (as in D). H) Association of 25 μM mant-GDP to the HflX•50S complex. I) Concentration dependence of k_{app} values for mant-GDP association to the HflX•50S complex. J) Dissociation of mant-GDP from the HflX•mant-GDP•70S complex. K) Association of 25 μM mant-GDP to the HflX•70S complex. (L) Concentration dependence of k_{app} values for mant-GDP association to the HflX•70S complex.

4.3.3 Kinetics of mant-GDPNP interacting with HflX and its ribosomal complexes.

As HflX rapidly hydrolyzes GTP in the presence of 50S and 70S ribosomal particles, mant-GTP cannot be used to study the nucleotide binding properties of the HflX•50S and HflX•70S. We therefore utilized the non-hydrolyzable analog mant-GDPNP to determine the kinetic constants describing the guanosine triphosphate interactions with free HflX and its complexes with 30S, 50S and 70S ribosomal particles. First we determined the kinetic parameters governing the mant-GDPNP interaction with free HflX, which have not been reported previously. Similar to the mant-GDP dissociation and association experiments with free HflX, fluorescence time courses obtained using mant-GDPNP were best fit with a two-exponential equation (Figures 4.3A and 4.3B respectively). In the mant-GDPNP association experiment the apparent rate constants for the first fast fluorescence signal increase ($k_{app1,GDPNP}$) was concentration dependent, while the slower second apparent rate constant ($k_{app2,GDPNP}$) was concentration independent. The association rate constant of mant-GDPNP to HflX ($k_{1,\ GDPNP}$ = 5.2 ± 0.8 x 10^5 $M^{-1}s^{-1}$) was calculated from the slope of the concentration dependence of $k_{app1,GDPNP}$ and is ~ 10 fold faster than that of mant-GTP association to free HflX (6.4 ± 0.3 x 10^4 $M^{-1}s^{-1}$ (Shields et al., 2009)). The rate constant for the second slower, concentration-independent phase was calculated as the average of $k_{app2,GDPNP}$ yielding a value of $k_{2,\ GDPNP}$ = 3.1 ± 0.6 s^{-1}. This again suggests, similar to the mant-GDP experiments, a two-step binding process for mant-GDPNP in which the rapid initial binding interaction is followed by a slower conformational change, leading to the respective nucleotide (GDP or GTP) bound conformation of the protein. When performing nucleotide chase experiments to determine the nucleotide dissociation rate constants from HflX•mant-GDPNP complexes, the observed fluorescence time courses were best fit with a two-exponential function, further supporting a two-step binding mechanism for the interaction of

mant-GDPNP and HflX. Interestingly, the fast first dissociation rate constant ($k_{-1,\ GDPNP}$ = 34 ± 2.0 s^{-1}) obtained from the two-exponential fits differs from the previously reported dissociation rate constant for mant-GTP obtained from the single exponential fluorescence time courses observed in (Shields et al., 2009). However, the previously determined mant-GTP dissociation rate constant from free HflX ($k_{-1,\ GTP}$ = 2.1 ± 0.1 s^{-1}) is very similar to the rate constant found for the slower second phase of the signal change ($k_{-2,\ GDPNP}$ = 2.3 ± 0.2 s^{-1}). Therefore, the observed transient initial interaction with mant-GDPNP is very likely to also occur during mant-GTP dissociation, but might have been missed due to its small signal amplitude and an improved signal-to-noise ratio in the current measurement. This is supported by the fact that the equilibrium binding constant for mant-GDPNP interaction with HflX ($K_{D,\ GDPNP}$ = 49 ± 13 µM) when calculated from the obtained rate constants (k_1, k_{-1}, k_2, k_{-2}) is very similar to the previously determined $K_{D,\ GTP}$ of 30 ± 1 µM for the mant-GTP HflX interaction (Shields et al., 2009).

Fluorescence time courses observed for the mant-GDPNP interactions with the HflX•30S complex (Figures 4.3D, 4.3E, and 4.3F) showed a biphasic behavior similar to the free protein (*vide supra*) yielding very similar association and dissociation rate constants ($k_{1,\ GDPNP,\ 30S}$ = 1.5 ± 0.5 x 10^6 $M^{-1}s^{-1}$, $k_{2,\ GDPNP,\ 30S}$ = 2.4 ± 1.6 s^{-1}, $k_{-1,\ GDPNP,\ 30S}$ = 35 ± 7.4 s^{-1} $k_{-2,\ GDPNP,\ 30S}$ = 2.6 ± 0.5 s^{-1}). This suggests that binding of HflX to the 30S subunit does not affect nucleotide-binding affinity, as the equilibrium dissociation constant calculated from the determined rate constants (K_D = 25 ± 20 µM) is comparable to the affinity for the free protein (as above).

For both the HflX•50S and the HflX•70S complexes, the mant-GDPNP association and dissociation experiments also resulted in biphasic fluorescence signals. However, when fluorescence time courses for the nucleotide association (Figures 4.3E, 4.3H) were analyzed using two-exponential fitting as well as global fitting, the initial association step was found to be

slightly slower for the 50S complex and ~ 30 fold slower for the 70S complex when compared either to the free HflX or 30S complex experiments ($k_{1,\ GDPNP,\ 50S}$ = 9.2 ± 1.2 x 10^4 $M^{-1}s^{-1}$ and $k_{1,\ GDPNP,\ 70S}$ = 1.7 ± 0.2 x 10^4 $M^{-1}s^{-1}$ respectively). In addition, the slow second step was ~ 10 fold slower for the 50S-complex and ~ 100 fold slower for the 70S-complex ($k_{+2,\ GDPNP,\ 50S}$ = 0.23 ± 0.09 s^{-1} and $k_{+2,\ GDPNP,\ 70S}$ = 0.019 ± 0.005 s^{-1} respectively). The dissociation rate constants obtained from the fluorescence time courses of the chase experiments in Figures 4.3G and 4.3J were also significantly smaller than for the free protein or the 30S complex ($k_{-1,\ GDPNP,\ 50S}$ = 0.012 ± 0.004 s^{-1} and $k_{-2,\ GDPNP,\ 50S}$ = 0.0012 ± 0.0001 s^{-1}, $k_{-1,\ GDPNP,\ 70S}$ 0.041 ± 0.02 s^{-1} and $k_{-2,\ GDPNP,\ 70S}$ = 0.0015 ± 0.0001 s^{-1}). These values reveal a drastic stabilizing effect of the 70S and in particular the 50S particles on mant-GDPNP binding, representing a 250 to 70 000 fold increased affinity for mant-GDPNP when compared to the free protein ($K_{D,GDPNP,\ 70S}$ = 0.19 ± 0.11 µM and $K_{D,GDPNP,\ 50S}$ = 0.7 ± 0.4 nM, Table 4.2).

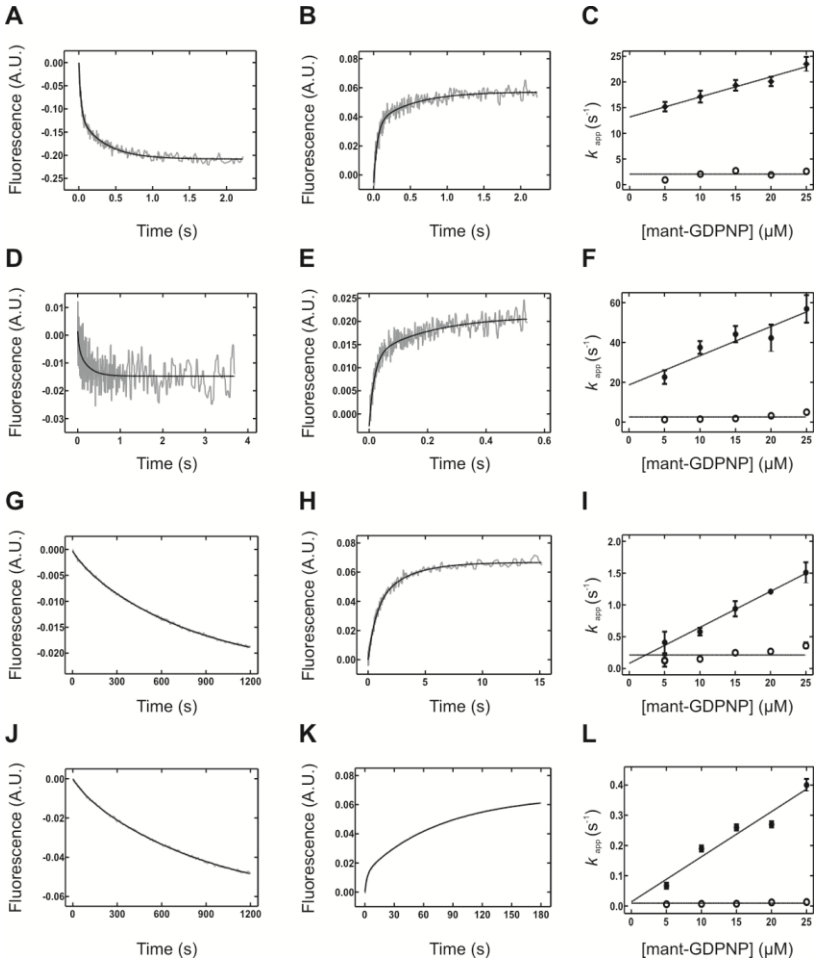

Figure 4.3. Interaction between mant-GDPNP and HflX•Ribosome Complexes.

Mant fluorescence was excited by FRET from the intrinsic tryptophan residues of HflX (λ_{ex} = 280 nm). All traces (grey) are fit as described in Experimental Procedures; solid black lines represent the resulting fits. Concentrations of components after mixing. A) Time course of the dissociation of mant-GDPNP from HflX•mant-GDPNP (1 μM HflX, 15 μM mant-GDPNP) in the presence of GDPNP (150 μM). B) Association of 25 μM mant-GDPNP to HflX. C) Concentration dependence of k_{app} values for mant-GDPNP association to HflX. D) Time course of the dissociation of mant-GDPNP from HflX•mant-GDPNP•30S (as in A), with 1 μM 30S) in the presence of GDPNP (150 μM). E) Association of 25 μM mant-GDPNP to HflX•30S. F) Concentration dependence of k_{app} values for mant-GDPNP association to HflX•30S. G) Dissociation of mant-GDPNP from the HflX•mant-GDPNP•50S complex in the presence of HflX•50S•GDPNP (150 μM GDPNP). H) Association of 25 μM mant-GDPNP to the HflX•50S complex. I) Concentration dependence of k_{app} values for mant-GDPNP association to the HflX•50S complex. J) Dissociation of mant-GDPNP from the HflX•mant-GDP•70S complex in the presence of HflX•70S•GDPNP. K) Association of 25 μM mant-GDPNP to the HflX•70S complex. L) Concentration dependence of k_{app} values for mant-GDPNP association to the HflX•70S complex. All data was fit according to a two exponential function. Closed circles, k_{app1}; open circles, k_{app2}.

Table 4.1. Rate Constants Governing the Interaction between mant-guanine Nucleotides and HflX•Ribosome Complexes.

Complex	nucleotide	k_{+1} ($M^{-1}s^{-1}$)	k_{-1} (s^{-1})	k_{+2} (s^{-1})	k_{-2} (s^{-1})
HflX	mant-GDP	$3.5 \pm 0.3 \times 10^5$	2.5 ± 0.1	0.14 ± 0.02	0.040 ± 0.007
HflX•30S	mant-GDP	$5.1 \pm 0.9 \times 10^5$	2.4 ± 0.2	N/A	N/A
HflX•50S	mant-GDP	$6.7 \pm 0.3 \times 10^5$	0.53 ± 0.01	N/A	N/A
HflX•70S	mant-GDP	$4.9 \pm 1.3 \times 10^5$	1.5 ± 0.1	N/A	N/A
HflX	mant-GDPNP	$5.2 \pm 0.8 \times 10^5$	34 ± 2.0	3.1 ± 0.6	2.3 ± 0.2
HflX•30S	mant-GDPNP	$1.5 \pm 0.5 \times 10^6$	35 ± 7.4	2.4 ± 1.6	2.6 ± 0.5
HflX•50S	mant-GDPNP	$9.2 \pm 1.2 \times 10^4$	0.012 ± 0.004	0.23 ± 0.09	0.0012 ± 0.0001
HflX•70S	mant-GDPNP	$1.7 \pm 0.2 \times 10^4$	0.041 ± 0.020	0.019 ± 0.005	0.0015 ± 0.0001

Table 4.2. Equilibrium Dissociation Constants Governing the Interaction between mant-guanine Nucleotides and HflX•Ribosome Complexes.

Complex	Nucleotide	K_D (μM)
HflX	mant-GDP	2.0 ± 0.5
HflX•30S	mant-GDP	4.7 ± 0.9
HflX•50S	mant-GDP	0.79 ± 0.02
HflX•70S	mant-GDP	3.1 ± 0.8
HflX	mant-GDPNP	49 ± 13
HflX•30S	mant-GDPNP	25 ± 20
HflX•50S	mant-GDPNP	0.0007 ± 0.0004
HflX•70S	mant-GDPNP	0.19 ± 0.11

4.3.4 Enzymatic probing of different conformational states of HflX.

During their functional cycle GTPases typically adopt different conformations depending on the nucleotide bound. Based on our observation that nucleotide binding to HflX free in solution is a two-step process, which entails a first initial binding step followed by a slower step that likely involves the rearrangement of the protein to its respective nucleotide bound conformation,

we have probed the structural dynamics of HflX using limited trypsinolysis. Limited trypsinolysis of the *apo* form of HflX produced 3 distinct fragments (Figure 4.4A, Fragment I, II, & III). Peptide mapping of the fragments using mass spectrometry indicated the presence of the G domain in these three fragments. When combined with a hypothetical trypsin digest using PeptideCutter (Gasteiger et al., 2005), these three fragments are most likely generated by trypsin cleavage of the full-length protein at amino acid K22, R103, and approximately R189/R192/K194, all located in the N-terminal HflX domain of the protein (Figure 4.4B and C). Interestingly, the cleavage site giving rise to the formation of fragment I (K22) showed great sensitivity to the nucleotide-bound state and seemed to be readily accessible for trypsin in the *apo* state of HflX, based on the rapid formation of this fragment (Fragment I in Figure 4.4A). Based on this information we probed for different conformations of HflX in the *apo*, GDP and GDPNP bound form as well as for the respective complexes in the presence of 30S, 50S and 70S ribosomal particles by measuring the time-dependence of HflX degradation in these complexes (Figure 4.5). To this end, we quantified the fraction of full-length HflX present at different time points during the trypsinolysis assay and determined half-life times ($t_{1/2}$) of HflX in the respective complex (summarized in Table 4.3). In the absence of ribosomal particles, HflX exhibits similar stability against trypsinolysis in all three nucleotide-bound states (Figure 4.5A), with the GDP and GDPNP bound states being slightly more stable than the *apo* form ($t_{1/2,HflX,GDP}$ = 7.9 ± 0.5 min, $t_{1/2,HflX,GDPNP}$ = 9.5 ± 0.7 min and $t_{1/2,HflX,apo}$ = 4.7 ± 0.3 min, respectively). In the presence of all three ribosomal particles, HflX is digested slower (Figure 4.5B, C, D), with increasing stabilization for the 50S and 70S complexes by the bound nucleotide in the following order *apo* < GDP < GDPNP. The strongest protection is observed for the GDPNP bound state in the 50S complex ($t_{1/2,HflXapo,50S}$ = 22 ± 3 min, $t_{1/2,HflX•GDP,50S}$ = 48 ± 5 min, and $t_{1/2,HflX•GDPNP,50S}$ =

154 ± 50 min). In the presence of 70S subunits (Figure 4.5B), similar results were observed ($t_{1/2,HflX\textit{apo},70S}$ = 17 ± 2 min, $t_{1/2,HflX•GDP,70S}$ = 32 ± 5 min, and $t_{1/2,HflX•GDPNP,70S}$ = 108 ± 8 min respectively for *apo*, GDP, and GDPNP states). Experiments with 30S subunits (Figure 4.5D) yielded comparable half-life values regardless of the nucleotide present ($t_{1/2,HflX\textit{apo},30S}$ = 21 ± 2 min, $t_{1/2,HflX•GDP,30S}$ = 31 ± 4 min, and $t_{1/2,HflX•GDPNP,30S}$ =24 ± 4 min).

In order to map the observed trypsinolysis fragments onto the three-dimensional structure of HflX, we have constructed a homology model of the *E. coli* enzyme (Figure 4.4C) based on the available X-ray structure of HflX from the archaeon *S. solfataricus* (Huang et al., 2010a; Wu et al., 2010). Based on this homology model, the locations of the putative trypsinolysis sites were visualized (Figure 4.4C, blue spheres). The cleavage at K22 removes the 22 N-terminal amino acids, located ~18 Å (Cα-3'OH) away from the bound nucleotide and only 22 Å from the switch II (G254). Only 7 of these amino acids are present in our model due to the absence of the additional amino acids in the *S. solfataricus* enzyme. The proximity of this cleavage site to the nucleotide binding site and the switch region is consistent with its sensitivity to the nucleotide-bound state of the enzyme, enabling the detection of different conformational states. Furthermore, R103 (Fragment II) is about 16 Å away (G254) from the switch II region and forms the N-terminal end of helix 4 in the HflX-domain, which is tightly packed against the switch II helix 2 in the G-domain. Trypsinolysis at this position will almost completely remove the N-terminal subdomain I identified in the *S. solfataricus* factor (Wu et al., 2010). The putative trypsinolysis site at (approximately) R189/R192/K194 is located in the junction between the HflX- and G-domain ~13 Å away from the C-terminal end of switch II helix 2 (A277) and about 14 Å away (L372) from the C-terminus of the *S. solfataricus* protein, which is followed by a 50 amino acid extension in the *E. coli* enzyme.

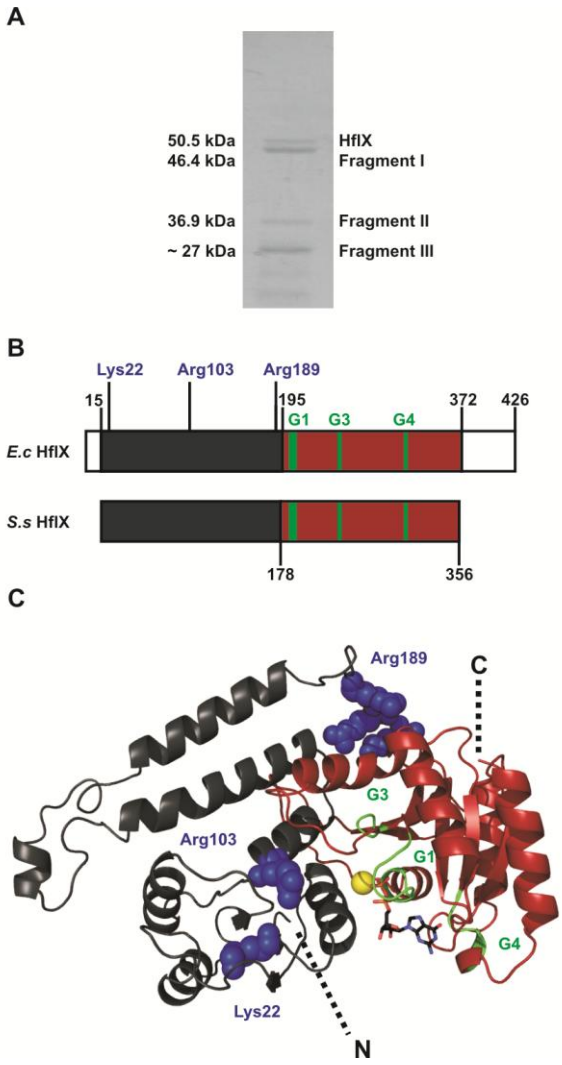

Figure 4.4. Structural Features of *E. coli* HflX.

A) Three major products of limited trypsinolysis after 4 minutes. Fragments were identified by mass spectrometry (Fragments I, II, and III). Based on mass spectrometry data, combined with a theoretical proteolysis of HflX using PeptideCutter (Gasteiger et al., 2005), likely cleavage sites were identified at Lys22, Arg103, and Arg189/Arg192/Lys194 respectively. B) Domain arrangement of *E. coli* (*E.c.*) and *S. solfataricus* (*S.s.*) HflX. *E. coli* HflX contains both an N-terminal and C-terminal extension (15 and 53 amino acids respectively; white) compared to the *S. solfataricus* protein. The N-terminal HflX domain (residues 16-195) is shown in grey; the G domain (residues 196-372) is shown in red; the domain organization of *S. solfataricus* HflX is as described in Wu *et al.* (Wu et al., 2010). The conserved G1, G3, and G4 motifs are shown in green. Likely sites sensitive to limited proteolysis (Lys22, Arg103, and Arg189/Arg192/Lys194) are indicated (blue). C) Homology model of *E. coli* HflX (residues 16-372 of 426) was generated using the structure of *S. solfataricus* HflX (PDBs 2QTF and 2QTH). Structural features are identified similarly to (B). Likely trypsinolysis sites are shown as blue (space fill), GDP (stick structure) and a magnesium ion (yellow) are also shown.

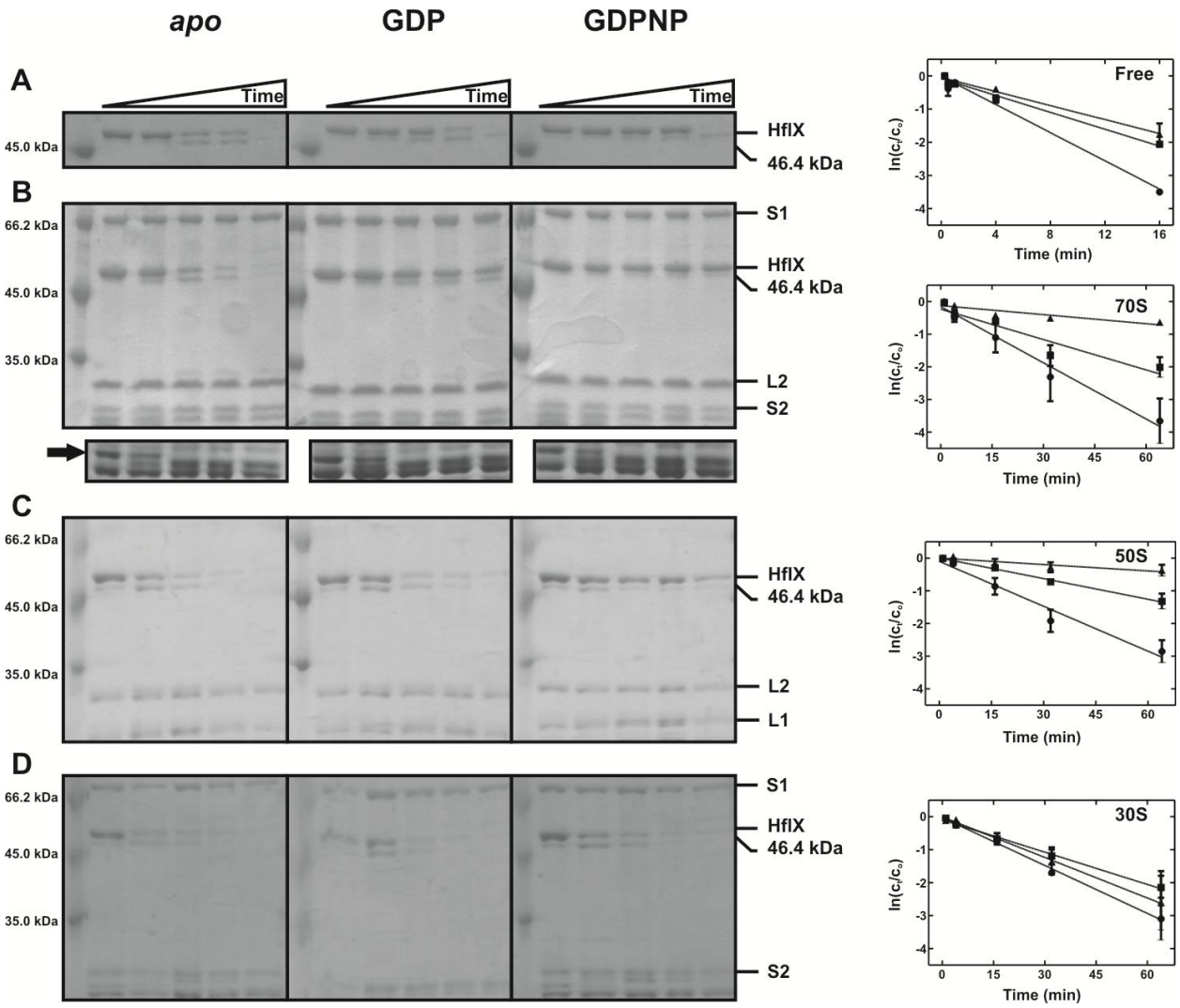

Figure 4.5. Enzymatic Probing of HflX Nucleotide Bound Conformations by Limited Trypsinolysis.

A) Enzymatic probing in the absence of ribosomal particles or the presence of B) 70S ribosomes (as an internal control, an unidentified ribosomal protein, indicated by an arrow, was found to be cleaved consistently after 16 minutes independent of the nucleotide present, forming a lower molecular mass fragment), C) 50S subunits, or D) 30S subunits. Samples were taken for SDS-PAGE analysis at 0, 0.25, 0.5, 1, 4, and 16 minutes in the absence of ribosomal particles and 1, 4, 16, 32, and 64 minutes in the presence of ribosomal particles. Also shown are digestion time courses of HflX alone (closed circles) or in complex with either GDP (closed squares) or GDPNP (closed triangles). $\ln(c_t/c_o)$ is plotted over time, where the slope indicates the rate of trypsinolysis of HflX, c_t is the amount (%) of HflX at time t and c_o is the initial amount of HflX present. Error bars reflect standard deviations (n = 3).

Table 4.3. Half-life Values ($t_{1/2,}$ in min) for the Proteolysis of HflX by Trypsin.

Nucleotide	HflX	+ 30S Rb	+ 50S Rb	+ 70S Rb
apo	4.7 ± 0.3	21 ± 2	22 ± 3	17 ± 2
GDP	7.9 ± 0.5	31 ± 4	48 ± 5	32 ± 5
GDPNP	9.5 ± 0.7	24 ± 4	154 ± 50	108 ± 18

4.4 Discussion

Using a highly purified reconstituted *in vitro* system, we were able to demonstrate for the first time that HflX from *E. coli* not only interacts with the 50S and 70S, but also with 30S ribosomal particles and that this interaction is independent of the nucleotide-bound state of HflX (*apo*, GDP or GDPNP). Our findings therefore reveal the promiscuous interaction of HflX with the three different ribosomal particles and that the previously observed interaction between the *apo* state of HflX and the 50S ribosomal subunit is not limited to the archaeon *S. solfataricus* (Blombach et al., 2011). Therefore it is likely that binding of HflX in the *apo*-form to ribosomal particles is a general feature of HflX. Promiscuous ribosome interactions have also been observed with IF-2, which interacts with 30S, 50S, and 70S particles with varying affinities depending on the nucleotide-bound state of the factor (Pon et al., 1985a) and its interaction with the initiator fMet-$tRNA^{fMet}$ (Peterson et al., 1979).

The findings reported here also provide the first insight into the structural dynamics of HflX during interaction with its two major interaction partners, the ribosome and guanine nucleotides. The observed structural states are in agreement with the typical GTPase cycle. Our trypsinolysis results indicate, based on the obtained half-life times of 12 different functional states, that HflX

is likely to exist in two different conformations, a compact (less accessibly to trypsin) GDPNP-bound GTP conformation and an open (easier accessible to trypsin) GDP/*apo* conformation (Figure 4.6). The existence of very similar conformations for the GDP and *apo* form of the protein is in agreement with the respective X-ray structures *S. solfataricus* HflX (Blombach et al., 2011). Furthermore, our detailed pre-steady-state kinetics analysis of nucleotide binding revealed a two-step binding mechanism for GDP to free HflX, in which a first rapid initial binding of GDP to HflX is followed by a transient exploration of a second GDP-bound form of the complex. The partitioning between the two states, based on the respective rate and equilibrium constants (k_{-1} = 2.5 s^{-1}, k_2 = 0.14 s^{-1}, $K_2 = k_{-2} / k_2$ = 0.29), suggests that the majority of the HflX•GDP complex exists in the initial binding complex (before conformational change). The equilibrium between the first conformation and the second conformation of HflX•GDP complex (described by K_2) does only partially lie on the right side, the second HflX•GDP conformation (Figure 4.6). Together with the 10 fold larger k_{-1} compared to k_2 and the observed sensitivity to limited trypsinolysis, which is similar to the *apo* form of free HflX, this suggests that the initial encounter state is predominantly populated and structurally resembles the *apo* state.

Interestingly, in the presence of ribosomal particles, HflX is biased towards a single conformation as reflected in the single exponential fluorescence time courses (GDP, Figure 4.2), suggesting a single binding step. This is further supported by the very similar GDP association and dissociation rate constants for the three ribosomal complexes. Therefore, HflX is most likely found in a single GDP-conformation when bound to the ribosome (30S, 50S and 70S, Figure 4.6), whereas the mant-GDPNP binding kinetics for the corresponding ribosomal complexes

point towards a two-step binding event with a final rearrangement into the GTP conformation (Figure 4.6).

The fact that mant-GDP binding to the HflX•30S, HflX•50S and HflX•70S complexes is a single-step binding event reported by a single-exponential fluorescence signal indicates that no rearrangement of the mant reporter group occurs following binding of the nucleotide to HflX. Accordingly, we conclude that the biphasic binding of mant-GDPNP reflects a true two-step binding event and not a mant reporter group rearrangement. Ultimately this suggests that interaction of nucleotide-free HflX with either the 70S, 50S or 30S ribosomal subunit induces a single very similar conformation, based on the determined rate constants for GDP association and dissociation and the very similar half-life times in the trypsinolysis assays (Figure 4.6).

Interestingly, the rate constants for nucleotide association of mant-GDPNP to the HflX•70S and HflX•50S, but not the HflX•30S complex, are an order of magnitude slower than for the association of mant-GDPNP to free HflX, which is essentially identical to the respective mant-GDP association rate constant. This suggests that the transition state for mant-GDPNP binding to the 50S and 70S bound form of HflX is energetically higher than for the free and 30S bound form of HflX. A tenfold reduction in association rate constant for mant-GDPNP binding to the 50S and 70S when compared to the 30S complex can be explained by either a slightly different or a less open conformation of the nucleotide binding pocket. Partial occlusion of the nucleotide binding pocket by the 50S ribosomal subunit either in the HflX•50S or the HflX•70S complex would provide a straightforward explanation for this effect. However, occlusion of the nucleotide-binding pocket by the ribosome is unlikely as no such effect was observed for the association of mant-GDP to the respective complexes. This is in contrast to the recent study on the *S. solfataricus* HflX that suggested that the orientation of HflX binding to the 50S subunit

would cause the guanine nucleotide binding pocket to form part of the interface between HflX and the ribosome (Blombach et al., 2011).

It is therefore more likely that the interaction of HflX with 50S and 70S particles (mainly through the interaction with the 50S subunit) induces a state different from the 30S bound or the free form of HflX, which is more sensitive to the presence of the nucleotide γ-phosphate. The presence of the γ-phosphate then triggers additional conformational changes (also seen in the free form of HflX), which are then stabilized with the help of the ribosome resulting in the formation of a closed conformation (Figure 4.6). This is also reflected in the significant protection of the N-terminus against limited trypsinolysis and the ~ 50 000-fold increase in affinity for GDPNP (from ~50 μM to ~1 nM). Mechanistically this mainly occurs by slowing down (~1 000 fold) the conversion between the second GDPNP-bound form and the initial conformation, essentially trapping the protein in the tight second conformation (from $k_{-2,GDPNP,HflX}$ = 2.3 s^{-1} to $k_{-2,GDPNP,HflX•70S}$ = 0.0015 s^{-1}). The effect is further increased by slowing down (~1 000 fold) the dissociation of the nucleotide from the initial bound complex (from $k_{-1,GDPNP,HflX}$ = 34 s^{-1} to $k_{-1,GDPNP,HflX•70S}$ = 0.041 s^{-1}, Figure 4.6). Together with the fact that 50S and 70S ribosomal particles are able to stimulate the intrinsic GTP-hydrolysis of HflX, it is most likely that this tight complex also resembles the GTPase-activated state of HflX on the ribosome. This behavior is very similar to the modulation of nucleotide binding and hydrolysis observed for the translational GTPase EF-G, which exhibits a 30 000 fold stabilization of the EF-G•GDPNP complex when bound to the 70S ribosomal particle (Wilden et al., 2006b). In conclusion, the ribosome not only is able to stimulate the GTPase activity of HflX and acts therefore as a GAP, but also to modulate the nucleotide-binding affinity for GTP, raising the question to how GTP-hydrolysis is regulated in the ribosomal complex.

Both the *S. solfataricus* and *E. coli* proteins share the common N-terminal HflX and C-terminal G domains. Overall, the factors share 40.4% similarity and 24.4% identity across the 356 amino acids present in the *S. solfataricus* factor. However, an additional 54 amino acids are present on the C-terminus of the G domain in *E. coli*. A detailed examination of this region in prokaryotes revealed that this region is poorly conserved and highly variable in length (not shown). Polkinghorne *et al*. reported that C-terminal or N-terminal *C. pneumoniae* HflX truncations lost 50S specificity or affinity, respectively (Polkinghorne et al., 2008). A similar behavior was also corroborated by Jain *et al.* for the *E. coli* protein (Jain et al., 2009). This would account for the observed association of HflX to all three ribosomal particles reported here. It is tempting to speculate that one molecule of HflX interacts with the 70S ribosome in a way that the C-terminal G-domain interacts with the 50S subunit, while the N-terminal HflX-domain interacts with the 30S subunit, thus bridging the two in the 70S complex. Binding of a single copy of HflX to both ribosomal subunits of the 70S ribosome would be consistent with the binding stoichiometry reported here. The fact that the N-terminal domain is required for regulation of the G domain (Huang et al., 2010a; Wu et al., 2010) would further support this model. Furthermore, the N-terminal 15 amino acid extension may play a crucial role in GTPase activation, accounting for the 1 000 fold stimulation of the *E. coli* factor compared to the more modest stimulation of the archaeal homolog (Blombach et al., 2011). Our limited proteolysis results in conjunction with mass spectrometry identification of the fragments indicate a protection of the N-terminal HflX domain, in particular, the N-terminal 22 amino acids in the 50S and 70S HflX complexes. It will be interesting to see how the removal of only the N-terminal region affects GTPase activity.

The combined data presented here allows us to develop a mechanistic/kinetic model describing the functional cycle of HflX (Figure 4.6) and to solve the mystery of the surprising low affinity of the protein for GTP (K_D = 187 μM (Shields et al., 2009)). Under cellular concentrations of nucleotides, HflX will adopt either the GDP (70%) or GTP bound forms (9%). Binding to the 50S and 70S ribosomal particles significantly enhances the binding affinity for GDPNP, the nonhydrolyzable GTP analog used here (due to the stimulatory effect on GTP hydrolysis by these ribosomal particles). In particular, the dissociation of mant-GDPNP is inhibited > 1 000 fold by the interaction with these two ribosomal particles. Given the cellular concentration of GTP and GDP and the high affinity for GDPNP/GTP in the 50S/70S bound form of HflX, association of HflX in the GDP bound form to the 50S or 70S ribosomal particle will result in the exchange of bound GDP for GTP. This will cause an effective shifting of the cellular forms of HflX from the mainly GDP-bound free form toward a mainly HflX•GTP•ribosome ternary complex.

Furthermore, our results reported here suggest that based on the high affinity binding of all three nucleotide states of HflX to the ribosome (Figure 4.1), almost all HflX will be bound to ribosomes under cellular ribosome concentration (~ 20 μM (Hirokawa et al., 2008)). Since HflX also interacts with the ribosome in the *apo* state, it is likely that the factor remains bound to ribosomal particles during all stages of its functional GTPase cycle. This raises the question of HflX's role during translation and how its GTPase activity is regulated. The fact that 50S and 70S ribosomal particles drastically stimulate the intrinsic nucleotide hydrolysis rate of HflX, together with the high affinity for both GTP and the ribosome, would cause a constant and most likely futile GTP-hydrolysis cycle *in vivo*. It is therefore likely that the functional cycle of HflX involves a signal from either within the ribosome or an additional factor that regulates the

GTPase activity of the HflX•GTP•50S/70S complex. Our previous studies indicate that a similar level of GTPase stimulation is observed with a post-termination like complex containing deacylated tRNA in the P-site and that GTP-hydrolysis can be modulated by the antibiotic chloramphenicol (Shields et al., 2009), which does not interfere with HflX binding to the ribosome (Figure 4.1). This suggests that the ribosome itself is in general able to modulate the GTPase activity of ribosome-bound HflX. It also suggests that a particular functional state of the ribosome during translation is required for HflX's function, placing this universally conserved GTPase in the realm of translation factors rather than ribosome biogenesis factors. This is particularly interesting as nothing is known about the catalytic mechanism used by HflX to hydrolyze the bound GTP. Other than the classical translational GTPases which belong to the family of Ras-like GTPases and which mainly bind to the GTPase activating center (GAC) in the ribosomal A-site, HflX belongs to a group of GTPases termed HAS-GTPases, including Era, YchF, EngA, and EngB (YihA) (Mishra et al., 2005), which have the catalytic residue (His in EF-Tu) replaced with a hydrophobic side chain (Phe in *E. coli* HflX). Due to the high level of evolutionary conservation of the GAC, this suggests a different mode of GTPase activation.

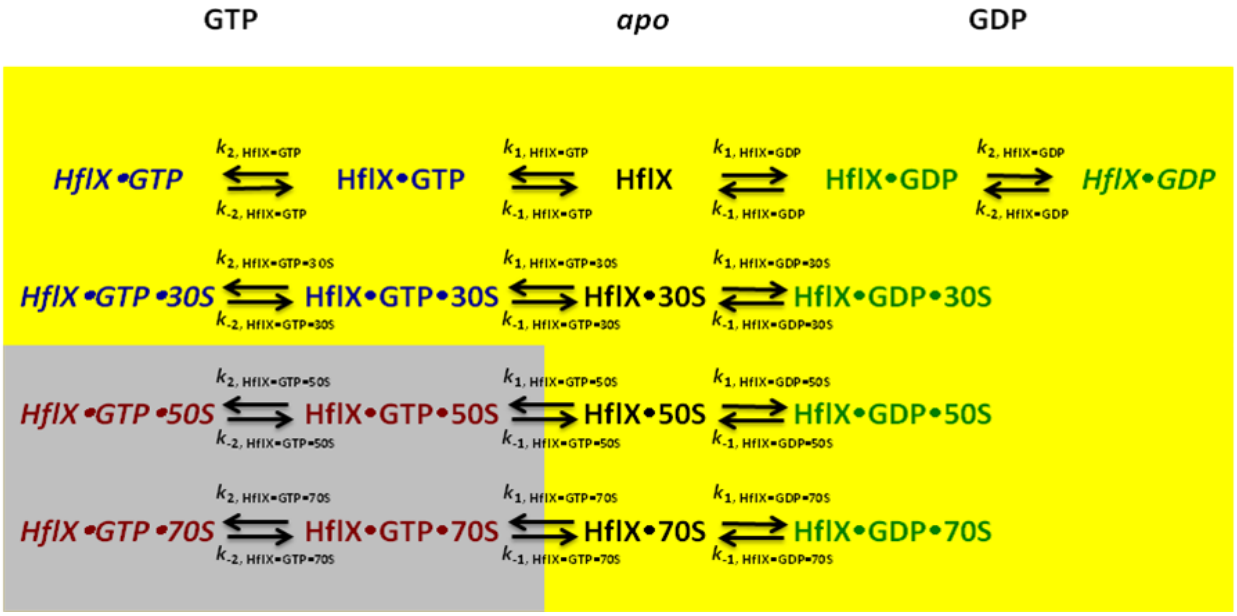

Figure 4.6. Model for Ribosome and Nucleotide Regulation of HflX.

Structural dynamics of HflX. Based on the available trypsinolysis data two distinct structural forms of HflX can be identified (yellow background represent the open GDP/*apo* form and light grey the closed GTP-bound form). Superimposed are the kinetically different states of the protein identified by their respective colors: GDP conformation (green), *apo* conformation (black), loose GTP conformation (blue) and tight GTP conformation (red). Observed rearrangement of a given nucleotide bound state is represented by the italicized font.

In summary, we have presented the first detailed kinetic study on the two molecular interaction partners (nucleotide and ribosome) of HflX known to date. The 50S and 70S ribosomal particles, which act as GAPs for HflX, also induce a tight nucleotide-binding form of the protein, likely through a movement of the N-terminal HflX domain of the protein relative to the C-terminal G domain. Thus, HflX will exist in the cell mainly in a ribosome bound GTP state.

5. The Mechanism of GTPase Activation of HflX

5.1 Introduction

All known translational guanosine 5'-triphosphatases (GTPases) constitute a family of proteins whose intrinsic GTPase activity is stimulated by the large ribosomal subunit. These include the essential canonical translation factors initiation factor (IF) 2, elongation factors (EFs) Tu and G, and release factor (RF)-3, as well as the non-essential factors LepA, BipA, SelB, Tet(O), and HflX. The available X-ray crystal structures of EF-Tu (Abel et al., 1996; Polekhina et al., 1996; Song et al., 1999), EF-G (Chen et al., 2010; Czworkowski et al., 1994; Hansson et al., 2005), RF-3 (Gao et al., 2007), LepA (Evans et al., 2008), and SelB (Leibundgut et al., 2005) reveal common structural features. These features include the GTP binding domain, followed by a β-barrel (domain II) and the α/β or all β-sheet domain III. Though X-ray structures are not available, the GI and GII domains of IF-2 are predicted to be similar to those in EF-G based on the protein sequence. Small-angle X-ray scattering (SAXS) and NMR experiments suggest that the C-terminal domains are also structurally similar to domains IV and V of EF-G (Rasmussen et al., 2008; Wienk et al., 2005). These results are supported by the Cryo-EM structure of the IF-2•GTP•$tRNA_i$•30S complex (Simonetti et al., 2008). BipA binds to the ribosome at the same site as its homologs EF-G and LepA (Owens et al., 2004), and shares structural similarity with these factors (DeLivron et al., 2009). Tet(O) also shares significant sequence similarity with these factors (Sanchez-Pescador et al., 1998; Taylor and Chau, 1996; Thakor et al., 2008). Structural similarity and a common ribosomal binding site for EF-Tu, EF-G, LepA, and BipA suggests not only a shared binding site on the ribosome for all the translational GTPases, but also a similar mechanism by which GTPase activation occurs. This mechanism involves the correct positioning of a conserved catalytic histidine residue in switch II of the translation factor by A2662 of the

23S rRNA (Voorhees et al., 2010b). According to the mechanism outlined by Voorhees *et al.*, the phosphate of A2662 (in the sarcin-ricin loop of the 23S rRNA) orders the catalytic His residue into a catalytic conformation. In this state, the His residue acts as a general base, allowing a nucleophilic attack by a water molecule on the γ-phosphate of bound GTP (Voorhees et al., 2010b).

Although the GTPase activity of HflX is increased ~ 1000 fold by 70S and 50S ribosomal particles (Shields et al., 2009), the crystal structure of HflX (Wu et al., 2010) reveals that the protein shares no significant structural similarity to the other translational GTPases (Figure 5.1). In contrast to the other translational GTPases, in which a key structural feature determining the function of the factor is a C-terminal domain that varies from factor to factor, HflX consist of a unique N-terminal "HflX" domain followed by a C-terminal G domain, and a poorly conserved and structurally undefined C-terminus (Wu et al., 2010). Furthermore, the catalytic His residue found in the canonical translational GTPases within the G domain immediately following the G3 motif (DxxGH) is replaced by a phenylalanine in HflX (Figure 5.1H); thus, HflX has been classified as a hydrophobic amino acid substituted (HAS) GTPase (Mishra et al., 2005). This suggests that HflX may not only bind to a distinct site on the ribosome, but that HflX may be the first translational GTPase that is not activated by the GTPase activating centre (GAC). GTP hydrolysis is likely therefore induced by a different mechanism outside that outlined by Voorhees *et al.* Additionally, chloramphenicol, an antibiotic targeting the peptidyl transferase centre, has been shown to inhibit the ribosome-stimulated GTPase activity of HflX (Shields et al., 2009). Interestingly, the chloramphenicol binding site is deep within the ribosome (Dunkle et al., 2010), suggesting that a distinct conformation of the ribosome depending on the conformation of the peptidyl transferase centre is required for GTPase activation. This suggests a

role of HflX during translation that is dependent on the conformation of the peptidyl transferase centre.

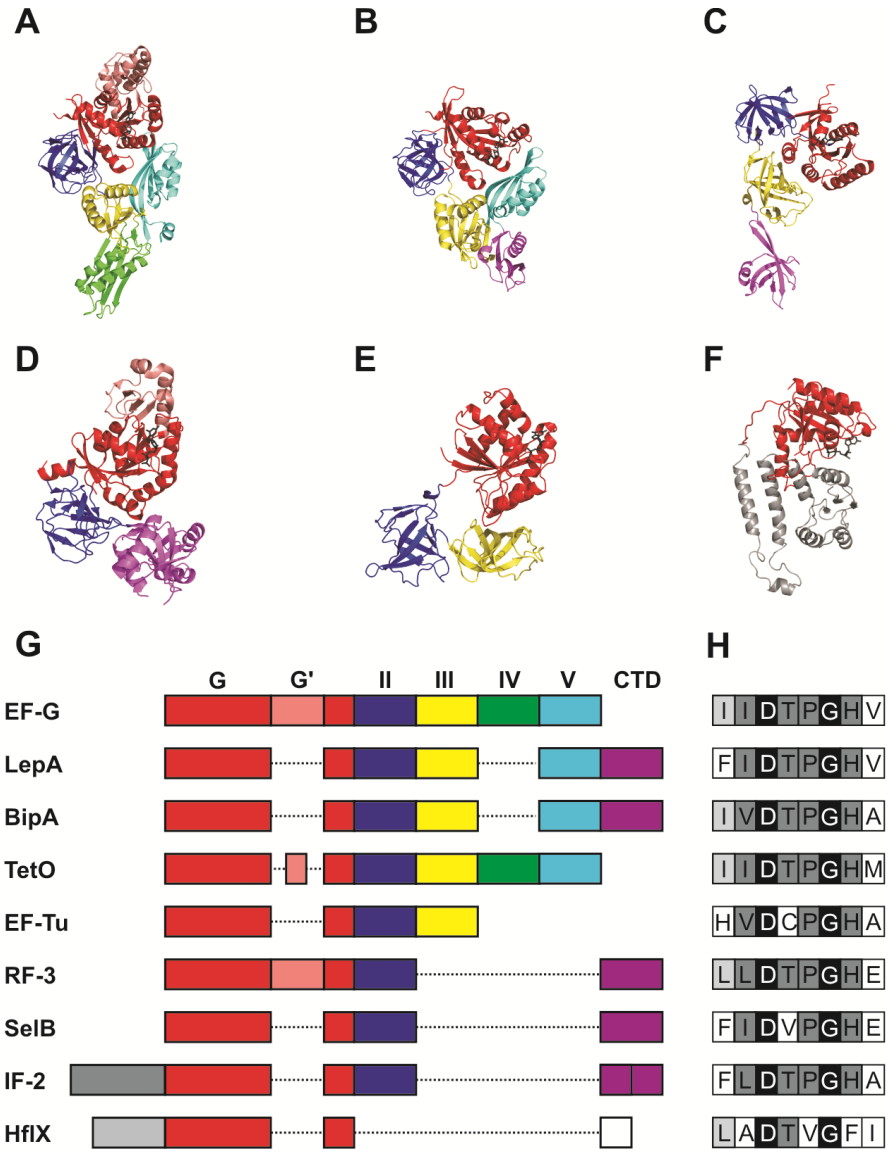

Figure 5.1. Structural Features of Known Translational GTPases.

Cartoon representations of GDP-bound A) EF-G (PDB 1FNM (Laurberg et al., 2000)), B) LepA (PDB 2YWH Kawazoe *et al.*, to be published), C) SelB (PDB 1WB1 (Leibundgut et al., 2005)), D) RF-3 (PDB 2H5E (Gao et al., 2007)), E) EF-Tu (PDB 1TUI (Polekhina et al., 1996)), and a homology model F) of HflX (Chapter 4). All factors are in the GDP-bound conformation. Colors of domains are as in G), which shows the relative domain arrangement of the known translational GTPases. Red, G domain; pink, G' domain; blue, conserved β-barrel domain; yellow, structurally conserved α/β domain; blue, cyan, and purple, variable C-terminal domains. Domains II-V can be spatially superimposed, though in some factors lack sequence similarity. H) Conservation of the G3 motif.

Ribosomal antibiotics target specific ribosomal complexes during protein synthesis, effectively "locking" the ribosome in a defined functional state. For example, fusidic acid has been used to trap the EF-G•GDP complex on the 70S ribosome and thus has allowed for crystallization of translocation intermediates for X-ray crystallography studies (Gao et al., 2009a), kirromycin (which binds to EF-Tu) and paromomycin have been used to trap EF-Tu on the ribosome to monitor aa-tRNA delivery and GTPase activation (Schmeing et al., 2009; Voorhees et al., 2010a). In order to assess potential ribosomal complexes that are targets *in vivo* for HflX, as well as obtain a tool to stabilize an HflX•Ribosome complex for X-ray crystallography and cryo-electron microscopy studies, the effect of different antibiotics on the GTPase activity of HflX were examined. Antibiotics that bind to the peptidyl transferase centre (chloramphenicol, azithromycin, erythromycin, lincomycin, and clindamycin) show significant inhibition of the ribosome-stimulated GTPase activity of HflX. Interestingly, the aminoglycoside tobramycin also showed a moderate inhibitory effect, whereas other aminoglycosides had no effect on GTP hydrolysis. This information demonstrates that HflX is indeed a target for antibiotic inhibition.

To assess if this inhibition is due to modulation of the nucleotide binding properties of HflX while bound the ribosome, a pre-steady state analysis was carried out, monitoring fluorescent nucleotide association to and dissociation from HflX in the presence of 50S ribosomal subunits. To confirm that antibiotics do not affect binding of HflX to the ribosome, microfiltration assays along the lines of previous experiments were performed (Chapter 4 of this work), and suggest that ribosome binding is not affected.

Furthermore, in an effort to localize a potential binding site for HflX on the 70S ribosomal particle, crosslinking experiments utilizing HflX conjugated to the UV-inducible photolabile crosslinking reagent 4-azidophenacyl bromide (AzP) revealed that HflX interacts with ribosomal proteins L2, L5, and S18. Interestingly, L2 is located in close proximity to the peptidyl transferase centre, thus suggesting that the presence of antibiotics targeting this region may cause a conformational change in L2 and thus interfere with the GTPase activation of HflX by the 50S subunit. Based on the available crosslinking data and the structural information available on HflX, the potential binding site for HflX would overlap with that of IF-3; thus, the effect of IF-3 on GTP hydrolysis by HflX in the presence of 70S ribosomes was examined. Surprisingly, IF-3 further stimulated GTP hydrolysis by ~ 2 fold (2 fold molar excess IF-3 compared to HflX).

Overall, this indicates a new ribosome binding site for a translational GTPase near the ribosomal E-site, and a potentially new mode of GTPase activation by the 50S subunit that may occur via a communication network from the peptidyl transferase centre through ribosomal protein L2. To examine a potentially new mechanism for GTPase activation, 50S and 70S ribosomes were depleted of L7/L12 (required for GTPase activation of A-site factors) along the lines of previous studies (Savelsbergh et al., 2000). In the presence of depleted ribosomes, the GTPase-stimulated activity of EF-G was reduced ~ 2 fold, while no effect was observed on the ribosome-stimulated GTPase activity of HflX. Further research is required to determine the exact functional requirement on the ribosome for GTPase activation of HflX; for example, cleavage of the GTPase activating centre (GAC) via sarcin or ricin along the lines of previous experiments (Garcia-Ortega et al., 2010).

5.2 Experimental Procedures

5.2.1 Materials

Antibiotics were purchased from BioBasic or Sigma. 50 or 100 mM stocks of antibiotics were made in either $TAKM_7$ (50 mM Tris-Cl pH 7.5 at 20 °C, 70 mM NH_4Cl, 30 mM KCl, 7 mM $MgCl_2$) buffer (kanamycin, paromomycin, streptomycin, tobramycin, hygromycin B, spectinomycin, neomycin, fusidic acid, lincomycin, clindamycin, and fusidic acid), 50% v/v $TAKM_7$/ethanol (azithromycin and erythromycin), or 100% ethanol (chloramphenicol and tetracycline), and diluted to working solutions with $TAKM_7$. All experiments were performed such that ethanol concentrations were less than 3% v/v. Control experiments with only ethanol were also performed and revealed no significant influence on GTP hydrolysis.

5.2.2 GTP hydrolysis assays

GTP hydrolysis assays were performed as described in section 3.2.7. Rates were calculated from the slope of each time course of GTP hydrolysis. IC_{50} values were calculated based on the initial rate of GTP hydrolysis at various concentrations of antibiotic.

5.2.3 Microfiltration of HflX•Rb•antibiotic complexes

To examine the effect of peptidyl transferase centre antibiotics on binding of HflX to 50S ribosomal subunits, microfiltration assays were carried out as described in section 4.2.2, in the presence of 500 μM antibiotic.

5.2.4 Pre-steady state kinetics

Mant-nucleotide binding and dissociation constants were determined as outlined in section 4.2.4, in the presence of 500 μM antibiotic.

Table 5.1. Antibiotics Examined for Inhibition of HflX.

Antibiotic (abbreviation)	Target	Classification	Step Inhibited
Kanamycin (Kan)	30S	Aminoglycoside	Translocation
Paromomycin (Par)	30S	Aminoglycoside	Initiation and elongation
Streptomycin (Strp)	30S	Aminoglycoside	Interferes with $tRNA_i$ binding
Tobramycin (Tob)	30S	Aminoglycoside	Translocation
Hygromycin B (HygB)	30S	Aminoglycoside	Translocation
Spectinomycin (Spec)	30S	Aminocyclitol	Translocation
Neomycin (Neo)	30S	Aminoglycoside	Translocation
Chloramphenicol (Cam)	50S	Phenicol	Blocks peptidyl transfer
Azithromycin (Azi)	50S	Azalide	Blocks peptidyl transfer
Erythromycin (Ery)	50S	Macrolide	Blocks peptidyl transfer
Lincomycin (Linc)	50S	Lincosamide	Blocks peptidyl transfer
Clindamycin (Clin)	50S	Lincosamide	Blocks peptidyl transfer
Tetracycline (Tet)	30S	Polyketide	Blocks aa-tRNA delivery
Fusidic Acid (Fus)	EF-G	Cyclic oligopeptide	Traps EF-G•GDP on the ribosome
Puromycin (Pur)	30S	aa-tRNA analog	Blocks peptide chain synthesis

5.2.5 UV-inducible crosslinking

HflX was labeled with the Cys-specific crosslinking reagent 4-azidophenacyl bromide (AzP). Briefly, 100 µM HflX was incubated with 300 µM AzP at 4 °C for 24 h. The sample was then dialyzed against $TAKM_7$ high salt buffer (50 mM Tris-Cl pH 7.5 at 20 °C, 70 mM NH_4Cl, 600 mM KCl, 7 mM $MgCl_2$) overnight to remove unreacted AzP. Small aliquots were flash frozen and stored at -80 °C prior to use. Complexes were formed in 20 µL volumes (100 pmol AzP-HflX, 20 pmol 70S Rb, with or without 10 000 pmol nucleotide and 20 000 pmol chloramphenicol) at 37 °C for 15 min in $TAKM_7$ buffer. Samples were then briefly placed on ice for 5 min, and diluted to 500 µL with $TAKM_7$. Samples were then subjected to microfiltration (Section 5.2.3) until 20 µL remained. 10 µL samples were placed in 96 well microtiter plates, and exposed to 365 nm UV light (Spectroline model ENF-280C UV light) placed ~ 1 cm above the sample for 15 min at 4 °C. Samples were then analyzed by SDS-PAGE fixed for 10 min in 50% v/v EtOH, 2% w/v H_3PO_4 and stained with 20% v/v MeOH, 10% w/v H_3PO_4, 10% w/v NH_4SO_4, and 0.1% w/v Coomassie G-250. Samples not exposed to UV light were also analyzed as a control. Crosslinks were excised from the SDS-PAGE gels and analyzed by mass spectrometry (University of Alberta).

5.2.6 Depletion of L7/L12 from ribosomal particles

50S and 70S ribosomal particles were depleted of L7/L12 essentially as previously described (Savelsbergh et al., 2000). Briefly, 450 pmol of 50S ribosomal particles was diluted in buffer $TAKM_7$ (final volume 450 µL). 250 µL depletion buffer was added (25 mM Tris-Cl pH 7.8 at 4°C, 10 mM $MgCl_2$, 500 mM NH_4Cl, 50% v/v ethanol). Samples were incubated on ice for 10

min; an additional 250 µL depletion buffer was added. After mixing followed by an additional 5 min incubation on ice, samples volumes were adjusted to 2.2 mL with depletion buffer and centrifuged at 80 000 xg for 24 h in a Beckman TLA 100.3 rotor. Ribosome pellets were resuspended in 50 µL $TAKM_7$. Concentrations of the resulting ribosome solution were determined via spectrophotometry at 260 nm using extinction coefficients of 39 103 438 and 25 457 162 $M^{-1}cm^{-1}$ for 70S and 50S particles respectively. Proteins present in supernatants were precipitated with 8 mL ice-cold acetone at -20 °C and centrifuged at 15 000 xg for 30 min. Pellets were resuspended in 20 µL 8 M urea and examined via SDS-PAGE.

5.3 Results

5.3.1 Antibiotic inhibition of HflX

As an initial screen for potential inhibitors of the ribosome-stimulated GTPase activity of HflX, the effect of several 30S and 50S-specific antibiotics were examined at a concentration of 500 µM. None of these antibiotics completely inhibited the ribosome-stimulated GTPase activity (Figure 5.2) of HflX under these conditions. However, significant decreases in the rate of GTP hydrolysis (14-21 fold) were observed in the presence of azithromycin, erythromycin, lincomycin, and clindamycin, which bind to the peptidyl transferase centre of the 50S ribosomal subunit (Bulkley et al., 2010; Dunkle et al., 2010; Hansen et al., 2002; Schlünzen et al., 2003), along with chloramphenicol (3.4 fold inhibition). Interestingly, although it is specific to the 30S subunit, the aminoglycoside tobramycin also exhibited inhibited ribosome-stimulated GTPase activity to a similar extent compared to chloramphenicol (3.4 fold inhibition). The macrolide erythromycin and its azalide derivative azithromycin exhibited slightly less potent inhibition (14 fold and 6-8 fold inhibition for 70S and 50S experiments respectively) compared to the

lincosamides lincomycin and clindamycin (16-21 fold and 10-12 fold for 70S and 50S experiments respectively). The observed inhibitory effects are presented in Table 5.2. In order to assess the efficiency with which these antibiotics inhibit the ribosome-stimulated GTPase activity of HflX, 50% inhibitory concentrations (IC_{50}) were determined by examining the rate dependence of GTP hydrolysis in the presence of 70S ribosomes and 50S subunits at various concentrations of antibiotics. Only those antibiotics that showed a greater than 2 fold inhibitory effect were examined: chloramphenicol, which has previously been described (Shields et al., 2009), lincomycin, clindamycin, azithromycin, and erythromycin. IC_{50} values for chloramphenicol were significantly larger compared to the lincosamides clindamycin and lincomycin, which in turn were greater than the azalide/macrolides (erythromycin and azitrhomycin). Interestingly, the IC_{50} values describing the inhibition of the 70S-stimulated GTPase were 15-25 fold lower for azithromycin and erythromycin compared to the 50S experiment, while a 3-12 fold difference was observed for the lincosamide antibiotics. IC_{50} values for lincomycin, clindamycin, azithromycin, and erythromycin are comparable to the binding affinities of the various antibiotics interacting with the 70S ribosome, and are significantly lower than the minimum inhibitory concentrations (MICs) required to prevent bacterial growth (Table 5.3). Chloramphenicol, by contrast, has a higher IC_{50} than the MIC value for growth inhibition of *E. coli;* the IC_{50} value is consistent with the binding affinity of the antibiotic for the peptidyl transferase centre. Data are summarized in table 5.3. None of the antibiotics examined had any effect on binding to the 50S subunit (as studied by microfiltration; Figure 5.2E).

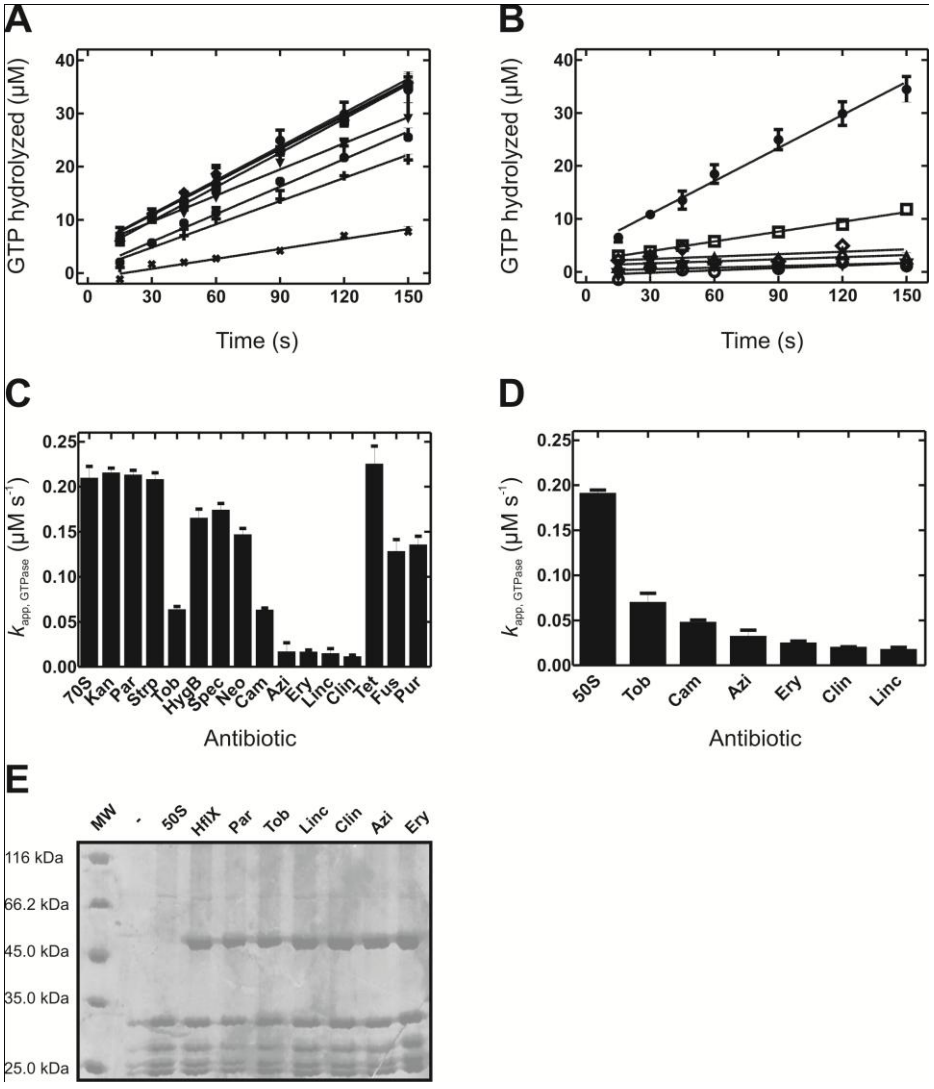

Figure 5.2. Antibiotic Inhibition of HflX.

A) Time courses of GTP hydrolysis by HflX in the presence of 70S ribosomes and 500 μM aminoglycosides: closed circles, no antibiotic; closed squares, kanamycin; closed triangles, paromomycin; closed diamonds, streptomycin; closed reverse triangles, hygromycin B; x, tobramycin; asterisk, spectinomycin; plus sign, neomycin. Time courses were fit to a linear regression. B) Time courses of GTP hydrolysis by HflX in the presence of 70S ribosomes and 500 μM peptidyl transferase centre antibiotics: closed circles, no antibiotic; open squares, chloramphenciol; open diamonds, azithromycin; open circles, erythromycin; open triangles, lincomycin; open reverse triangles, clindamycin. Time courses were fit to a linear regression. C) Effect of antibiotics on the apparent rate of GTP hydrolysis in the presence of 70S ribosomes (abbreviations are given in table 5.1). Error bars represent standard deviations of the linear fits shown in A) and B); each time course was performed in triplicate. D) Effect of antibiotics on the apparent rate of GTP hydrolysis in the presence of 50S ribosomal subunits. E) Microfiltration of 50S complexes in the presence of various antibiotics.

Table 5.2. GTP Hydrolysis by HflX in the Presence of Ribosomal Particles and Antibiotics.

Antibiotic	GTP hydrolysis rate ($\mu M\ s^{-1}$); + 70S	Ratio of rates of GTP hydrolysis (70S/70S + antibiotic)	GTP hydrolysis rate ($\mu M\ s^{-1}$); + 50S	Ratio of rates of GTP hydrolysis (50S/50S + antibiotic)
None	0.21 ± 0.01	1	0.19 ± 0.01	1
Kan	0.21 ± 0.01	1	N/D	N/D
Par	0.21 ± 0.01	1	N/D	N/D
Strp	0.21 ± 0.01	1	N/D	N/D
Tob	0.062 ± 0.004	3.4	0.067 ± 0.011	2.8
HygB	0.16 ± 0.01	1.3	N/D	N/D
Spec	0.17 ± 0.01	1.2	N/D	N/D
Neo	0.15 ± 0.01	1.4	N/D	N/D
Cam	0.062 ± 0.004	3.4	0.046 ± 0.004	4.1
Azi	0.015 ± 0.001	14	0.031 ± 0.008	6.1
Ery	0.015 ± 0.004	14	0.023 ± 0.004	8.3
Linc	0.013 ± 0.006	16	0.016 ± 0.004	12
Clin	0.010 ± 0.001	21	0.019 ± 0.002	10
Tet	0.23 ± 0.02	0.91	N/D	N/D
Fus	0.13 ± 0.01	1.6	N/D	N/D
Pur	0.13 ± 0.02	1.6	N/D	N/D

N/D, not determined

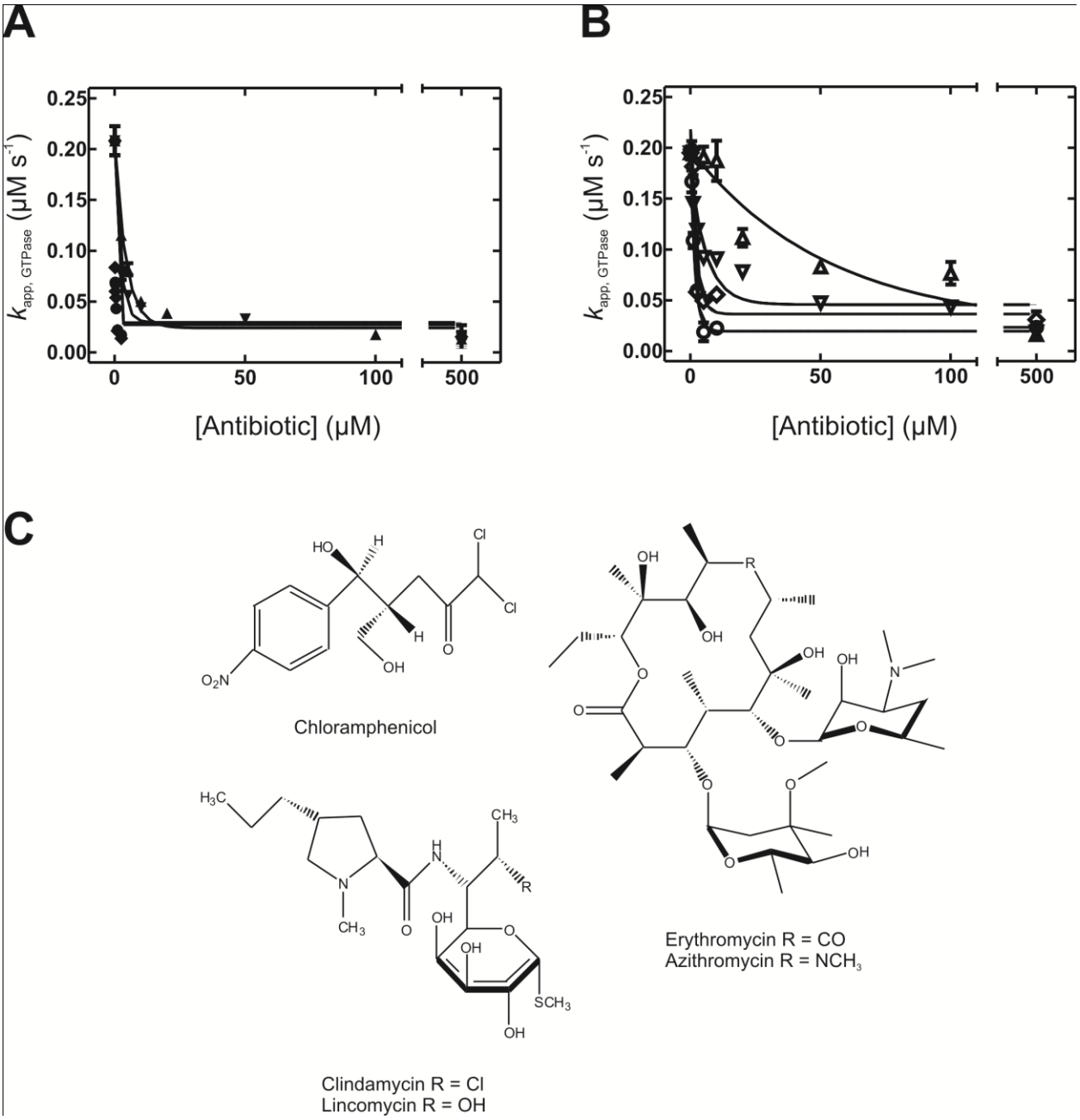

Figure 5.3. HflX Inhibition by Peptidyl Transferase Centre Antibiotics.

A) Antibiotic concentration dependence of GTP hydrolysis by HflX in the presence of 70S ribosomes and B) 50S ribosomal subunits. Diamonds, azithromycin; circles, erythromycin; triangles, lincomycin; reverse triangles, clindamycin. Open symbols are in the presence of 50S subunits. C) Structures of peptidyl transferase centre antibiotics.

Table 5.3. IC_{50}s, MICs, and Binding Affinities of Peptidyl Transferase Centre Antibiotics.

Antibiotic	$IC_{50, 70S}$ (μM)	$IC_{50, 50S}$ (μM)	MIC (μM) for *E. coli*	K_D for binding to 70S ribosomes (μM)
Cam	150 ± 32	210 ± 22	0.97-3.9 (Feldman and Manning, 1983)	2 (A-site); 200 (peptidyl transferase centre)*
Azi	0.06 ± 0.03	1.5 ± 0.4	11 (Chayani et al., 2009)	0.020 - 0.050†
Ery	0.07 ± 0.03	1.1 ± 0.4	44 (Werner et al., 1978)	0.075 – 0.52†
Clin	1.5 ± 0.7	4.4 ± 1.1	220 (Douthwaite, 1992)	1.0-5.0†‡
Linc	3.0 ± 0.9	37 ± 7.5	4500 (Douthwaite, 1992)	5.0†‡

* From references (Long and Porse, 2003; Schlunzen et al., 2001)
† Dependent on ionic strength and presence of polyamines (Douthwaite, 1992; Kouvela et al., 2006; Petropoulos et al., 2008; Petropoulos et al., 2009)
‡ Affected by mutations in rRNA residues in the peptidyl transferase centre (Douthwaite, 1992)

5.3.2 Dissociation of mant-nucleotides from HflX•Rb•Antibiotic complexes

The initial screen for antibiotic inhibitors of HflX indicated that the 50S/70S-stimulated GTPase activity is strongly inhibited by those antibiotics that bind to the peptidyl transferase centre, but these antibiotics have no effect on HflX binding to ribosomal particles. To examine if this effect is due to altering the binding of guanine nucleotides to HflX or adoption of the proposed GTPase activated state, a pre-steady state analysis of the interaction between HflX•ribosome complexes and guanine nucleotides was performed in the presence of 500 μM antibiotic. These studies were performed along the lines of experiments performed in sections 4.3.2 and 4.3.3.

Fluorescence traces representative of the dissociation of mant-GDP from HflX•mant-GDP•50S•antibiotic complexes (Figure 5.4A) were best fit with a single exponential function, which describes a single step dissociation as described by the scheme below. These experiments showed that the signal amplitudes of experiments in the presence of chloramphenicol, lincomycin, or azithromycin were ~ 6 fold smaller compared to the same experiment lacking antibiotic. However, the obtained rate constants did not vary more than ~ 2 fold compared to the control experiment lacking antibiotic (Table 5.4). The obtained mant-GDP dissociation rate constant for experiments in the presence of chloramphenicol were slightly lower ($k_{-1,\,GDP}$ = 0.31 ± 0.03 s^{-1}) than experiments lacking antibiotic ($k_{-1,\,GDP}$ = 0.53 ± 0.01 s^{-1}), whereas experiments in the presence of azithromycin and lincomycin yielded slightly larger rate constants ($k_{-1,\,GDP}$ = 0.75 ± 0.08 s^{-1} and 1.2 ± 0.12 s^{-1} respectively).

$$\text{HflX + mant-GDP} \underset{k_{-1}}{\overset{k_1}{\leftrightarrow}} \text{HflX•mant-GDP} \qquad \text{(Scheme 1)}$$

Fluorescence traces describing the dissociation rate constants for mant-GDPNP dissociating from HflX•mant-GDPNP•50S•antibiotic complexes (Figure 5.4B) were best fit with two exponential functions. These data best describe a two-step dissociation mechanism, outlined in Scheme 2 (as per Scheme 1 in Chapter 4).

$$\text{HflX + mant-GDPNP} \underset{k_{-1}}{\overset{k_1}{\leftrightarrow}} \text{HflX•mant-GDPNP} \underset{k_{-2}}{\overset{k_2}{\leftrightarrow}} \textit{HflX•mant-GDPNP} \qquad \text{(Scheme 2)}$$

Unlike in mant-GDP dissociation experiments, the fluorescence amplitude changes were higher in the presence of antibiotics, particularly in the presence of chloramphenicol (~ 8 fold).

Rate constants describing mant-GDPNP dissociation varied to a greater degree compared to mant-GDP dissociation rate constants: in the presence of chloramphenicol, mant-GDPNP dissociation ($k_{-1,\ GDPNP}$) is ~ 5 fold faster (0.055 ± 0.007 s^{-1}), while in the presence of clindamycin, this rate is 3 fold slower (0.0040 ± 0.0006 s^{-1}) compared to the same experiment without antibiotic (0.012 ± 0.004 s^{-1}). The second fluorescence phase ($k_{-2,\ GDPNP}$) again showed little difference between the various antibiotics compared to the experiment with no antibiotic ($k_{-2,\ GDPNP}$ = 0.0012 ± 0.0001 s^{-1}), with the greatest effect (~ 7 fold faster) again in the presence of chloramphenicol ($k_{-2,\ GDPNP}$ = 0.0086 ± 0.0006 s^{-1}). The fluorescence traces in the presence of chloramphenicol did have a 2-3 fold increase in the amplitude of the observed fluorescence signal. Comparison of the various dissociation rates revealed that the rate constants of mant-GDPNP dissociation vary from 5 fold faster (in the presence of chloramphenicol) to 3 fold slower (in the presence of clindamycin), while values for k_{-2} are ~ 10 fold larger (in the presence of chloramphenicol) to only slightly lower (in the presence of lincomycin).

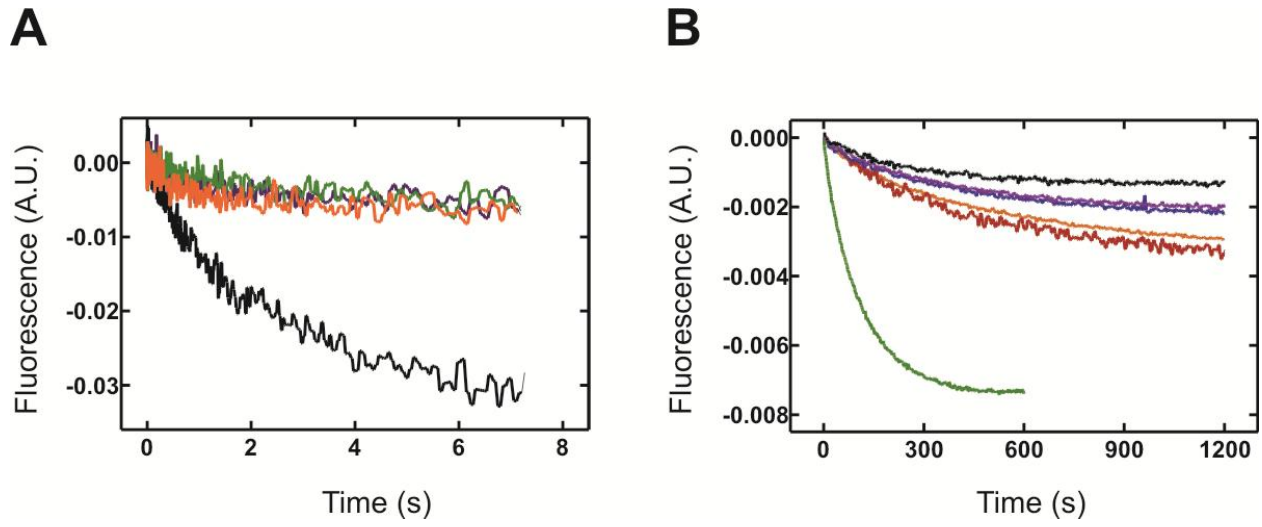

Figure 5.4. Dissociation of mant-nucleotides from HflX•mant-nucleotide•50S•Antibiotic Complexes.

A) Fluorescence traces for the dissociation of mant-GDP from HflX•mant-GDP•50S complex (black) in the presence of chloramphenicol (green), lincomycin (orange), or azithromycin (purple). B) Fluorescence traces for the dissociation of mant-GDPNP from HflX•mant-GDPNP•50S complex (black) in the presence of chloramphenicol, lincomycin, azithromycin (as above), clindamycin (red), or erythromycin (blue).

Table 5.4. Rate Constants for the Dissociation of mant-GDP from HflX•mant-GDP•50S•Antibiotic Complexes.

Antibiotic	$k_{-1,\,GDP}$ (s^{-1})	k_{-1} fold change
None	0.53 ± 0.01	1.0
Cam	0.31 ± 0.03	1.7
Azi	0.75 ± 0.08	0.71
Linc	1.2 ± 0.12	0.44

Table 5.5. Rate Constants for the Dissociation of mant-GDPNP from HflX•mant-GDPNP•50S•Antibiotic Complexes.

Antibiotic	$k_{-1,\ GDPNP}$ (s^{-1})	k_{-1} fold change	$k_{-2,\ GDPNP}$ (s^{-1})	k_{-2} fold change
None	0.012 ± 0.004	1.0	0.0012 ± 0.0001	1.0
Cam	0.055 ± 0.007	0.22	0.0086 ± 0.0006	0.14
Azi	0.013 ± 0.005	0.92	0.0024 ± 0.0001	0.50
Ery	0.029 ± 0.008	0.41	0.0023 ± 0.0007	0.52
Clin	0.0040 ± 0.0006	3.0	0.0021 ± 0.003	0.57
Linc	0.010 ± 0.001	1.2	0.0016 ± 0.0007	0.75

5.3.3 Association of mant-nucleotides to HflX•Rb•Antibiotic complexes

Association of mant-nucleotides to various antibiotic-bound HflX•50S complexes was examined using the stopped-flow technique. Similar to experiments in the absence of antibiotics, association of mant-GDP resulted in a single exponential increase in fluorescence due to FRET between the intrinsic tryptophan residues of HflX and the mant moiety of mant-GDP, and were fit accordingly. Similar to experiments studying the dissociation of mant-GDP from HflX•50S•antibiotic complexes, the signal amplitudes of observed fluorescence traces were lower compared to similar experiments lacking antibiotic (Figure 5.5A; ~ 3 fold maximum difference for experiments with chloramphenicol). Fitting the concentration dependence of association experiments (Figure 5.5B) with a linear function yielded association rate constants lower than experiments lacking antibiotic (~ 2 fold; summarized in Table 5.6). The *y* axis intercepts, which in section 3.3.2 have been shown to provide accurate estimates for nucleotide dissociation rate constants, were consistently ~ 5 fold higher compared to values determined in the nucleotide dissociation experiments (in Table 5.4).

Experiments examining the association of mant-GDPNP to HflX•50S•antibiotic complexes exhibited two exponential fluorescence traces similar to experiments lacking antibiotics, with ~ 3 fold lower fluorescence signal amplitudes (Figure 5.5C). Only one phase of the two exponential function showed a linear concentration dependence; linear regression of this faster fluorescence signal yielded mant-GDPNP association rate constants for experiments in the presence of antibiotics that were up to ~ 3 fold lower ($7.7 \pm 0.6 \times 10^4$, $4.5 \pm 1.1 \times 10^4$, and $2.9 \pm 0.6 \times 10^4$ $M^{-1}s^{-1}$ in the presence of chloramphenicol, azithromycin, and lincomycin respectively) compared to experiments lacking antibiotic ($k_{+1,\ GDPNP} = 9.2 \pm 1.2 \times 10^4$ $M^{-1}s^{-1}$). Values for the concentration independent fluorescence phase, corresponding to the proposed conformational change in HflX outlined in Chapter 4, had similar rate constants, with chloramphenicol having a ~ 3 fold larger rate constant (0.60 ± 0.09 s^{-1}) compared to control experiments (0.23 ± 0.09 s^{-1}), while azithromycin experiments had a slightly larger rate constant (1.5 fold) and lincomycin experiments showed similar values for $k_{+2,\ GDPNP}$ (rate constants of 0.15 ± 0.05 and 0.23 ± 0.04 s^{-1} respectively). Values obtained from the k_{app} plots of $k_{+1,\ GDPNP}$ provided poor estimates of k_{-1} compared to experimentally determined values (in Table 5.5), especially in experiments with chloramphenicol and lincomycin. Thus, for determining equilibrium dissociation constants, only the experimentally determined rate constants were used.

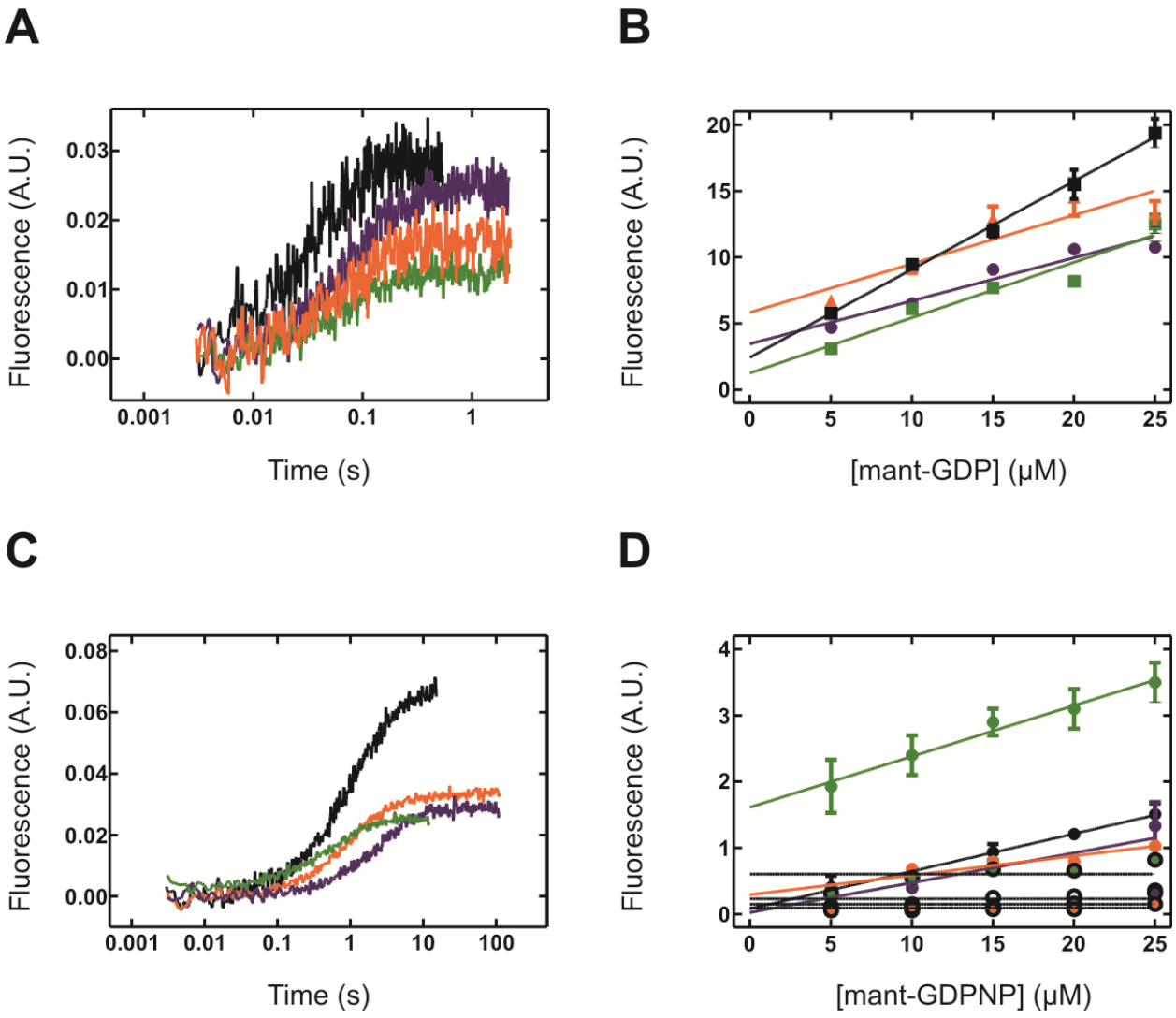

Figure 5.5. Association of mant-nucleotides to HflX•50S•Antibiotic Complexes.

A) Fluorescence traces for the association of mant-GDP (25 μM) to HflX•50S•antibiotic complexes in the absence (black trace) or presence of chloramphenicol (green), lincomycin (orange), or azithromycin (purple). B) concentration dependence of mant-GDP association to HflX•50S•antibiotic complexes. C) Fluorescence traces for the association of mant-GDPNP (25 μM) to HflX•50S•antibiotic complexes (colors as in A). D) k_{app} plot for mant-GDPNP association to HflX•50S•antibiotic complexes.

Table 5.6. Rate Constants for the Association of mant-GDP to HflX•50S•Antibiotic Complexes.

Antibiotic	$k_{+1, GDP}$ ($M^{-1}s^{-1}$)	k_{+1} Ratio (50S/50S + antibiotic)	$k_{-1, GDP}$ from y axis intercept (s^{-1})
None	$6.7 \pm 0.3 \times 10^5$	1.0	2.4 ± 0.4
Cam	$4.2 \pm 0.7 \times 10^5$	1.6	1.3 ± 1.1
Azi	$3.2 \pm 0.5 \times 10^5$	2.1	3.5 ± 0.8
Linc	$3.7 \pm 1.1 \times 10^5$	1.8	5.8 ± 1.7

Table 5.7. Rate Constants for the Association of mant-GDPNP to HflX•50S•Antibiotic Complexes.

Antibiotic	$k_{+1, GDPNP}$ ($M^{-1}s^{-1}$)	k_{+1} Ratio (50S/50S + antibiotic)	$k_{+2, GDPNP}$ (s^{-1})	k_{+2} Ratio (50S/50S + antibiotic)	$k_{-1, GDPNP}$ from y axis intercept (s^{-1})
None	$9.2 \pm 1.2 \times 10^4$	1.0	0.23 ± 0.09	1.0	0.081 ± 0.050
Cam	$7.7 \pm 0.6 \times 10^4$	1.2	0.60 ± 0.09	0.38	1.6 ± 0.1
Azi	$4.5 \pm 1.1 \times 10^4$	2.0	0.15 ± 0.05	1.5	0.025 ± 0.19*
Linc	$2.9 \pm 0.6 \times 10^4$	3.2	0.23 ± 0.04	1.0	0.29 ± 0.10

* Large uncertainty in *y* axis intercept value

Comparison of the nucleotide binding affinities for HflX interacting with mant-GDP or mant-GDPNP (Table 5.8) shows that the K_D value for mant-GDP (calculated from the ratio of $k_{-1, GDP}$ / $k_{+1, GDP}$) does not significantly differ in the presence of chloramphenicol ($K_D = 0.74 \pm 0.14$ μM) compared to experiments lacking antibiotic ($K_D = 0.79 \pm 0.02$ μM), whereas the affinity for mant-GDP is lowered by ~ 4 fold in the presence of either azithromycin or lincomycin (2.3 ± 0.4

and 3.2 ± 1.0 μM respectively). The affinity of HflX•50S•antibiotic complexes for mant-GDPNP is reduced in the presence of antibiotics, with a 15 fold decrease in affinity in the presence of chloramphenicol (K_D = 10 ± 2.1 nM) compared to experiments lacking antibiotic, which have a calculated sub-nanomolar affinity (0.68 ± 0.37 nM). Azithromycin and lincomcyin had a similarly lowered (approximately 10 fold) affinity for mant-GDPNP (K_D values of 4.6 ± 2.4 and 2.4 ± 1.2 nM). This indicates that the presence of the appropriate antibiotic may induce a conformational change in the ribosome that reduces the affinity of HflX for mant-GDPNP. This likely occurs due to interference of the initial binding step (k_{+1}, table 5.7) as opposed to the subsequent conformational change in HflX (reflected by k_{+2} and k_{-2}, which vary only ~ 2 fold compared to experiments in the absence of antibiotic).

Table 5.8. Equilibrium Dissociation Constants Governing the Interaction between mant-nucleotides and HflX while Bound to 50S Ribosomal Particles.

Antibiotic	$K_{D, GDP}$ (μM)	Ratio (50S/50S + antibiotic)	$K_{D, GDPNP}$ (μM)	Ratio (50S/50S + antibiotic)
None	0.79 ± 0.02	1.0	0.00068 ± 0.00037	1.0
Cam	0.74 ± 0.10	1.1	0.010 ± 0.002	0.068
Azi	2.3 ± 0.4	0.34	0.0046 ± 0.0024	0.15
Linc	3.2 ± 1.0	0.25	0.0024 ± 0.0012	0.28

5.3.4 Crosslinking of HflX to ribosomal proteins

In order to determine a potential ribosome binding site for HflX, the protein was reacted with the cysteine-specific photolabile crosslinking reagent 4-azidophenacyl bromide (AzP; Figure 5.6A), an approach previously utilized to study (for example) the interaction between EF-G and

the *E. coli* ribosome (Nechifor, 2007). *E. coli* HflX contains three intrinsic cysteine residues at positions 96, 98, and 415 that may react with AzP and thus become potential probes for the interaction with various ribosomal components. Upon exposure to UV light, proteins within ~ 11 Å of the cysteine residue may react with the AzP-conjugated protein. HflX•ribosome complexes were pre-formed in the presence of various nucleotides and with or without chloramphenicol. Incubation of complexes in the absence of UV light caused no additional bands to be observed upon separation by SDS-PAGE (70S control in Figure 5.6B, 70S -UV). However, upon UV light exposure, several additional bands of molecular masses higher than HflX were reproducibly observed in several experiments when visualized with Coomassie Brilliant Blue, independent of the complex formed (Figure 5.5B). These bands were excised and analyzed by mass spectrometry. Table 5.9 shows the identity of potential crosslinks based on mass spectrometric analysis of peptide fragments found in each band after proteolysis. In all experiments, a high molecular mass band of ~ 100 kDa was observed, that was found to only contain peptide fragments from HflX in all complexes examined, indicating the formation of an HflX•HflX dimer. In 70S complexes, the second high molecular mass band (Figure 5.6, band 1) also contained 9 distinct peptides from ribosomal protein L2 (29.9 kDa), covering 42.1% of the primary sequence of L2. Additional, lower intensity crosslinks containing peptides from L5 (Figure 5.6, band 2, 4 distinct peptides with 30.3% coverage) and S18 (Figure 5.6, band 3, 2 distinct peptides with 35.1% coverage) were also observed in 70S complexes. By contrast, no distinct peptides from ribosomal proteins were identified in 50S experiments, while in 30S complexes, an additional S18 crosslink with a single distinct peptide was identified (18.9% coverage). These data indicate that HflX crosslinks to proteins near the ribosomal E-site, and may suggest different conformations of HflX on the 70S compared to the 50S-bound complexes.

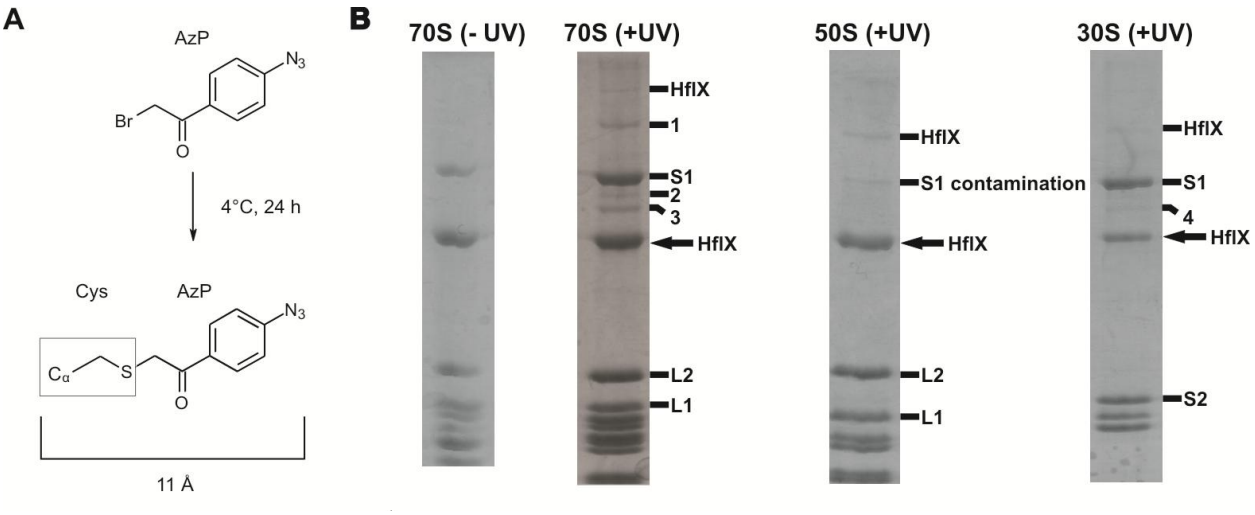

Figure 5.6. Crosslinking of AzP-HflX to Ribosomal Particles.

A) 4-azidophenacyl bromide chemistry. Reaction of 4-azidophenacyl bromide with cysteine residues forms a photolabile crosslinkable conjugate with a probing range of ~ 11 Å. (B) left, AzP-HflX complex without UV irradiation. AzP-HflX-ribosome complexes formed crosslinks (higher molecular mass band labeled HflX is an HflX-HflX crosslink; bands 1, 2, and 3 are indicated) in the presence of 70S ribosomes, 50S ribosomal subunits (only the HflX-HflX crosslink was observed), and 30S subunits (HflX-HflX crosslink and band 4). Contamination of the 50S subunit preparation with ribosomal protein S1 was detected (as determined by mass spectrometry). Identical crosslinks were observed regardless of nucleotide bound or the presence of chloramphenicol (data not shown). Additional ribosomal proteins (S1, S2, L1, and L2) were identified by mass spectrometry and are labeled.

Table 5.9. HflX-Ribosomal Protein Crosslink Identification by Mass Spectrometry.

Band	Description	Distinct peptides	Coverage (%)	Intensity
1	L2	9	42.1	+++
2	L5	4	30.3	+
3	S18	2	35.1	++
4	S18	1	18.9	+

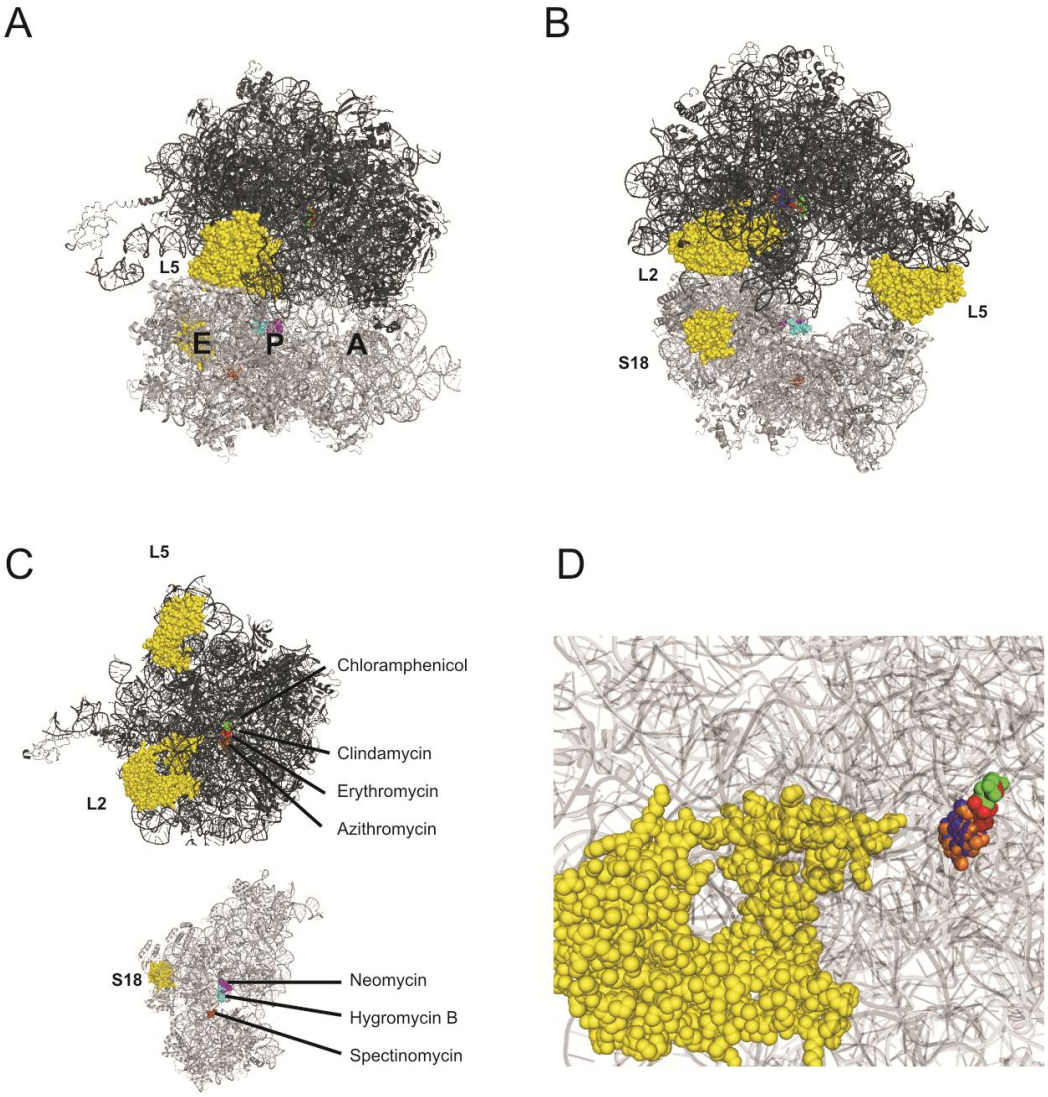

Figure 5.7. Binding Sites of Ribosomal Antibiotics and HflX Crosslinks.

Cartoon representation of rRNA with HflX-ribosomal protein crosslinks. A) Crosslinks of HflX to ribosomal proteins L2, L5, and S18 with respect to the ribosomal A, P, and E-sites. B) View of ribosomal crosslinks from the ribosomal E-site. C) View of the 50S (top) and 30S (bottom) subunits from the subunit interface. Antibiotics are labeled. D) Zoomed-in view of L2 in relation to the peptidyl transferase centre antibiotics (50S cartoon images made transparent). In all figures, the 50S ribosomal subunit is shown in dark grey; the 30S, in light grey. Antibiotics, shown as spheres, are chloramphenicol (green), azithromycin (orange), erythromycin (blue), clindamycin (red), hygromycin B (cyan), spectinomcyin (brown), and neomycin (purple). Antibiotics were superimposed using PYMOL on ribosomes using PDB files 2QAL (Neomycin, 30S), 2QOY (Spectinomycin, 30S), 3DF1 (Hygromycin B, 30S), 3OFR (Erythromycin, 50S), 3OFZ (Clindamycin, 50S), 3OHZ (Azithromycin), and 3OFC (Chloramphenicol, 50S). From references (Borovinskaya et al., 2007a; Borovinskaya et al., 2008; Borovinskaya et al., 2007b; Bulkley et al., 2010; Dunkle et al., 2010).

The locations of crosslinks to L2, S18, and L5 are distant from the ribosomal A-site common to other known TRAFAC GTPases, and are located near the ribosomal E-site. This information, combined with the replacement of the catalytic His residue in the switch II region of the canonical GTPases with a Phe residue in HflX and the observation that HflX lacks common structural domains crucial for interacting with the ribosomal GTPase activating centre indicates that the ribosome might possess an additional GTPase activating site. Ribosomal protein L7/L12 is an essential requirement for the ribosome-stimulated GTPase activity of EF-G (Datta et al., 2005; Savelsbergh et al., 2005a; Savelsbergh et al., 2000) and EF-Tu (Diaconu et al., 2005; Kothe et al., 2004). To examine if L7/L12 influences the ribosome-stimulated GTPase activity of HflX, L7/L12 was depleted by washing 50S ribosomal subunits with NH_4CL and EtOH, conditions which remove L7/L12, along the lines of previous assays (Savelsbergh et al., 2000). In a preliminary assay, examining the 50S-stimulated GTPase activity of HflX and EF-G (Figure 5.8) demonstrates that EF-G alone does not have any significant GTPase activity in the absence of 50S ribosomes ($k_{app,\ GTPase} \sim 0.0002\ \mu M\ s^{-1}$), whereas in the presence of 50S subunits, the rate of hydrolysis increases 1000 fold ($k_{app,\ GTPase} = 0.20 \pm 0.01\ \mu M\ s^{-1}$). In the presence of 50S subunits treated with 500 mM NH_4Cl and ethanol (conditions that remove L7/L12), this rate is reduced ~ 2-3 fold ($k_{app,\ GTPase} = 0.088 \pm 0.004\ \mu M\ s^{-1}$). By contrast, washing of 50S subunits had no effect on the multiple turnover rate of GTP hydrolysis by HflX, though the rate in this experiment was ~ 25% slower than reported in Figure 5.2 ($k_{app,\ GTPase} = 0.15 \pm 0.01\ \mu M\ s^{-1}$ without NH_4Cl/ethanol treatment and $k_{app,\ GTPase} = 0.14 \pm 0.02\ \mu M\ s^{-1}$ in the presence of NH_4Cl/ethanol washed 50S particles). This may be due to inaccuracies in determining the concentration of L7/L12-depleted ribosomes.

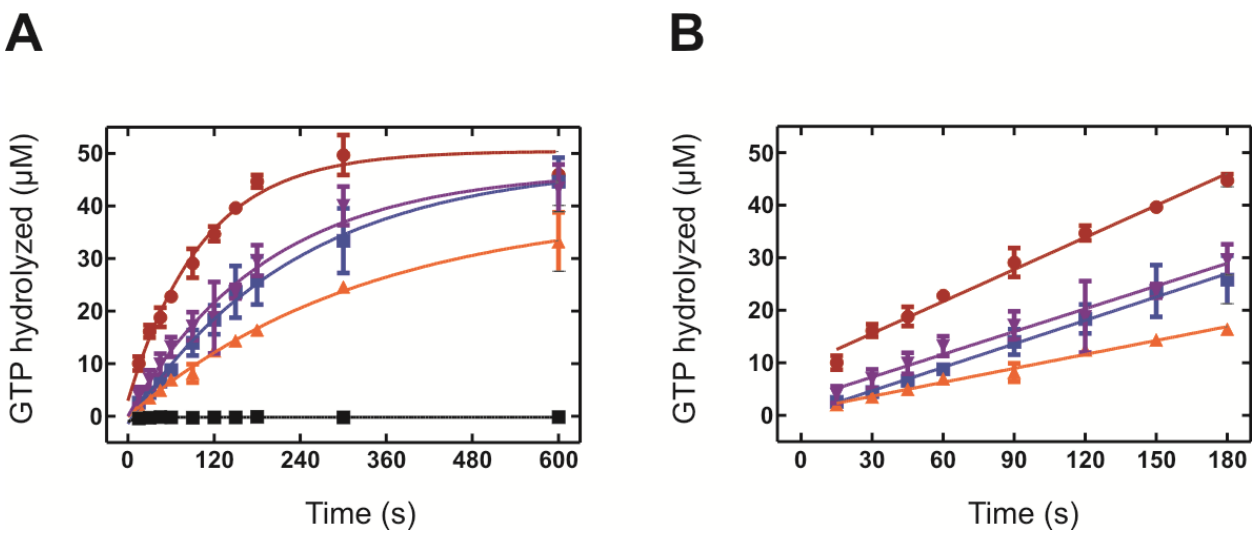

Figure 5.8. Effect of L7/L12 Depletion on the Ribosome-stimulated GTPase activity of HflX and EF-G.

A) Time course for initial rates of GTP hydrolysis by EF-G in the presence of 50S subunits (red), 50S subunits washed with NH_4Cl and ethanol to remove L7/L12 (orange), EF-G alone (black), HflX in the presence of 50S subunits (blue) and 50S subunits washed with NH_4Cl and ethanol (magenta). B) Initial time course for GTP hydrolysis used to calculate the apparent rate of GTP hydrolysis.

Interestingly, extrapolating the potential binding site for HflX based on crosslinking data also indicates that the putative binding site for HflX on the ribosome may overlap with that of initiation factor 3 (Figure 5.9), as shown by X-ray crystallography studies and RNA protection mapping (Moazed et al., 1995; Pioletti et al., 2001). In order to investigate a potential interaction between HflX and IF-3, GTP hydrolysis experiments in the presence of 70S ribosomes were performed (Figure 5.10). IF-3 alone had no significant GTPase activity; nor did HflX alone or HflX in the presence of IF-3. Surprisingly, rather than inhibit GTP hydrolysis by HflX, experiments in the presence of IF-3 and 70S ribosomes further enhanced the GTP hydrolysis rate of HflX by an additional 2-fold (to a maximum rate of 0.38 ± 0.02 μM s^{-1} at 2 μM IF-3 under

these conditions) over the already 1000-fold stimulatory effect by the 70S ribosome (Figure 5.10B).

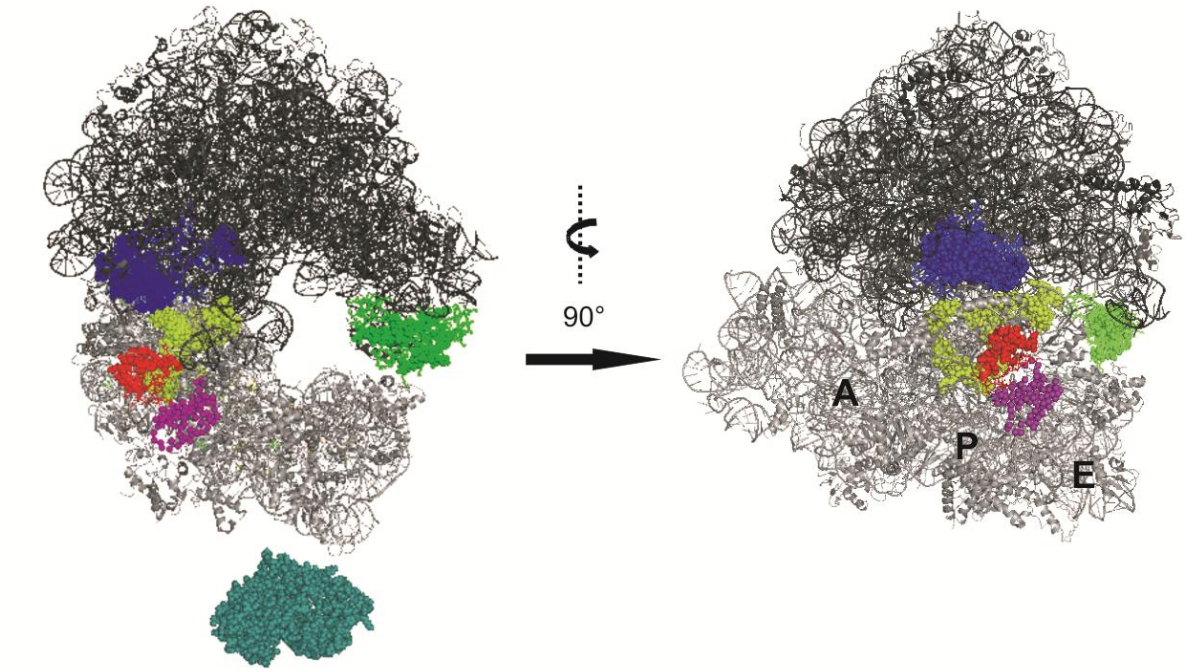

Figure 5.9. Binding Sites of IF-3 on the 30S Subunit Relative to HflX Crosslinks.

Cartoon representation of ribosomal RNA with HflX-crosslinked ribosomal proteins visualizing the binding site of IF-3 relative to HflX crosslinks. The 50S subunit (PDB ID 2AW4) is shown in dark grey, 30S (PDB ID 2AVY) in light grey. Left panel, view from the ribosomal E-site, similar to Figure 5.5B. Ribosomal protein L5 is shown in green, L2 in blue, and S18 in red (stick models). Peptides identified from crosslinking and mass spectrometry analysis are shown as spheres. For perspective, the homology model of HflX is shown below in cyan. The binding site of IF-3 (purple spheres) was visualized by superimposing the crystal structure of IF-3 bound to the 30S subunit (PDB ID 1I96) reported in (Pioletti et al., 2001). 16S rRNA nucleotides protected from chemical protection, determined in (Moazed et al., 1995), are shown as dark yellow spheres.

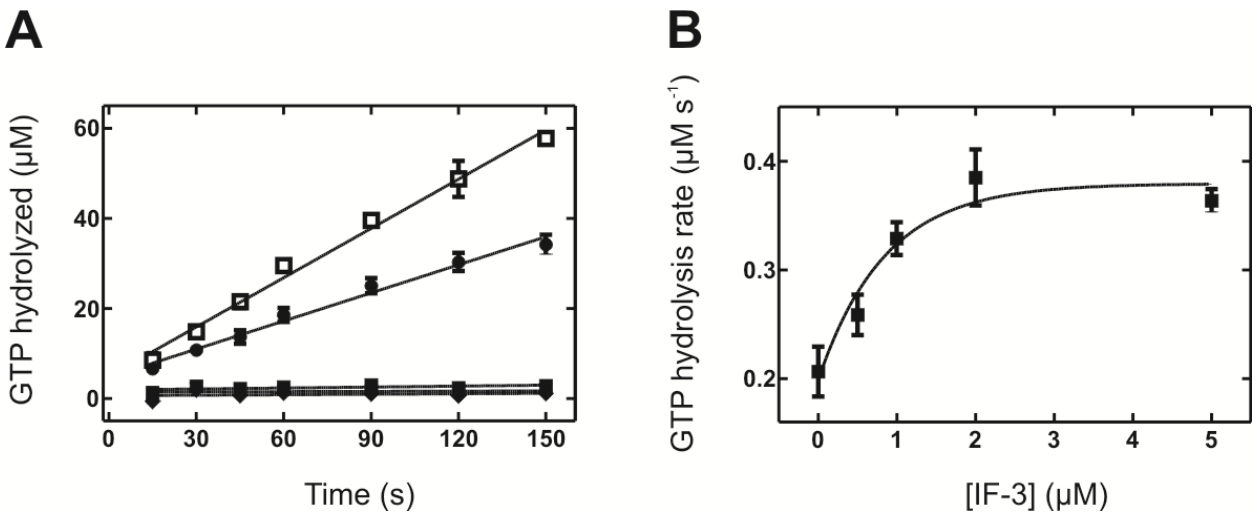

Figure 5.10. GTPase Stimulation of HflX by 70S Ribosomes and IF-3.

A) GTP hydrolysis (125 μM GTP) by 1 μM HflX was monitored alone (closed squares), in the presence of 2 μM IF-3 (closed diamonds), 1 μM 70S ribosomes (closed circles), or in the presence of both 70S ribosomes and IF-3 (open squares). IF-3 alone (closed reversed triangles) had no detectable GTPase activity. B) IF-3 concentration dependence of GTP hydrolysis by HflX in the presence of HflX. IF-3 stimulated the rate of GTP hydrolysis ($k_{GTPase,\ max}$ = 0.38 ± 0.02 μM s^{-1} based on the fit in B) by an additional 2-fold compared to 70S ribosomes alone.

5.4 Discussion

HflX exhibits a 50S and 70S ribosome-stimulated GTPase activity that is also exhibited by the known TRAFAC GTPases IF-2, EF-Tu, EF-G, RF-3, LepA, BipA, Tet(O), and SelB. This GTPase activity of HflX has been shown to be inhibited by the peptidyl transferase centre antibiotic chloramphenicol (Chapter 3). In an effort to dissect the functional role of GTP hydrolysis by HflX, additional antibiotics were screened for inhibitory effects on GTPase activation. Interestingly, antibiotics of different classes (a phenicol, lincosamides, and a macrolide and ketolide derivative) that interact with the peptidyl transferase centre are inhibitors of the ribosome-stimulated activity of HflX. Additionally, the aminoglycoside tobramycin also exhibited a modest inhibitory effect. However, other inhibitors of TRAFAC GTPases (tetracycline, which binds EF-Tu (Heffron et al., 2006), or fusidic acid, which targets EF-G (Chen et al., 2010)) have no effect on GTPase activation, nor do other aminoglycosides (Streptomycin, for example, reduces both cognate codon-anticodon recognition and GTP hydrolysis by EF-Tu (Gregory et al., 2009; Gromadski and Rodnina, 2004)). By contrast, erythromycin has been shown to have no effect on the ribosome-coupled GTPase activity of EF-G and EF-Tu (Chinali et al., 1988), but is an inhibitor of HflX.

While the pre-steady state analysis of mant-nucleotides interacting with HflX•50S complexes the peptidyl transferase centre antibiotics shows an approximately 10 fold reduction in the affinity for mant-GDPNP and little effect on the interaction with mant-GDP. This is insufficient to fully explain the overall 10-20 fold inhibition in GTP hydrolysis in the presence of these antibiotics. The signal amplitudes of the pre-steady state analysis vary depending on the antibiotic present: mant-GDP experiments show a smaller signal amplitude change in the presence of PTC antibiotics, whereas mant-GDPNP experiments show antibiotics increase the

signal amplitude in mant-GDPNP dissociation experiments yet decrease the signal amplitude in association experiments. Examination of raw fluorescence data of these experiments shows no significant difference in the starting fluorescence of the system, suggesting that PTC antibiotics do not directly influence the structure of HflX bound to the 50S subunit (not shown). Microfiltration assays indicate that binding to the 50S is not influenced by antibiotics. These data suggest that a subpopulation of different complexes exists in these experiments, reflecting different signal amplitudes. This is unlikely, due to saturating concentrations of antibiotics used. It is possible that the changed signal amplitude in these experiments is due to an additional contribution of ribosomal particles to the fluorescence of the system, i.e. that intrinsic tryptophan residues contribute to the energy transfer to the mant group of mant-nucleotides. If the nucleotide binding pocket were on the interface between HflX and the ribosomal particle, any tryptophan residues nearby would contribute to the FRET signal. If the conformation of this region alters due to binding of an antibiotic to the ribosomal particle, such a residue may be more distant from the fluorophore, leading to a decreased fluorescence signal. Thus, it is highly unlikely that antibiotic binding to the 50S subunit has any effect on the structural dynamics of HflX. Rather, the fluorescence amplitude of the system likely differs due to the FRET contribution of the ribosome to the mant group.

Crosslinking data presented here reveals for the first time that HflX crosslinks to ribosomal proteins L2, L5, and S18, which lie in close proximity to the ribosomal E-site. L2 has previously been shown to affect the ATPase activity of the *E. coli* Hsp90 homolog HptG *in vitro* (Motojima-Miyazaki et al., 2010), suggesting that L2 perhaps has some mechanism for activation of NTPase activity of an exogenous factor. It would be of interest to examine if the

GTPase activity of HflX could be stimulated by purified L2; if so, this would demonstrate that an additional ribosomal protein acts as a GTPase modulator.

The additional GTPase stimulation of HflX by IF-3 in the presence of 70S ribosomes is particularly intriguing, and supports crosslinking experiments that indicate a shared or similar binding site for the two factors. However, the observation that IF-3 alone is not capable of stimulating the GTPase activity of HflX may indicate that binding of IF-3 to the ribosome potentially causes a conformational change in the ribosome (perhaps inducing a transint ratcheting motion such as that outlined in Figure 1.6C). This in turn may expose an additional region of the ribosome to HflX, or aid in positioning a catalytic residue. It is tempting, based on this interaction to speculate that HflX has a role in modulating either translation initiation or ribosome recycling. Further studies aimed at reconstituting an HflX•IF-3 binary complex will be required to examine the role of IF-3 as a modulator of the GTPase activity of HflX.

Different antibiotic inhibitors, unique domain architecture, structural replacement of a key conserved His residue with Phe, a unique binding site, and no requirement for L7/L12 for efficient GTPase activation of HflX indicate that a unique catalytic mechanism exists that activates the GTPase activity of HflX. Unlike the A-site TRAFAC factors, which contain the conserved catalytic His residue that is correctly positioned for GTP hydrolysis by the ribosomal GTPase activating centre (GAC) upon interaction with the ribosome (Voorhees et al., 2010b), this factor could potentially be supplied by an external factor. For example, an external Arginine finger could be supplied by a ribosomal protein (in analogy to activation of Ras by its GAPs, reviewed in (Gamblin and Smerdon, 1998)) to stabilize HflX in its GTPase-activated form.

Due to the close proximity of L2 to the peptidyl transferase centre, it is tempting to envision a communication network between the PTC and the putative binding site of HflX. The presence of

a PTC antibiotic could potentially affect communication across this distance (~ 90 Å) by changing the conformation of the 50S ribosome, in particular the externally supplied catalytic residue such that efficient GTP hydrolysis by HflX cannot occur. This may also explain the puzzling fluorescence amplitude variation observed in the pre-steady state analysis; the presence of ribosomal particles may in fact contribute to the observed fluorescence signals due to FRET if the nucleotide binding pocket is indeed located at the interface of HflX and the 50S subunit as proposed (Blombach et al., 2011). Thus, GTPase activation may not be caused by the ribosome inducing a conformational change in HflX, but rather by the conformation of the ribosome itself. Information regarding the occupancy and functional state of the ribosome (i.e. presence of mRNA, aa-tRNA, deacyl-tRNA in various positions in the ribosome) and its effect on the GTPase activation of HflX will be pivotal to further understanding the functional role of HflX.

In summary, a detailed antibiotic-based inhibition study, coupled with structural information, crosslinking experiments, and examination of potential interaction partners (L7/L12 and IF-3) suggests a novel communication pathway through ribosomal protein L2 to HflX that is influenced by the peptidyl transferase centre. This has important implications for understanding the functional role of HflX in the cell, as L2 has been shown to be essential for ribosomal subunit association, as well as binding of aa-tRNA to the ribosomal P-site (Diedrich et al., 2000), which in turn may indicate a role for HflX in subunit association or sensing the functional state of the peptidyl transferase centre. Additionally, L2 has been previously shown to regulate both DNA replication (Chodavarapu et al., 2011) and transcription of DNA (Rippa et al., 2010), which may also indicate a role for HflX in regulating expression of certain proteins, such as those involved in stress response.

6. HflX has a Ribosomal Subunit Anti-association Activity

6.1 Introduction

In an effort to elucidate the three-dimensional structure of HflX bound to the 70S ribosome, HflX•70S ribosome complexes were formed as described in section 5.2 and examined in a cryo-electron microscope (Holger Stark lab at the Max Planck Institute for Biophysical Chemistry). Serendipitously, examination of the resulting micrographs revealed intact 50S and 30S ribosomal subunits with no additional factors attached, but no 70S ribosomes present. As HflX shares a binding site overlapping that of IF-3, which was shown in section 5.3 to further stimulate the GTPase activity of HflX in the presence of 70S ribosomes, the stability of 70S ribosomes was examined using Rayleigh light scattering in the presence of HflX while bound to guanine nucleotides along the lines of previous experiments (Görisch et al., 1976). IF-3 has a potent 70S ribosome anti-association function thought to be key in regulating both translation initiation (Section 1.2.1) and ribosome recycling (Section 1.5.1) and can slowly dissociate ribosomes into 50S and 30S subunits (Hirokawa et al., 2007; Singh et al., 2005b).

Here it is demonstrated that HflX can dissociate 70S ribosomes in a nucleotide-dependent manner (*apo*<GDP<GTP). While hydrolysis of GTP accelerates this process, it is not required for ribosome dissociation as HflX in complex with the non-hydrolyzable GTP analog GDPNP is also capable of dissociating 70S ribosomes to a similar extent, albeit 10 fold more slowly compared to experiments with GTP. Dissociation of 70S ribosomes is inhibited by polyamines, high concentrations of Mg^{2+}, and the aminoglycoside paromomycin. However, as paromomycin does not influence GTP hydrolysis (Chapter 5), nor does the phosphate analog vanadate, it is likely that GTP hydrolysis and subsequent release of inorganic phosphate are not required for efficient ribosome dissociation. Given the promiscuous ribosome binding properties of HflX, the

ability of HflX to prevent subunit association was also examined. These experiments suggest that the ribosome dissociation function of HflX is due to preventing subunit re-association; thus, HflX has a similar function to IF-3 in that it functions as an "anti-association" factor (Hirokawa et al., 2007). While HflX functions as a guanine-nucleotide dependent anti-association factor, this activity can be decoupled from its GTPase activity based on aminoglycoside inhibition of 70S dissocation but not GTPase activity. Determining the affinity of the nucleotide bound states of HflX for 30S, 50S, and 70S ribosomal particles will be pivotal for development of a model for this activity and observed preferential association to the 50S subunit *in vivo* (Jain et al., 2009; Polkinghorne et al., 2008).

6.2 Experimental Procedures

6.2.1 Purification of Initiation Factor 3

Initiation factor 3 was purified as an N-terminally 6X His-tagged protein from an *E. coli* expression construct obtained from the National BioResource Project (NBRP (Kitagawa et al., 2005)). The obtained expression construct was grown in LB media supplemented with chloramphenicol (30 μg/mL) at 37 ºC to an OD_{600} of ~ 0.6. Overexpression was induced by addition of IPTG to a final concentration of 1 mM. Cells were grown at 37 ºC until the mid log phase, harvested by centrifugation at 5000 xg, and flash frozen prior to use. To monitor protein expression levels, small culture samples were taken, lysed in 8 M urea, and analyzed by 12% SDS-PAGE. Gels were stained with Coomassie brilliant blue.

Previously frozen cells were resuspended in 7 mL buffer A (50 mM Tris-Cl pH 8.0 at 4 ºC, 60 mM NH_4Cl, 300 mM KCl, 7 mM $MgCl_2$, 7 mM β-mercaptoethanol, 10 mM imidazole, 15% v/v glycerol, 1 mM PMSF) per gram of cells and opened by incubation with 1 mg/mL

lysozyme for 30 min. Sodium deoxycholate was added to a final concentration of 12.5 mg/g of cells. Following an increase in viscosity, several crystals of DNase I were added; resulting in a decrease in viscosity, the cell mixture was centrifuged at 3000 xg (4 ºC) to remove cell debris. The resulting supernatant was centrifuged at 30 000 xg (4 ºC) to obtain a cleared cell lysate. This cleared lysate was applied to Ni^{2+} Sepharose columns (GE Healthcare) equilibrated in buffer A, washed in 50 column volumes buffer A and 50 column volumes buffer B (buffer A with 20 mM imidazole). His tagged initiation factors were eluted with several 90% column volume elutions of buffer C (buffer A with 250 mM imidazole). Fractions containing eluted proteins were pooled prior to size exclusion chromatography: fractions were dialyzed against a 1 000 fold volume of buffer D (50 mM Tris-Cl pH 7.5 at 4 ºC, 70 mM NH_4Cl, 600 mM KCl, 7 mM $MgCl_2$) prior to concentration (Vivaspin 20; 3000 MWCO, Sartorius). Protein samples were then purified by size exclusion chromatography (superdex 75 resin packed in an XK26/100 column, GE Healthcare). Fractions containing the pure initiation factor were pooled and concentrated. Protein concentration was calculated photometrically using an extinction coefficient 4 470 $M^{-1}cm^{-1}$. Protein samples were aliquoted, flash frozen, and stored at -80 ºC prior to use.

6.2.2 Rayleigh Light Scattering

Dissociation of 70S ribosomes into 50S and 30S particles was monitored by Rayleigh light scattering with a KinTek SF-2004 Stopped-flow apparatus at 20 ºC. Samples were illuminated at 436 nm; scattering of light was monitored at 90 º. 25 µL samples containing HflX, nucleotides, initiation factors, and antibiotics (as described in figure captions) in $TAKM_5$ buffer (50 mM Tris-Cl pH 7.5 at 20 ºC, 70 mM NH_4Cl, 30 mM KCl, 5 mM $MgCl_2$) were rapidly mixed with 0.15 µM 70S ribosomes (final concentration) in the same buffer. As a control, ribosomes

were also mixed with an equal volume of TAK buffer (50 mM Tris-Cl pH 7.5 at 20 ºC, 70 mM NH_4Cl, 30 mM KCl), resulting in a decrease in the Mg^{2+} concentration. At 2.5 mM Mg^{2+}, 70S ribosomes completely dissociate (Görisch et al., 1976) (70S = 0 µM at 29% signal decrease). Light scattering signals were normalized with respect to the initial light scattering of the ribosome solution, which is indicative of 100% 70S ribosomes present. The changes in light scattering were fit with either one or two exponential functions (equations 2 and 3), where LS is the light scattering at time t, LS_∞ is the final light scattering value, A is the signal amplitude, and k_{app} is the apparent rate constant for ribosome dissociation.

$$LS = LS_\infty + A_1\exp(-k_{app1}t) \quad \text{(equation 2)}$$

$$LS = LS_\infty + A_1\exp(-k_{app1}t) + A_2\exp(-k_{app2}t) \quad \text{(equation 3)}$$

6.2.3 Nucleotide Hydrolysis Assays

Hydrolysis assays involving polyamines, antibiotics, and initiation factors were performed as previously described in section 3.2.7. Experiments performed in the presence of sodium metavanadate (2 mM) were performed similarly but using thin layer chromatography (TLC) to separate hydrolysis products. Briefly, samples were quenched in 50 µL 6 M formic acid, dried via vacuum centrifugation and resuspended in 10 µL 1:1 6 M formic acid/$TAKM_7$ buffer. 3 µL aliquots were spotted onto CCM Cellulose PEI plates (EMD Chemicals), hydrolysis products were resolved by TLC utilizing 1.5 M KH_2PO_4 pH 3.4 as the mobile phase. Radioactivity was detected using a Typhoon Trio phosphorimager (GE Healthcare). Liberated inorganic phosphate and unhydrolyzed GTP was quantified using ImageJ software (Abramoff et al., 2004).

6.3 Results

6.3.1 HflX induces subunit dissociation in a nucleotide-dependent manner

Initial experiments on 70S ribosome dissociation (Figure 6.1) were performed by rapidly mixing 70S ribosomes (0.15 μM final concentration) in buffer containing 5 mM Mg^{2+} with buffer lacking magnesium. Under these conditions, 70S ribosomes dissociate completely into 50S and 30S subunits (Görisch et al., 1976). Upon mixing 70S ribosomes with $TAKM_5$ buffer, a small ~ 1% decrease in light scattering was observed. By contrast, mixing 70S ribosomes with TAK buffer resulted in a 29% decrease in the light scattering signal at a rate of 0.055 ± 0.001 s^{-1}. In the presence of HflX•nucleotide complexes (1 μM HflX, 125 μM nucleotide final concentrations), the extent of ribosome dissociation as reflected by the change in light scattering signal varied, as did the rate of dissociation. Light scattering signals were best fit with a two exponential function. *Apo* HflX and HflX•GDP dissociated ribosomes to the least extent (~1.5% light scattering change, k_{app1} = 0.027 ± 0.008 s^{-1} and k_{app2} = 0.0038 ± 0.0002 s^{-1} for *apo* HflX; ~ 1.5% LS change, k_{app1} = 0.0069 ± 0.0002 s^{-1} and k_{app2} = 0.0014 ± 0.0002 s^{-1} for HflX•GDP). By contrast, HflX•GDPNP dissociated ribosomes to a greater extent though at approximately the same rate (Depending on the experiment performed, %LS change was between 20 to 25%; k_{app1} = 0.017 ± 0.007 s^{-1} and k_{app2} = 0.0044 ± 0.0002 s^{-1}), while HflX•GTP rapidly split 70S ribosomes to the greatest extent (~ 25 to 30% LS change, k_{app1} = 0.065 ± 0.001 s^{-1} and k_{app2} = 0.0018 ± 0.0001 s^{-1}). The rates of ribosome dissociation by HflX•GTP are approximately equal to the rate of ribosome dissociation by EF-G•GTP and RRF (Hirokawa et al., 2008).

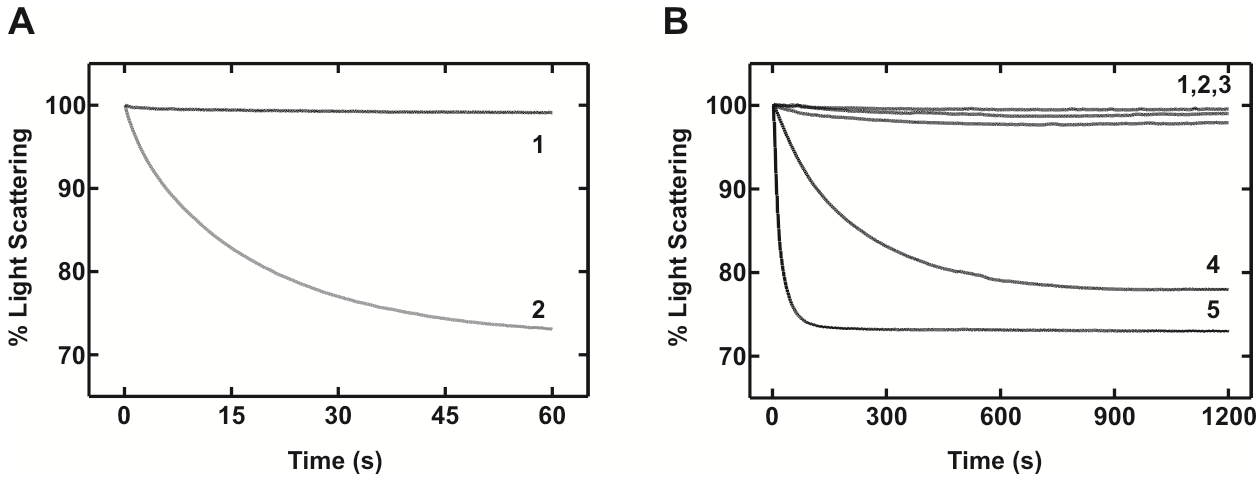

Figure 6.1. 70S Ribosome Dissociation by HflX.

A) 70S ribosomes mixed rapidly with $TAKM_5$ (1) or with with TAK (2). B) 70S ribosomes rapidly mixed with $TAKM_5$ (1), HflX (2), HflX•GDP (3), HflX•GDPNP (4), or HflX•GTP (5).

Ribosome recycling, of the post-termination complex by EF-G and RRF is dependent on the concentration of GTP present (Hirokawa et al., 2008). Exhaustion of GTP in experiments by Hirokawa *et al.* resulted in the re-association of split subunits back into 70S ribosomes, unless IF-3 was present to prevent subunit re-association (Hirokawa et al., 2008). These experiments also demonstrated that increasing concentrations of EF-G not only induced more rapid dissociation of 70S ribosomes, but also induced dissociation to a greater extent (Hirokawa et al., 2008). To examine if HflX-induced subunit dissociation exhibits similar properties, 70S ribosomes were rapidly mixed with increasing concentrations of HflX, in the presence of 125 µM GTP. At low concentrations of HflX, the light scattering signal was monophasic, while at concentrations of HflX greater than 0.3 µM, signals required two exponential functions to fit. Along the lines of experiments with EF-G•GTP and RRF (Hirokawa et al., 2008), the GTP concentration dependence of these experiments (Figure 6.2) yielded estimates for the Michaelis-Menten parameters $K_{M,1}$ and $k_{cat,1}$ values of 3.9 µM and 0.036 min^{-1} and $K_{M,2}$ and $k_{cat,2}$ values of

1.8 μM and 0.0073 min^{-1} respectively. The K_M values are significantly higher than the reported value for the EF-G•GTP RRF recycling system (K_M = 0.59 μM), while k_{cat} is significantly lower (0.35 min^{-1}) (Hirokawa et al., 2008). Additionally, the light scattering signal reached its maximum at 3 μM HflX, at which point the light scattering signal change decreased (Figure 6.2B). These data indicate that similar to the EF-G/RRF ribosome recycling system, increasing amounts of HflX induce greater extents of 70S dissociation, and that hydrolysis of GTP to GDP allows subunit re-association. Preliminary experiments examining the concentration dependence of HflX•GDPNP and HflX•GDP indicate that GDPNP also induces dissociation both at a slower rate and to a lesser extent, while GDP has very little effect on either rate or extent of 70S dissociation (data not shown).

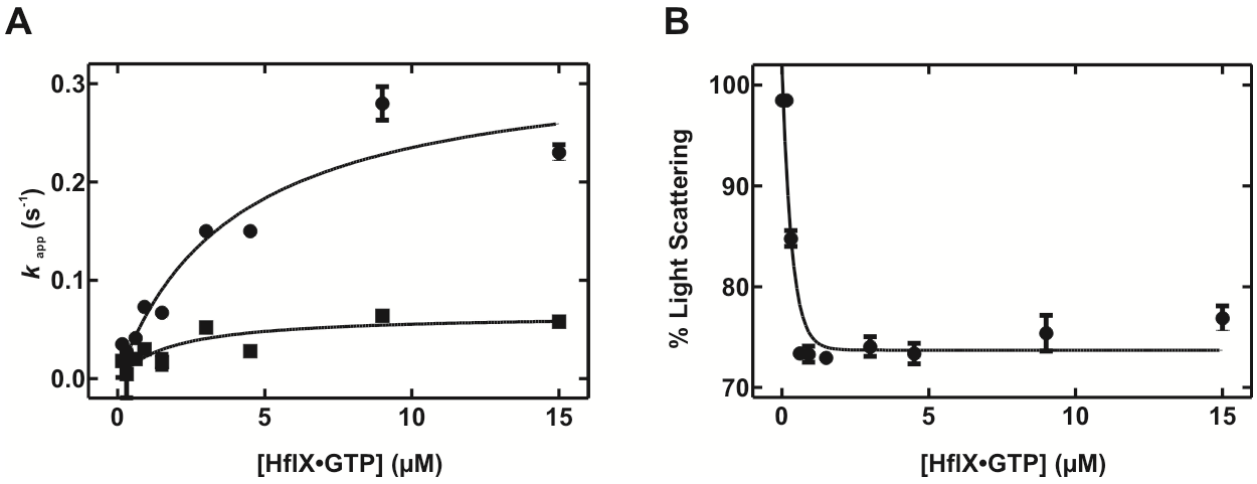

Figure 6.2. 70S Ribosome Dissociation by HflX•GTP.

A) 70S ribosomes mixed rapidly with increasing concentrations of HflX•GTP (black). Apparent rates k_{app1} and k_{app2} are plotted as closed circles and closed squares respectively. B) Change in light scattering at various concentrations of HflX•GTP.

6.3.2 Ribosome stabilizing agents inhibit HflX-induced ribosome dissociation

The nucleotide dependence of ribosome dissociation suggests one of two mechanisms by which HflX splits the ribosome: either through an active dissociation, as in the case of EF-G•GTP RRF recycling of the post-termination complex, or through passive interruption of the equilibrium between ribosomal subunits and the 70S ribosomes. To examine the latter possibility, the effect of the non-specific ribosome stabilizing polyamines spermine and spermidine were examined, along with increasing concentrations of magnesium ions. In the presence of polyamines in buffer $TAKM_5$ (0.6 mM spermine, 0.4 mM spermidine), 70S dissociation is almost completely abolished (Figure 6.3, trace 1); ribosome-stimulated GTP hydrolysis was not affected in buffer containing spermine and spermidine. Polyamines have also been shown to stabilize 70S ribosomes even in the presence of the EF-G•GTP RRF recycling system as well as IF-3 (Hirokawa et al., 2008; Umekage and Ueda, 2006). To confirm the effect of non-specific stabilizing agents on HflX-induced ribosome dissociation, splitting experiments were carried out in buffers containing increasing concentrations of Mg^{2+}. In the presence of 20 mM Mg^{2+}, both the rate and extent of 70S splitting were significantly reduced compared to experiments with lower Mg^{2+} concentrations (Figure 6.3B). The rates of ribosome dissociation in this figure are inconsistent with those reported in Figures 6.1 and 6.2, possibly due to a new preparation of ribosomes being used. However, the stabilizing effect of Mg^{2+} is still clearly shown.

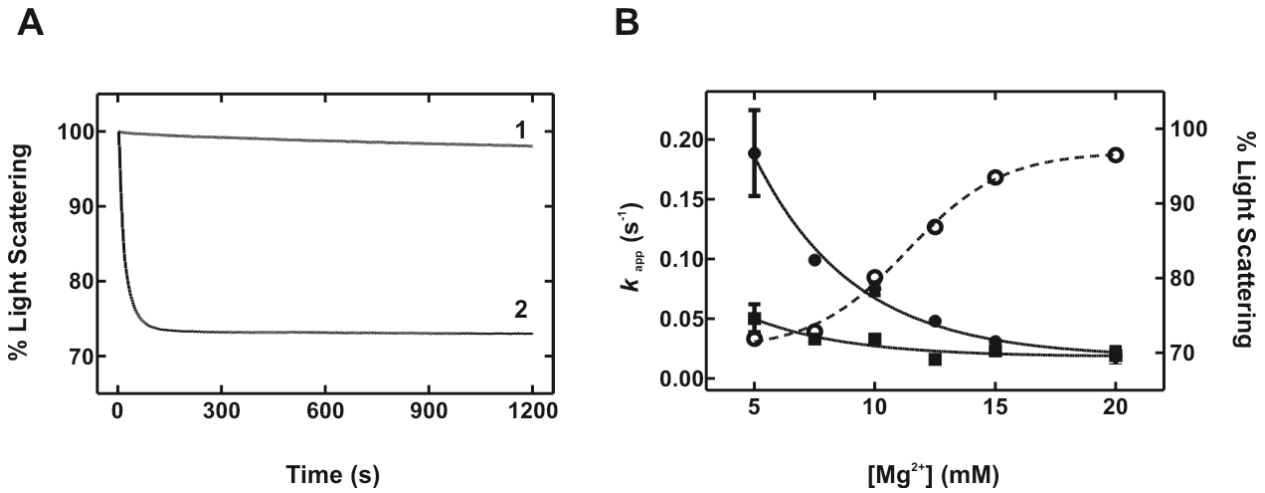

Figure 6.3. Effect of Polyamines and Magnesium ions on HflX-induced Ribosome Dissociation.

A) 0.15 µM 70S ribosomes were mixed rapidly with HflX•GTP (1 µM HflX, 125 µM GTP) in the presence of $TAKM_5$ with 0.6 mM spermine and 0.4 mM spermidine (trace 1) or just $TAKM_5$ (trace 2). B) Effect of magnesium concentration on the apparent rates of ribosome dissociation (k_{app1} and k_{app2} are plotted as closed circles and closed squares respectively) by HflX•GTP. The light scattering signal amplitude is also shown (open circles, dashed line) to indicate the extent of splitting.

To examine the effect of a specific inhibitor of ribosome dissociation on the activity of HflX, the aminoglycoside paromomycin was utilized in ribosome splitting assays. Paromomycin is also an inhibitor of the anti-association activity of IF-3 (Hirokawa et al., 2007). Figure 5.2 (Chapter 5) demonstrates that even high concentrations (500 µM) of paromomycin do not affect the ribosome-stimulated hydrolysis of GTP by HflX. This was confirmed using TLC separation of hydrolysis products (Figure 6.4B). However, Figure 6.4A below demonstrates that the rate of 70S splitting is significantly slowed by paromomycin (IC_{50} = 1 µM). The extent of 70S dissociation is also decreased significantly, at 100 µM paromomycin, no detectable ribosome dissociation was observed (data not shown). Similar to IF-3, paromomycin is a potent inhibitor of HflX•GTP induced ribosome dissociation (Hirokawa et al., 2007).

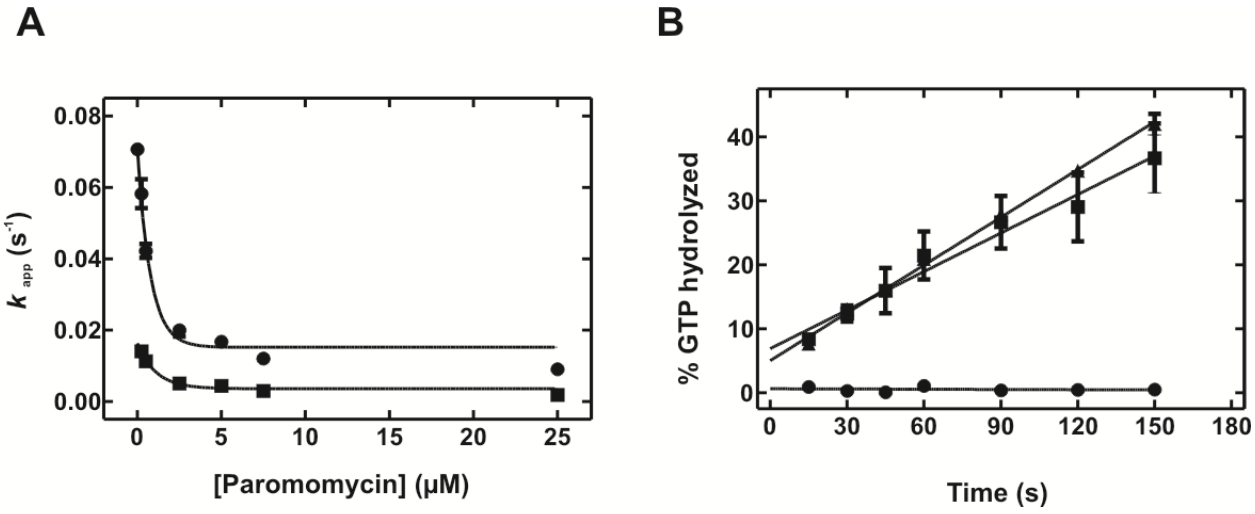

Figure 6.4. Paromomycin Inhibition of Ribosome Dissociation by HflX•GTP.

A) 0.15 μM 70S ribosomes were mixed rapidly with HflX•GTP (1 μM HflX, 125 μM GTP) in the presence of increasing concentrations of paromomycin. (k_{app1} and k_{app2} are plotted as closed circles and closed squares respectively). B) GTP hydrolysis by HflX in the presence of 70S ribosomes was examined by TLC separation as described in section 6.2.3. Closed squares, no antibiotic; closed triangles, with 500 μM paromomycin; closed circles, 500 μM paromomycin but no 70S ribosomes.

6.3.2 Release of inorganic phosphate is not required for ribosome dissociation

Release of inorganic phosphate is required for the turnover of EF-G during translocation of mRNA and tRNA molecules during the elongation phase (though not single turnover GTP hydrolysis), and is required for efficient ribosome recycling by the EF-G RRF mediated subunit dissociation (Savelsbergh et al., 2005b; Savelsbergh et al., 2009). To determine if P_i release from HflX after GTP hydrolysis is required for efficient subunit dissociation, ribosome dissociation experiments were carried out along the lines of previous experiments in the presence of 2 mM sodium metavanadate (Savelsbergh et al., 2009). Metavanadate forms a mixture of both meta- and orthovanadate (VO_3^- and VO_4^{3-} respectively) in neutral aqueous solution (Savelsbergh et al.,

2009). Metavanadate acts as an analog of P_i by occupying the inorganic phosphate binding site of the nucleotide binding pocket, and has previously been used to study the role of P_i release in myosin (Wilson et al., 1995). Even in the presence of 2 mM sodium metavanadate, HflX•GTP induced subunit dissociation is not inhibited (Figure 6.5). GTPase assays in the presence of 70S ribosomes and sodium metavanadate show that vanadate does not inhibt the ribosome-dependent GTPase activity of HflX.

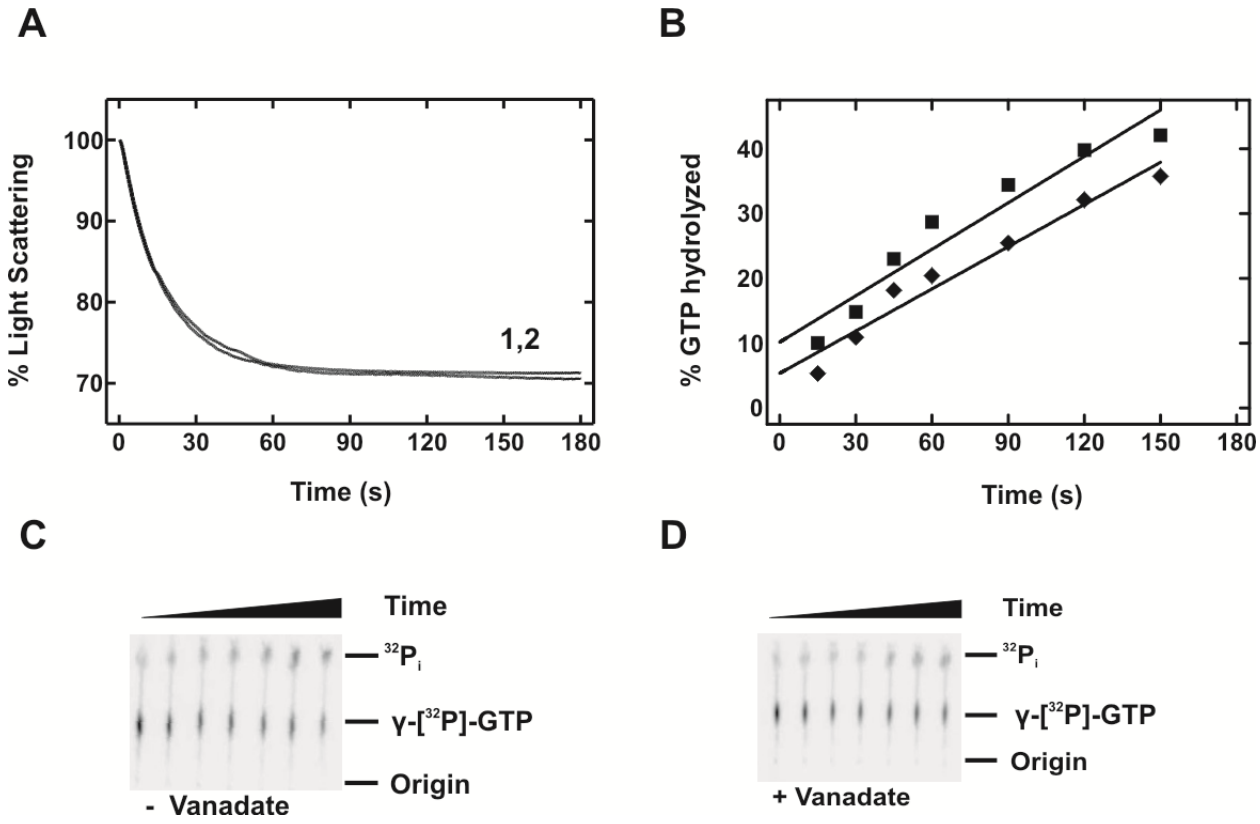

Figure 6.5. Effect of Vanadate on Ribosome Dissociation and the GTPase Activity of HflX.

A) Light scattering of ribosomes was monitored after rapid mixing with HflX•GTP (trace 1, as described Section 6.3.1) and in the presence of sodium metavanadate (2 mM final concentration; trace 2). B) GTP hydrolysis was monitored over time in the absence (closed squares) or presence (closed diamonds) of sodium metavanadate. C), D) Sample TLC plates from experiments in B) were resolved as described in Section 6.2.3. C) GTP hydrolysis in the absence of metavanadate and D) presence of metavanadate. $^{32}P_i$ was quantified using ImageJ (Abramoff et al., 2004).

6.3.3 HflX prevents subunit reassociation depending on the nucleotide present

Dissociation of 70S ribosomes by EF-G and RRF is reversible as GTP is depleted from the system, unless IF-3 is present to prevent subunit re-association (Hirokawa et al., 2008) the ability of HflX to prevent subunit association was examined by light scattering. In the presence of 5 mM Mg^{2+}, 30S and 50S subunits (0.15 µM each, final concentration), when rapidly mixed together, showed a biphasic, small change in light scattering amplitude (~ 3%; k_{app1} = 0.20 ± 0.01 s^{-1}, k_{app2} = 0.059 ± 0.004 s^{-1}). In order to improve this signal, this experiment was performed in the presence of 20 mM Mg^{2+}, which increased both the signal amplitude (~ 28% increase in LS) and the rate of subunit association (k_{app1} = 1.0 ± 0.1 s^{-1}, k_{app2} = 0.069 ± 0.001 s^{-1}). When HflX (1 µM final concentration) was preincubated for 15 min with GDPNP (125µM final concentration) and 50S subunits, the extent of ribosome association was completely blocked in 5 mM Mg^{2+} and impaired in the presence of 20 mM Mg^{2+} (~ 8% LS change, k_{app1} = 0.16 ± 0.01 s^{-1}, k_{app2} = 0.026 ± 0.002 s^{-1}). This data indicates that HflX•GPDNP inhibits the extent of ribosomal subunit association into 70S ribosomes. To investigate the nucleotide dependence of this antiassociation ability, HflX and 50S subunits were preincubated with different guanine nucleotides prior to mixing with 30S subunits. These experiments were performed with a different preparation of ribosomal subunits; thus, while the rates of subunit association in these experiments differ, the change in signal amplitude information is likely accurate. In general, subunit association was impaired in the presence of HflX, with the general trend of inhibition being no HflX<*apo*<GDP<GDPNP (~ 24%, 22%, 18%, and 10% LS changes respectively).

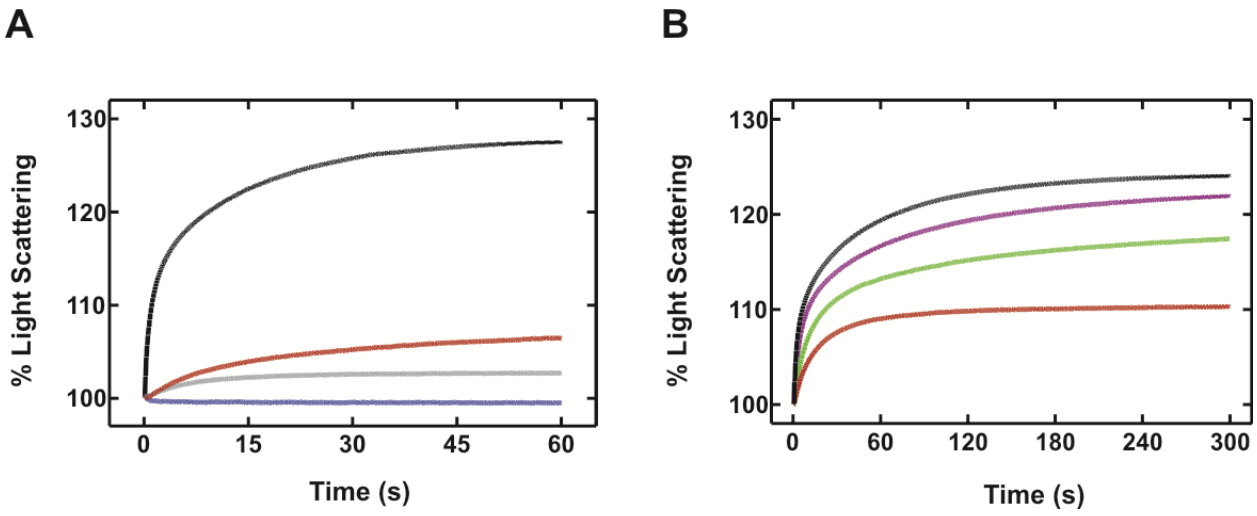

Figure 6.6. Inhibition of Ribosomal Subunit Association by HflX.

A) Magnesium ion dependence of subunit association. Grey trace, 50S and 30S subunits rapidly mixing in buffer containing 5 mM Mg^{2+} (blue trace, with HflX•GDPNP preincubated with 50S subunits); black trace, 50S and 30S subunits mixed with 20 mM Mg^{2+} (red trace, with HflX•GDPNP preincubated with 50S subunits). B) nucleotide dependence of subunit association inhibition by HflX in buffer containing 20 mM Mg^{2+}. Black trace, no HflX, purple, HflX, green, HflX•GDP, red, HflX•GDPNP.

6.3.4 IF-3 inhibits ribosomal subunit dissociation by HflX•GTP

HflX exhibits a ribosomal subunit antiassociation property similar to IF-3. The GTPase activity of HflX is also stimulated an additional 2 fold in the presence of both IF-3 and 70S ribosomes in addition to the 1000 fold stimulatory effect of ribosomes. To investigate potential interaction or competition between IF-3 and HflX on subunit dissociation, the ability of IF-3 to dissociate 70S ribosomes was examined. IF-3 induced 70S ribosome dissociation occurred at a much slower rate compared to HflX•GTP induced subunit dissociation, to a lesser extent (LS change of ~ 20% at 0.9 µM IF-3; k_{app1} = 0.023 ± 0.001 s^{-1}, k_{app2} = 0.0041 ± 0.0001 s^{-1}); though the extent of light scattering varied, the apparent rates of IF-3 induced ribosome dissociation did not significantly vary with IF-3 concentration. Despite the ribosome-stimulated GTPase activity

of HflX being enhanced by IF-3, the rate of HflX•GTP induced ribosome dissociation was inhibited by IF-3. This may indicate that IF-3 competes for a similar binding site with HflX, accounting for the slowed rate of 70S dissociation, but may also interact directly with HflX to aid in its positioning to the novel GTPase activation region of the 50S ribosomal subunit.

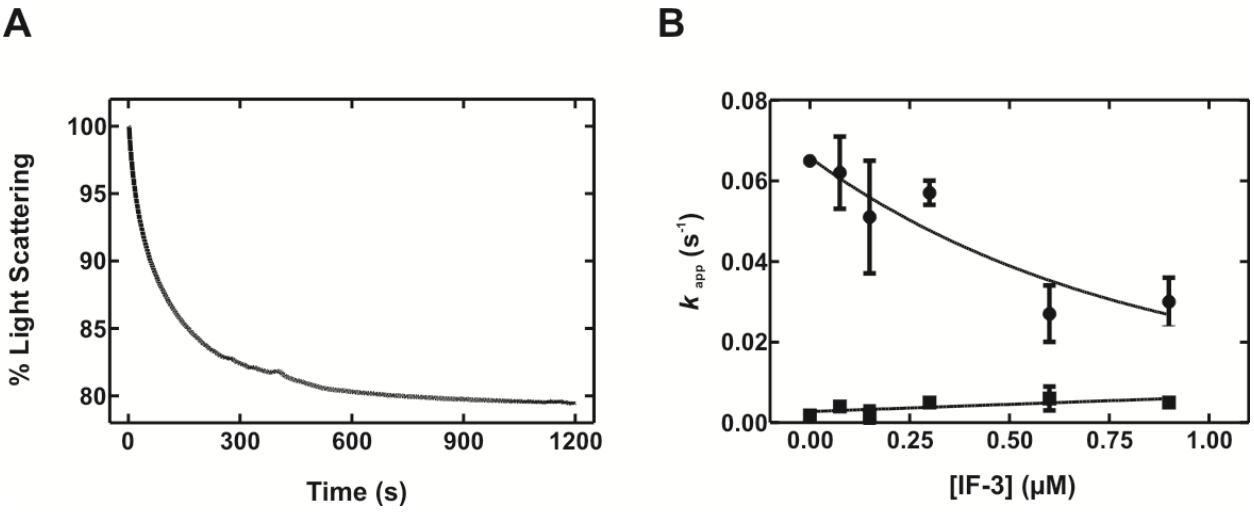

Figure 6.7. IF-3 competition of HflX•GTP Induced Subunit Dissociation.

A) Light scattering was monitored upon mixing 0.9 μM IF-3 with 0.15 μM 70S ribosomes. B) 0.15 μM 70S ribosomes were mixed rapidly with HflX•GTP (1 μM HflX, 125 μM GTP) in the presence of increasing concentrations of IF-3. The resulting light scattering traces were fit to two exponential functions, and the rates plotted as a function of IF-3 concentration (k_{app1} and k_{app2} are plotted as closed circles and closed squares respectively).

6.4 Discussion

A serendipitous discovery that 70S•HflX complexes, when examined under an electron microscope, only showed 50S and 30S subunits with no additional density attached to either subunit led to the discovery of the ability of HflX to induce dissociation of 70S ribosomes. The dissociation of 70S ribosomes by HflX is nucleotide-dependent, with both the rate and extent of 70S ribosome dissociation greatest in the presence of GTP. Indeed, the extent of ribosome dissociation by HflX•GTP is similar compared to experiments in which the magnesium ion concentration is reduced to 2.5 mM, conditions in which the 70S ribosome completely dissociates (Görisch et al., 1976) (~ 29% signal change, k_{app-}= 0.055 ± 0.001 s^{-1} , Figure 6.1). While the extent of dissociation is similar, HflX•GTP experiments show a two phase decrease in the light scattering signal (k_{app1} = 0.065 ± 0.001 s^{-1} and k_{app2} = 0.0018 ± 0.001 s^{-1}). Experiments where 70S ribosomes are mixed with buffer lacking Mg^{2+} show light scattering traces best fit to a single exponential function, therefore, the two phase signal is not likely due to heterogeneity of the ribosome sample. To confirm the observed effects of HflX during light scattering experiments, multiple preparations of 70S ribosomes have been utilized. Nor are these biphasic signals likely to be caused by heterogeneity of HflX preparations, as the nucleotide concentrations are at sufficiently high levels to ensure complete binding and multiple HflX preparations have been used. If the anti-association ability of HflX is like that of IF-3, the initial fast rate, which composes most of the light scattering signal, is likely due to a fast 70S dissociation, followed by a structural rearrangement of HflX on whichever subunit it preferentially binds to after 70S dissociation (based on purified ribosomes from *C. pneumonia* and *E. coli*, likely the 50S subunit (Jain et al., 2009; Polkinghorne et al., 2008)). Alternatively, HflX could induce a structural change in the 70S ribosome initially, thereby inducing a transient

ratcheted state which is required for a second dissociation step (analogous to that proposed for IF-3 in Figure 1.6C).

Ribosome dissociation is nucleotide-dependent; HflX bound to the non-hydrolyzable GTP analog GDPNP causes dissociation to an approximately similar extent (Figure 6.1), yet at a ~ 4 fold slower rate with respect to the first phase of the light scattering signal and ~ 2 fold faster with respect to the second light scattering signal compared to GTP (k_{app1} = 0.017 ± 0.007 s^{-1} and k_{app2} = 0.0044 ± 0.0002 s^{-1} for experiments with GDPNP). Likewise, the rates of70S dissociation in the presence of *apo* HflX and HflX•GDP are similar to the GDPNP experiment (1.6 fold and 4 fold faster for k_{app1} and 1.2 and 3.1 fold slower for k_{app2}, respectively), yet the extent of 70S dissociation is significantly lower (Figure 6.1). This, combined with the observation that the aminoglycoside paromomycin is a potent inhibitor of ribosome dissociation but has no effect on the 70S-stimulated GTPase activity of HflX (Section 5.3.1), suggests that while the presence of various guanine nucleotides dictates the extent of dissociated ribosomes, hydrolysis of GTP is decoupled from the ribosome splitting activity and likely plays another role during protein synthesis. Indeed, Figure 6.2 shows that the ribosomes are fully dissociated at approximately equimolar concentrations of HflX•GTP (consistent with the proposed high affinity for HflX binding to the 50S ribosome and the estimated $K_{M,1}$ value of 0.11 μM for Michaelis-Menten experiments in Figure 6.2A). Non-specific stabilizing agents such as polyamines and increased magnesium ion concentration stabilize the 70S ribosomes. Similar to paromomycin, these stabilizing agents were found to have no significant effect on the ribosome-stimulated GTPase activity of HflX, further supporting distinct roles for HflX-induced anti-association and GTP hydrolysis.

Inorganic phosphate release by EF-G is essential for the efficient dissociation of 70S ribosomes by EF-G and RRF (Savelsbergh et al., 2009). To further investigate a potential role of GTP hydrolysis, and a potential role for release of inorganic phosphate from HflX upon GTP hydrolysis, the P_i analog metavanadate (VO_3^-) was utilized to inhibit release of P_i. Such studies have been performed on EF-G (Savelsbergh et al., 2005b; Savelsbergh et al., 2009) and myosin (Wilson et al., 1995). Neither 70S dissociation nor GTP hydrolysis were affected (Figure 6.5), indicating that release of inorganic phosphate is not temporally regulated by 70S ribosomes, unlike EF-G. This is in line with the previous observation that GTPase stimulation of HflX is not affected by ribosomal proteins L7/L12 (Figure 5.8), which also regulates P_i release by EF-G upon translocation (Savelsbergh et al., 2005b). It is tempting to speculate that GTP hydrolysis, which is decoupled from ribosome dissociation, may be required for some additional activity on the ribosome, perhaps related to subunit association via L2. L2 has been previously shown to be required for ribosomal subunit association and also binding of aminoacyl-tRNA to the ribosomal P-site (Diedrich et al., 2000). Therefore, HflX may act as a sensor reacting to the occupancy of the ribosomal P-site of the 70S ribosome (Figure 6.9).

Figure 6.6 confirms that the observed 70S ribosome dissociation is indeed due to preventing subunit re-association. If HflX associates to the 70S ribosome as proposed in Chapter 4 with the N-terminal domain associated to the 50S subunit and the C-terminal G domain associated with the 50S subunit, then it is likely that the G domain acts as a sensor, and changes the conformation of the N-terminal HflX domain in response to tight GTP (GDPNP) binding. This conformational change may alter the affinity of HflX for the 50S and reduce the affinity for HflX binding to the 30S (also explaining results by Polkinghorne *et al.* and Jain *et al.* (Jain et al., 2009; Polkinghorne et al., 2008), and perhaps induce the HflX domain to pack against the 50S subunit

at the intersubunit interface, thereby disrupting key intersubunit interactions. However, one of these crucial intersubunit bridges, helix 69 of the 23S rRNA, lies ~ 63 Å away to nearest Cα of HflX. However, the less crucial intersubunit bridge B7b (consisting of G773,

G774, G775, and G776), which is crucial for $tRNA_i$ selection during initiation (Sun et al., 2011), lies in close proximity to L2 as well as the peptidyl transferase centre; thus, is a possible target for disruption via HflX interacting with L2 (Figure 6.8).

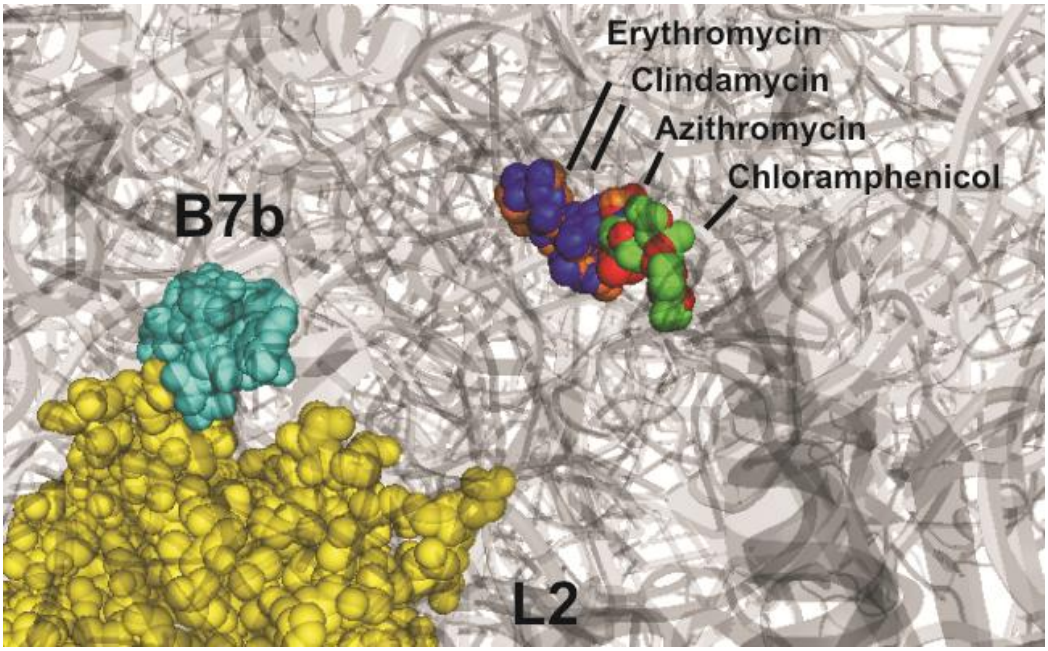

Figure 6.8. Location of Intersubunit Bridge B7b.

The location of intersubunit bridge B7b is shown (G773-G776, cyan spheres) in relation to the peptidyl transferase centre antibiotics chloramphenicol (green), azithromycin (orange), erythromycin (blue), and clindamycin (red). Ribosomal protein L2 is shown (yellow spheres). The view is from the intersubunit space looking into the 50S particle.

HflX may have a binding site on the 70S ribosome within close proximity to that of IF-3, and currently only indirect evidence is present for a functional interaction. The observed 2-fold

increase in GTP hydrolysis in the presence of IF-3 and 70S ribosomes may be explained by IF-3 inducing a conformational change in the ribosome that facilitates the binding of HflX; this may be a functional state to which HflX associates more readily. The fact that ribosome dissociation in the presence of HflX is slowed in the presence of IF-3 suggests that the two factors compete for the same binding site, and that HflX has a lower affinity than IF-3 for the ribosome. Alternatively, IF-3 and HflX may function synergistically during ribosome recycling: IF-3 may prevent subunit reassociation while bound to the 30S, while HflX may perform the same function while bound to the 50S. The fact that the preferred *in vivo* state of HflX is to associate to the 50S subunit (Blombach et al., 2011; Jain et al., 2009), combined with the fact that HflX is non-essential under optimal conditions (Baba et al., 2006), would seem to indicate that HflX performs a specific function, most likely stress or starvation conditions. It may be that HflX is expressed to sequester 50S ribosomal subunits under starvation conditions or viral challenge, accounting for why this factor was not earlier discovered as part of the translation machinery.

Figure 6.9 provides a model for the activity of HflX. The cellular concentration of 70S ribosomes is ~ 20 µM (Hirokawa et al., 2008), and that of HflX under optimal conditions, ~ 0.4 µM (Ishihama et al., 2008). Thus, HflX will only associate to a subfraction of ribosomal particles present in the *E. coli* cell. Both empty and poly(U) programmed ribosomes stimulate the GTPase activity of HflX (Chapter 3), but peptidyl transferase centre antibiotics that block peptide elongation (Chapter 5) inhibit this activity. This indicates that the elongating ribosome (i.e. ribosome with a nascent peptide being synthesized) is unlikely to be the cellular target for HflX. This is supported by the fact that the overexpression of HflX for purification (outlined in Chapter 3) has no significant effect on cellular growth (data not shown), otherwise, the cellular translation machinery would be inhibited by high concentrations of HflX upon IPTG induction.

Under starvation conditions, however, translation is inhibited and the concentration of deacyl-tRNA compared to that of aminoacyl-tRNA is significantly increased (Goldman and Jakubowski, 1990), thereby reducing the number of elongating ribosomes and increasing the concentration of ribosomes lacking bound peptidyl-tRNA. HflX•GDP binds to these non-translating 70S ribosomes, "senses" the state of the peptidyl transferase centre, and binds GTP. Binding of GTP would cause HflX to adopt a different conformation (perhaps described by the pre-steady state analysis described in Chapter 4), likely driving the N-terminal HflX subdomain I (up to residue R103) into the intersubunit region, disrupting contacts near the B7b intersubunit bridge and promoting dissociation of the 70S ribosome complex into 50S and 30S subunits (Chapter 6). Following GTP hydrolysis, HflX would adopt its inactive, GDP-bound form, either dissociating from the 50S subunit or remaining bound. In the later event, an additional factor would be required to regulate GTP binding by HflX, ensuring futile cycles of GTP hydrolysis do not occur. If HflX dissociates from the 50S subunit in its GDP bound form, then IF-3 could associate with the 30S subunit and therefore prevent subunit re-association.

A pivotal information required to either prove or disprove this model is knowledge of the equilibrium binding affinities for HflX interacting with 30S, 50S, and 70S ribosomal particles, information critical for developing a model for the anti-association activity of HflX. Based on current biochemical data, as well as interaction with IF-3 and ribosomal subunit anti-association activity of HflX, it is tempting to speculate a role for HflX in regulating translation during stress response, thereby regulating gene expression.

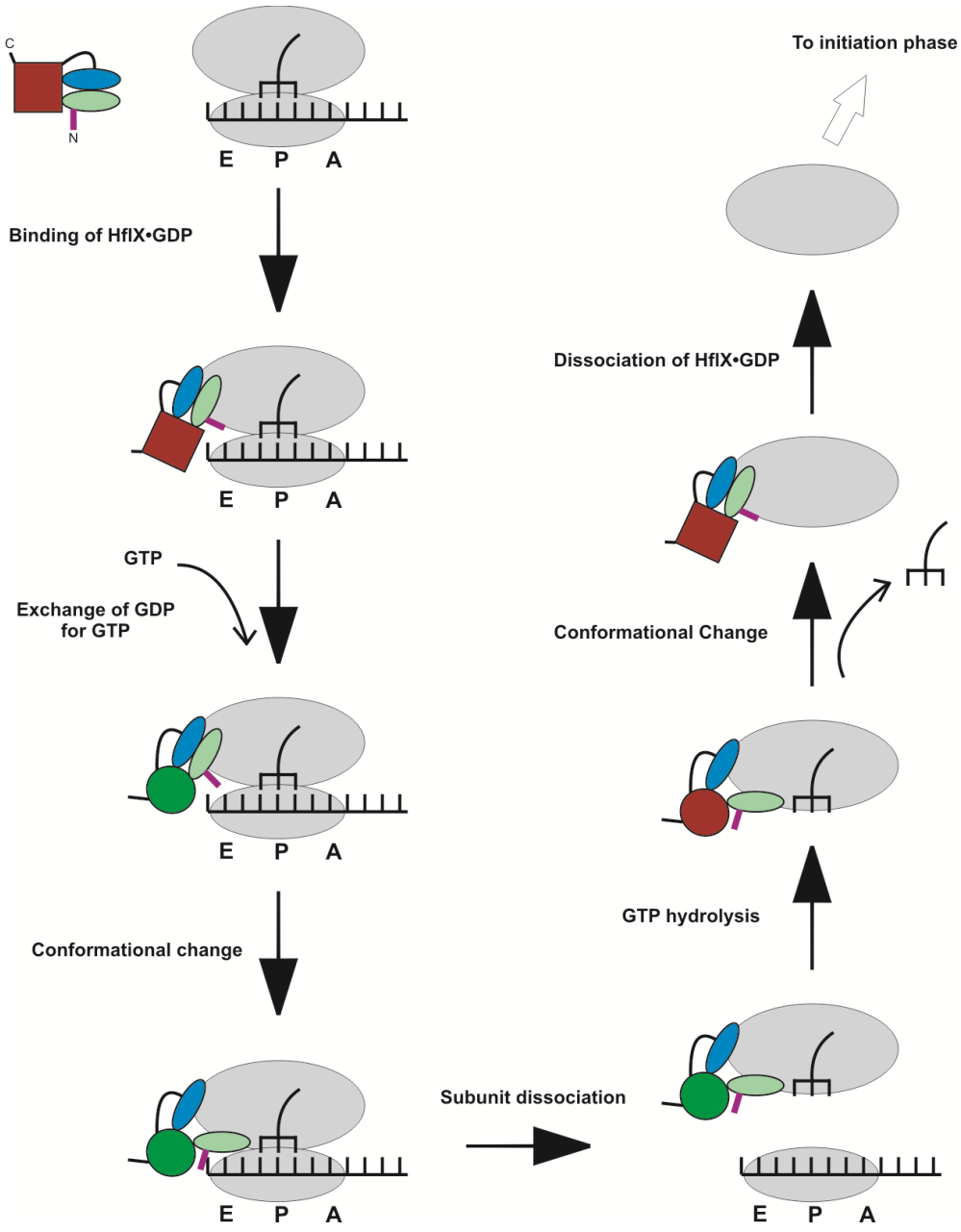

Figure 6.9. Model for the Activity of HflX in the *E. coli* cell.

Under stress conditions, the concentration of either empty 70S ribosomes or ribosomes bound to deacyl-tRNA increases. Free HflX, bound to GDP (based on data from Chapter 3), associates to the ribosome and exchanges GDP for GTP. HflX•GTP undergoes a conformational change to a "GTPase activated"state. The 70S ribosome dissociates into 50S and 30S ribosomal subunits, and GTP is hydrolyzed. HflX likely reverts to its GDP bound form and dissociates from the 50S subunit. Alternatively, another factor (possibly the alarmone guanosine pentaphosphate) prevents futile rounds of GTP hydrolysis by HflX. IF-3 prevents subunit re-association (not shown).

7. Future Directions

The role of HflX during protein synthesis remains unclear. In an effort to define a functional state of the ribosome that is the cellular target of HflX, multiple antibiotics targeting the ribosome were screened to examine the GTPase and anti-association activity of HflX. The aminoglycosides (such as paromomycin), which target processes such ribosome recycling (Borovinskaya et al., 2007a; Hirokawa et al., 2007) and elongation processes (Sohmen et al., 2009), do not affect ribosome-stimulated GTP hydrolysis by HflX. However, paromomycin, which is a potent inhibitor of the subunit anti-association activity of IF-3 (Hirokawa et al., 2007), also inhibits subunit dissociation in the presence of HflX. Preliminary data also indicates that tobramycin also inhibits this anti-association property, and is a promising candidate for stabilizing a HflX•Ribosome complex for structural studies by X-ray crystallography and Cryo-EM. Other antibiotics, such as fusidic acid (Gao et al., 2009b), kirromycin (Schmeing et al., 2009), tetracycline (Pioletti et al., 2001), and paromomycin (Selmer et al., 2006) have all been used to stabilize ribosomal complexes for structural studies. Tetracycline, which blocks delivery of the EF-Tu•GTP•aa-tRNA ternary complex to the ribosomal A-site, streptomycin, which increases the affinity of the A-site for aa-tRNA, and spectinomycin, which prevents subunit rotation and thus translocation, all have no effect on the ribosome-stimulated GTPase activity of HflX, suggesting that the elongation phase ribosomes may not be an *in vivo* target for HflX.

By contrast, antibiotics that target the peptidyl transferase centre (chloramphenicol, azithromycin, erythromycin, lincomycin, and clindamycin) are all inhibitors of the ribosome-stimulated GTPase activity of HflX, yet preliminary data also suggests that chloramphenicol does not inhibit the anti-association activity of HflX. These antibiotics inhibit the peptidyl transferase reaction (chloramphenicol, lincomycin, clindamycin (Brock, 1961; Douthwaite,

1992; Long and Porse, 2003; Sohmen et al., 2009; Vannuffel and Cocito, 1996)) and egress of the nascent polypeptide chain (azithromycin and erythromycin (Petropoulos et al., 2008; Petropoulos et al., 2009; Sohmen et al., 2009); interestingly, by preventing peptidyl transferase and polypeptide chain elongation, these antibiotics may reduce the affinity of ribosomes for aa-tRNA and peptidyl-tRNA (Kouvela et al., 2006; Menninger and Coleman, 1993). It would be of great interest to examine the GTPase and anti-association activities of HflX in the presence of different ribosomal complexes and antibiotics; for example, with P-site peptidyl-tRNA and one of azithromycin, erythromycin, lincomycin, or clindamycin. The rates of mant-GDPNP dissociation from HflX in the presence of these antibiotics and 50S ribosomal subunits do not significantly vary, though experiments with chloramphenicol present are ~ 5-10 fold faster. Preliminary data on association rates in of various nucleotides suggests nucleotide binding is not affected; thus, the presence of chloramphenicol may reduce the affinity of HflX for mant-GDPNP while bound to the 50S subunit. A reduced affinity may therefore account for the observed decrease in GTPase activity by HflX. Additional studies along these lines are underway.

It is interesting that the proposed binding site of HflX near the ribosomal E-site (based on crosslinking data) is near ribosomal protein L2. This protein is involved in subunit association, tRNA binding to the ribosomal A- and P-sites, and peptidyl transferase activity (Diedrich et al., 2000). If binding to this location was confirmed by structural studies, this would represent a new binding site for a translational GTPase on the 50S subunit, though the bacterial homolog of eukaryotic heat shock protein Hsp90 has been proposed to interact with and be stimulated by L2 (Motojima-Miyazaki et al., 2010). L2 lies within close proximity to the peptidyl transferase centre and hence binding sites for identified antibiotic inhibitors. It is tempting to speculate that

binding of a peptidyl transferase centre antibiotic induces a conformation in L2 that either reduces the stabilization of the nucleotide binding pocket of HflX while bound to the 50S subunit, or reduces the affinity of HflX for the 50S subunit, thereby preventing GTPase activation. Elucidating the effect of antibiotics on the affinities HflX for binding to ribosomal particles will address this question. In particular, the fact that IF-3 competes with HflX for inducing 70S ribosome dissociation suggests that the affinity of IF-3 for the 70S ribosome is greater than that of HflX, contradicting ultracentrifugation experiments that suggest the HflX binds to ribosomal particles with high affinity. The promiscuous binding of HflX to 30S, 50S, and 70S particles *in vitro* is also puzzling, given that only 70S and 50S particles stimulate the GTPase activity of HflX. Determining the affinity of HflX for ribosomal particles will be crucial for determining the precise interaction partner of HflX in the cell. Further experiments examining the influence of GTPase inhibitors (azithromycin, erythromycin, clindamycin, lincomycin, tobramycin, and chloramphenciol) on 70S ribosome splitting would confirm the decoupling of GTP hydrolysis and ribosome dissociation. The role of the HflX domain in splitting the 70S ribosome must also be examined, using truncated forms of HflX designed with respect to the domain arrangement of HflX.

8. Summary

The universally conserved GTPases are involved in protein synthesis. The roles of the canonical translation factors IF-2, EF-G, EF-Tu, as well as the protein secretion factors Ffh and FtsY, have been determined based on structural and kinetic data. To elucidate the role of HflX during protein synthesis, similar techniques have been applied. Results presented in this work have revealed that HflX is a promiscuous ribosome-associated factor that possesses a 50S-stimulated GTPase activity, likely through stabilization of a "GTPase activated" state. Crosslinking data indicates a new binding site on the ribosome for a translational GTPase near that of IF-3, and suggests a novel mechanism of GTPase activation of HflX compared to the canonical translational GTPases. Antibiotics targeting the peptidyl transferase centre inhibit the ribosome-stimulated GTPase activity of HflX, suggesting a long range communication network between the peptidyl transferase centre and the putative binding site of HflX. The splitting of 70S ribosomes can be induced by HflX•nucleotide complexes (GTP>GDPNP>GDP>*apo*), an activity that can be inhibited by the aminoglycoside paromomycin. This indicates a decoupling of GTP hydrolysis by HflX and the ribosome dissociation activity. While the role of this factor has yet to be fully understood, this work represents the first steps toward understanding the function of the universally conserved GTPase HflX.

References

Abel, K., Yoder, M.D., Hilgenfeld, R., and Jurnak, F. (1996). An alpha to beta conformational switch in EF-Tu. Structure *4*, 1153-1159.

Abramoff, M.D., Magalhaes, P.J., and Ram, S.J. (2004). Image processing with ImageJ. Biophotonics International *11*, 36-42.

Agrawal, R.K., Sharma, M.R., Kiel, M.C., Hirokawa, G., T.M., B., Spahn, C.M.T., Grassucci, R.A., Kaji, A., and Frank, J. (2004). Visualization of ribosome-recycling factor on the *Escherichia coli* ribosome: Functional implications. Proc Natl Acad Sci U S A *101*, 8900-8905.

Arigoni, F., Talabot, F., Peitsch, M., Edgerton, M.D., Allet, E., Fish, R., Jamotte, T., Curchod, M.-L., and Loferer, H. (1998). A genome-based approach for the identification of essential bacterial genes. Nat. Biotechnol. *16*, 851-856.

Arnold, K., Bordoli, L., Kopp, J., and Schwede, T. (2006). The SWISS-MODEL Workspace: A web-based environment for protein structure homology modelling. Bioinformatics *22*, 195-201.

Ataide, S.F., Schmitz, N., Shen, K., Ke, A., Shan, S., Doudna, J.A., and Ban, N. (2011). The crystal structure of the signal recognition partilce in complex with its receptor. Science *331*, 881-886.

Baba, T., Ara, T., Hasegawa, M., Takai, Y., Okumura, Y., Baba, M., Datsenko, K.A., Tomita, M., Wanner, B.L., and Mori, H. (2006). Construction of *Escherichia coli* K-12 in-frame, single-gene knock-out mutants: the Keio collection. Mol Syst Biol *doi:10.1038/msb4100050*

Banuett, F., and Herskowitz, I. (1987). Identification of polypeptides encoded by an *Escherichia coli* locus (*hflA*) that governs the lysis-lysogeny decision of bacteriophage lambda. J Bacteriol *169*, 4076-4085.

Barat, C., Datta, P.P., Raj, V.S., Sharma, M.R., Kaji, H., Kaji, A., and Agrawal, R.K. (2007). Progression of the ribosome recycling factor through the ribosome dissociates the two ribosomal subunits. Mol Cell *27*, 250-261.

Blombach, F., Launay, H., Zorraquino, V., Swarts, D.C., Cabrita, L.D., Benelli, D., Christodoulou, J., Londei, P., and van der Oost, J. (2011). An HflX-type GTPase from *Solfalobus solfataricus* binds to the 50S ribosomal subunit in all nucleotide-bound states. J Bacteriol *193*, 2861-2867.

Borovinskaya, M.A., Pai, R.D., Zhang, W., Schuwirth, B.S., Holton, J.M., Hirokawa, G., Kaji, A., and Cate, J.H.D. (2007a). Structural basis for aminoglycoside inhibition of bacterial ribosome recycling. Nat. Struct. Mol. Biol. *14*, 727-732.

Borovinskaya, M.A., Shoji, S., Frederick, K., and Cate, J.H.D. (2008). Structural basis for hygromycin B inhibition of protein biosynthesis. RNA *14*, 1590-1599.

Borovinskaya, M.A., Shoji, S., Holton, J.M.F., K., and Cate, J.H.D. (2007b). A steric block in translation caused by the antibiotic spectinomycin. ACS Chem Biol *2*, 545-552.

Bourne, H.R., Sanders, D.A., and McCormick, F. (1991). The GTPase superfamily: conserved structure and molecular mechanism. Nature *349*, 117-127.

Brock, T.D. (1961). Chloramphenicol. Bacteriol Rev *25*, 32-48.

Brown, E.D. (2005). Conserved P-loop GTPases of unknown function in bacteria: an emerging and vital ensemble in bacterial physiology. Biochem Cell Biol *83*, 738-746.

Brunelle, J.L., Shaw, J.J., Youngman, E.M., and Green, R. (2008). Peptide release on the ribosome depends critically on the 2' OH of the peptidyl-tRNA substrate. RNA *14*, 1526-1531.

Buckstein, M.H., He, J., and Rubin, H. (2008). Characterization of nucleotide pools as a function of physiological state in *Escherichia coli*. J Bacteriol *190*, 718-726.
Bulkley, D., Innis, C.A., Blaha, G., and Steitz, T.A. (2010). Revisiting the structures of several antibiotics bound to the bacterial ribosome. Proc Natl Acad Sci U S A *107*, 17158-17163.
Caldon, C.E., and March, P.E. (2003). Function of the universally conserved GTPases. Curr Opin Microbiol *6*, 135-139.
Chayani, N., Tiwari, S., Sarangi, G., Mallick, B., Mohapatra, A., Paty, B.P., and Das, P. (2009). Role of azithromycin against clinical isolates of family enterobacteriaceae: A comparison of its minimum inhibitory concentration by three different methods. Indian J Med Microbiol *27*, 107-110.
Chen, Y., Koripella, R.K., Sanyal, S., and Selmer, M. (2010). *Staphylococcus aureus* elongation factor G-structure and analysis of a target for fusidic acid. FEBS J *277*, 3789-3803.
Cheng, H.H., Muhlrad, P.J., Hoyt, A., and Echols, H. (1988). Cleavage of the cII protein of phage λ by purified HflA protease: Control of the switch between lysis and lysogeny. Proc Natl Acad Sci U S A *85*, 7882-7886.
Cheung, M.-Y., Xue, Y., Zhou, L., Li, M.-W., S, S.-M., and Lam, H.-M. (2010). An ancient P-loop GTPase in rice is regulated by a higher plant-specific regulatory protein. J Biol Chem.
Chinali, G., Nyssen, E., Di Giambattista, M., and Cocito, C. (1988). Action of erythromycin and virginiamycin S on polypeptide synthesis in cell-free systems. Biochim Biophys Acta *951*, 42-52.
Chodavarapu, S., Felczak, M.M., and Kaguni, J.M. (2011). Two forms of ribosomal protein L2 of *Escherichia coli* that inhibit DnaA in DNA replication. Nucleic Acids Res *39*, 4180-4191.
Christodoulou, J., Larsson, G., Fucini, P., Connell, S.R., Pertinhez, C., Hanson, C.L., Redfield, C., Nierhaus, K.H., Robinson, C.V., Schleucher, J., *et al.* (2004). Heteronuclear NMR investigations of dynamic regions of intact *Escherichia coli* ribosomes. Proc Natl Acad Sci U S A *101*, 10949-10954.
Clark, B.F.C., and Nyborg, J. (1997). The ternary complex of EF-Tu and its role in protein biosynthesis. Curr Opin Struct Biol *7*, 110-116.
Connell, S.R., Trieber, C.A., Dinos, G.P., Einfeldt, E., Taylor, D.E., and Nierhaus, K.H. (2003). Mechanism of Tet(O)-mediated tetracycline resistance. EMBO J *22*, 945-953.
Cooper, E.L., Garcia-Lara, J., and Foster, S.J. (2009). YsxC, an essential protein in *Staphylococcus aureus* crucial for ribosome assembly/stability. BMC Microbiol *9*, 266-277.
Czworkowski, J., Wang, J., Steitz, T.A., and Moore, P.B. (1994). The crystal structure of elongation factor G complexes with GDP, at 2.7 Å resolution. EMBO J *13*, 3661-3668.
Dahl, L.D., Wieden, H.J., Rodnina, M.V., and Knudsen, C.R. (2006). The importance of P-loop and domain movements in EF-Tu for guanine nucleotide exchange. J Biol Chem *281*, 21139-21146.
Datta, P.P., Sharma, M.R., Qi, L., Frank, J., and Agrawal, R.K. (2005). Interaction of the G' domain of elongation factor G and the C-terminal domain of ribosomal protein L7/L12 during translocation as revealed by cryo-EM. Mol Cell *20*, 723-731.
Daviter, T., Wieden, H.J., and Rodnina, M.V. (2003). Essential role of histidine 84 in Elongation Factor Tu for the chemical step of GTP hydrolysis on the ribosome. J Mol Biol *332*, 689-699.
DeLano, W.L. (2006). PyMOL. DeLano Scientific.

DeLivron, M.A., Makanji, H.S., Lane, M.C., and Robinson, V.L. (2009). A novel domain in translational GTPase BipA mediates interaction with the 70S ribosome and influences GTP hydrolysis. Biochemistry *48*, 10533-10541.
Diaconu, M., Kothe, U., Schlunzen, F., Fischer, N., Harms, J.M., Tonevitsky, A.G., Stark, H., Rodnina, M.V., and Wahl, M.C. (2005). Structural basis for the function of the ribosomal L7/L12 stalk in factor binding and GTPase activation. Cell *121*, 991-1004.
Diedrich, G., Spahn, C., Stelzl, U., Schäfer, M., Wooten, T., Bochkariov, D., Cooperman, B., Traut, R., and Nierhaus, K. (2000). Ribosomal protein L2 is involved in the association of the ribosomal subunits, tRNA binding to the A and P sites and peptidyl transfer. EMBO J *19*, 5241-5250.
Douthwaite, S. (1992). Interaction of the antibiotics clindamycin and lincomycin with *Escherichia coli* 23S ribosomal RNA. Nucleic Acids Res *20*, 4717-4720.
Dovas, A., and Couchman, J.R. (2005). RhoGDI: multiple functions in the regulation of Rho family GTPase activities. Biochem J *390*, 1-9.
Dunkle, J.A., Xiong, L., Mankin, A.S., and Cate, J.H.D. (2010). Structures of the *Escherichia coli* ribosome with antibiotics bound near the peptidyl transferase center explain spectra of drug action. Proc Natl Acad Sci U S A *107*, 17152-17157.
Dutta, D., Bandyopadhyay, K., Datta, A.B., Sardesai, A.A., and Parrack, P. (2009). Properties of HflX, an enigmatic protein from *Escherichia coli*. J Bacteriol *191*, 2307-2314.
Estrozi, L.F., Boehringer, D., Shan, S., Ban, N., and Schaffitzel, C. (2011). Cryo-EM structure of the *E. coli* translating ribosome in complex with SRP and its receptor. Nat Struct Mol Biol *18*, 88-90.
Evans, R.N., Blaha, G., Bailey, S., and Steitz, T.A. (2008). The structure of LepA, the ribosomal back translocase. Proc Natl Acad Sci U S A *105*, 4673-4678.
Feldman, W.E., and Manning, N.S. (1983). Effect of growth phase on the bactericidal action of chloramphenicol against *Haemophilus influenzae* type b and *Escherichia coli* K-1. Antimicrob Agents Chemother *23*, 551-554.
Fujiwara, T., Ito, K., Yamami, T., and Nakamura, Y. (2004). Ribosome recycling factor disassembles the post-termination ribosomal complex independent of the ribosomal translocase activity of elongation factor G. Mol Microbiol *53*, 517-528.
Gamblin, S.J., and Smerdon, S.J. (1998). GTPase-activating proteins and their complexes. Curr Opin Struct Biol *8*, 195-201.
Gao, H., Valle, M., Ehrenberg, M., and Frank, J. (2004). Dynamics of EF-G interaction with the ribosome explored by classification of a heterogeneous cryo-EM dataset. J Struct Biol *147*, 283-290.
Gao, H., Zhou, Z., Rawat, U., Huang, C., Bouakaz, L., Wang, C., Cheng, Z., Liu, Y., Zavialov, A.V., Gursky, R., *et al.* (2007). RF3 induces ribosomal conformational changes responsible for dissociation of class I release factors. Cell *129*, 929-941.
Gao, Y.-G., Selmer, M., Dunham, C.M., Weixlbaumer, A., Kelley, A.C., and Ramakrishnan, V. (2009). The structure of the ribosome with elongation factor G trapped in the posttranslocational State. Science *326*, 694-699.
Garcia-Ortega, L., Alvarez-Garcia, E., Gavilanes, J.G., Martinez-del-Pozo, A., and Joseph, S. (2010). Cleavage of the sarcin-ricin loop of 23S rRNA differentially affects EF-G and EF-Tu binding. Nucleic Acids Res *38*, 4108-4119.

Gasteiger, E., Hoogland, C., Gatiker, A., Duvaud, S., Wilkins, M.R., Appel, R.D., and Bairoch, A. (2005). Protein identification and analysis tools on the ExPASy server (New York, N.Y.: Springer-Verlag New York, LLC).
Goldman, E., and Jakubowski, H. (1990). Uncharged tRNA, protein synthesis, and the bacterial stringent response. Mol Microbiol *4*, 2035-2040.
Görisch, H., Goss, D., and Parkhurst, L. (1976). Kinetics of ribosome dissociation and subunit association studied in a light-scattering stopped-flow apparatus. Biochemistry *15*, 5743-5753.
Goyal, A., Muthu, K., Panneerselvam, M., Pole, A., and Ramadas, K. (2011). Molecular dynamics simulation of the *Staphylococcus aureus* YsxC protein: molecular insights into ribosome assembly and allosteric inhibition of the protein. J Mol Model, doi: 10.1007/s00894-00011-00998-00893.
Gradia, D.F., Rau, K., Umaki, A.C.S., deSouza, F.S.P., Probst, C.M., Correa, A., Holetz, F.B., Avila, A.R., Krieger, M.A., Goldenberg, S., *et al.* (2009). Characterization of a novel Obg-like ATPase in the protozoan *Trypanosoma cruzi*. Int J Parasitol *39*, 49-58.
Gregory, S.T., Carr, J.F., and ADahlberg, A.E. (2009). A signal relay between ribosomal protein S12 and elongation factor Tu during decoding of mRNA. RNA *15*, 208-214.
Gromadski, K., and Rodnina, M.V. (2004). Streptomycin interferes with conformational coupling between codon recognition and GTPase activation on the ribosome. Nat Struct Mol Biol *11*, 316-322.
Gromadski, K.B., Wieden, H.J., and Rodnina, M.V. (2002). Kinetic mechanism of elongation factor Ts-catalyzed nucleotide exchange in elongation factor Tu. Biochemistry *41*, 162-169.
Gualerzi, C.O., Brandi, L., Caserta, E., La Teana, A., Spurio, R., Tomsic, J., and Pon, C.L. (1991). Molecular dissection of translation initiation factor IF2. Evidence for two structural and functional domains. J Biol Chem *266*, 16356-16362.
Guex, N., and Peitsch, M.C. (1997). SWISS-MODEL and the Swiss-PdbViewer: An environment for comparative protein modelling. Electrophoresis *18*, 2714-2723.
Hansen, J.L., Ippolito, J.A., Ban, N., Nissen, P.M., P.B., and Steitz, T.A. (2002). The structrues of four macrolide antibiotics bound to the large ribosomal subunit. Mol Cell *10*, 117-128.
Hansen, J.L., Moore, P.B., and Steitz, T.A. (2003). Structures of five antibiotics bound at the peptidyl transferase center of the large ribosomal subunit. J Mol Biol *330*, 1061-1075.
Hansson, S., Singh, R., Gudkov, A.T., Liljas, A., and Logan, D.T. (2005). Crystal structure of a mutant elongation factor G trapped with a GTP analog. FEBS Lett *579*, 4492-4497.
Hauryliuk, V., Mitkevich, V.A., Draycheva, A., Tankov, S., Shyp, V., Ermakov, A., Kulikova, A.A., Makarov, A.A., and Ehrenberg, M. (2009). Thermodynamics of GTP and GDP binding to bacterial initiation factor 2 suggests two types of structural transitions. J Mol Biol *394*, 621-626.
He, S.L., and Green, R. (2010). Visualization of codon-dependent conformational rearrangements during translation termination. Nat Struct Mol Biol *17*, 465-470.
Heffron, S.E., Mui, S., Aorora, A., Abel, K., Bergmann, E., and Jurnak, F. (2006). Molecular complementarity between tetracycline and the GTPase active site of elongation factor Tu. Acta Crystallogr D Biol Crystallogr *62*, 1392-1400.
Herskowitz, I., and Hagen, D. (1980). The lysis-lysogeny decision of phage lambda: explicit programming and responsiveness. Annu. Rev. Genet. *14*, 399-445.
Higgins, D.G., Thompson, J.D., and Gibson, T.J. (1996). Using CLUSTAL for multiple sequence alignments. Methods Enzymol. *266*, 383-402.

Hirashima, A., and Kaji, A. (1972). Factor-dependent release of ribosomes from messenger RNA. J Mol Biol *65*, 43-58.
Hirokawa, G., Iwakura, N., Kaji, A., and Kaji, H. (2008). The role of GTP in transient splitting of 70S ribosomes by RRF (ribosome recycling factor) and EF-G (elongation factor G). Nucleic Acids Res *36*, 6676-6687.
Hirokawa, G., Kaji, H., and Kaji, A. (2007). Inhibition of antiassociation activity of translation initiation factor 3 by paromomycin. Antimicrob Agents Chemother *51*, 175-180.
Hobbie, S.N., Pfister, P., Brüll, C., Westhof, E., and Böttger, E.C. (2005). Analysis of the contribution of individual substituents in 4,6-aminoglycoside-tibosome interaction. Antimicrob Agents Chemother *49*, 5112-5118.
Huang, B., Wu, H., Hao, N., Blombach, F., Van der Oost, J., Li, X., Zhang, X.C., and Rao, Z. (2010a). Functional study on GTP hydrolysis by the GTP-binding protein from *Sulfolobus solfataricus*, a member of the HflX family. J Biochem *148*, 103-113.
Huang, C., Mandava, C.S., and Sanyal, S. (2010b). The ribosomal stalk plays a key role in IF2-mediated association of the ribosomal subunits. J Mol Biol *339*, 145-153.
Ishihama, Y., Schmidt, T., Rappsilber, J., Mann, M., Hartl, F.U., Kerner, M.J., and Frishman, D. (2008). Protein abundance profiling of the *Escherichia coli* cytosol. BMC Genomics *9*, 102.
Jagath, J.R., Rodnina, M.V., and Wintermeyer, W. (2000). Conformational changes in the bacterial SRP receptor FtsY upon binding of guanine nucleotides and SRP. J Mol Biol *295*, 745-753.
Jain, N., Dhimole, N., Khan, A.R., De, D., Tomar, S.K., Sajish, M., Dutta, D., Parrack, P., and Prakash, B. (2009). *E. coli* HflX interacts with 50S ribosomal subunits in presence of nucleotides. Biochem Biophys Res Commun *379*, 201-205.
Janosi, L., Shimizu, I., and Kaji, A. (1994). Ribosome recycling factor (ribosome releasing factor) is essential for bacterial growth. Proc Natl Acad Sci U S A *91*, 4249-4253.
Jerinic, O., and Joseph, S. (2000). Conformational changes in the ribosome induced by translational miscoding agents. J Mol Biol *304*, 707-713.
Jiang, M., Datta, K., Walker, A., Strahler, J., Bagamasbad, P., Andrews, P.C., and Maddock, J.R. (2006). The *Escherichia coli* GTPase $CgtA_E$ is involved in late steps of large ribosome assembly. J Bacteriol *188*, 6757-6770.
Kiefer, F., Arnold, K., Künzli, M., Bordoli, L., and Schwede, T. (2009). The SWISS-MODEL repository and associated resources. Nucleic Acids Res *37*, D387-D392.
Kitagawa, M., Ara, T., Arifuzzaman, M., Ioka-Nakamichi, T., Inamoto, E., Toyonaga, H., and Mori, H. (2005). Complete set of ORF clones of *Escherichia coli* ASKA library (A Complete Set of E. coli K-12 ORF Archive): unique resources for biological research. DNA Res *12*, 291-299.
Koller-Eichhorn, R., Marquardt, T., Gail, R., Wittinghofer, A., Kostrewa, D., Kutay, U., and Kambach, C. (2007). Human OLA1 defines an ATPase subfamily in the Obg family of GTP-binding proteins. J Biol Chem *282*, 19928-19937.
Kothe, U., Wieden, H.J., Mohr, D., and Rodnina, M.V. (2004). Interaction of helix D of elongation factor Tu with helices 4 and 5 of protein L7/L12 on the ribosome. J Mol Biol *336*, 1011-1021.
Kouvela, E.C., Petropoulos, A.D., and Kalpaxis, D.L. (2006). Unraveling new features of clindamycin interaction with functional ribosomes and dependence of the drug potency on polyamines. J Biol Chem *281*, 23103-23110.
Kozak, M. (1999). Initiation of translation in prokaryotes and eukaryotes. Gene *231*, 187-208.

Kuriki, Y., and Kaji, A. (1968). Factor- and guanosine 5'-triphosphate-dependent release of deacylated transfer RNA from 70S ribosomes. Proc Natl Acad Sci U S A *61*, 1399-1405.
Laurberg, M., Kristensen, O., Martemyanov, K., Gudkov, A.T., Nagaev, I., Hughes, D., and Liljas, A. (2000). Structure of a mutant EF-G reveals domain III and possibly the fusidic acid binding site. J Mol Biol *303*, 593-603.
Laursen, B.S., Sorensen, H.P., Mortensen, K.K., and Sperling-Peterson, H.U. (2005). Initiation of protein synthesis in bacteria. Microbiol Mol Biol Rev *69*, 101-123.
Lehoux, I.E., Mazzulla, M.J., Baker, A., and Petit, C.M. (2003). Purification and characterization of YihA, an essential GTP-binding protein from *Escherichia coli*. Protein Expr Purif *30*, 203-209.
Leibundgut, M., Frick, C., Thanbichler, M., Boeck, A., and Ban, N. (2005). Selenocysteine tRNA-specific elongation factor SelB is a structural chimaera of elongation and initiation factors. EMBO J *24*, 11-22.
Leipe, D.D., Wolf, Y.I., Koonin, E.V., and Aravind, L. (2002). Classification and evolution of P-loop GTPases and related ATPases. J Mol Biol *317*, 41-72.
Lin, B., Covalle, K.L., and Maddock, J.R. (1999). The *Caulobacter crescentus* CgtA protein displays unusual guanine nucleotide binding and exchange properties. J Bacteriol *181*, 5825-5832.
Long, K.S., and Porse, B.T. (2003). A conserved chloramphenicol binding site at the entrance to the ribosomal peptide exit tunnel. Nucleic Acids Res *31*, 7208-7215.
Marzi, S., Knight, W., Brandi, L., Caserta, E., Soboleva, N., Hill, W.E., Gualerzi, C.O., and Lodmell, J.S. (2003). Ribosomal localization of translation initiation factor IF2. RNA *9*, 958-969.
Menninger, J.R., and Coleman, R.A. (1993). Lincosamide antibiotics stimulate dissociation of peptidyl-tRNA from ribosomes. Antimicrob Agents Chemother *37*, 2027-2029.
Milon, P., Carottie, M., Konevega, A.L., Wintermeyer, W., Rodnina, M.V., and Gualerzi, C.O. (2010). The ribosome-bound initiation factor 2 recruits initiator tRNA to the 30S initiation complex. EMBO Rep *11*, 312-316.
Milon, P., Tischenko, E., Tomsic, J., Caserta, E., Folkers, G., La Teana, A., Rodnina, M.V., Pon, C.L., Boelens, R., and Gualerzi, C.O. (2006). The nucleotide-binding site of bacterial translation initiation factor 2 (IF-2) as a metabolic sensor. Proc Natl Acad Sci USA *103*, 13962-13967.
Mishra, R., Gara, S.K., Mishra, S., and Prakash, B. (2005). Analysis of GTPases carrying hydrophobic amino acid substitutions in lieu of the catalytic glutamine: implications for GTP hydrolysis. Proteins *59*, 332-338.
Moazed, D., and Noller, H.F. (1987). Interaction of antibiotics with functional sites in 16S ribosomal RNA. Nature *327*, 389-394.
Moazed, D., Samaha, R.R.G., C., and Noller, H.F. (1995). Specific protection of 16S rRNA by translational initiation factors. J Mol Biol *248*, 207-210.
Motojima-Miyazaki, Y., Yoshida, M., and Motojima, F. (2010). Ribosomal protein L2 associates with *E. coli* HtpG and activates its ATPase activity. Biochem Biophys Res Commun *400*, 241-245.
Nechifor, R.W., K.S. (2007). Crosslinking of translation factor EF-G to proteins of the bacterial ribosome before and after translocation. J. Mol. Biol. *368*, 1412-1425.
Neuhard, J., and Nygaard, P. (1987). Purines and pyrimidines, Vol 1 (Washington, DC: American Society for Microbiology).

Noble, J.A., Innis, M.A., Koonin, E.V., Rudd, K.E., Banuett, F., and Herskowitz, I. (1993). The *Escherichia coli hflA* locus encodes a putative GTP-binding protein and two membrane proteins, one of which contains a protease-like domain. Proc Natl Acad Sci USA *90*, 10866-10870.
Nyborg, J. (1998). Possible evolution of factors involved in protein biosynthesis. Acta Biochim Pol *45*, 883-894.
Owens, R.M., Pritchard, G., Skipp, P., Hodey, M., Connell, S.R., Nierhaus, K.H., and O'Connor, C.D. (2004). A dedicated translation factor controls the synthesis of the global regulator Fis. EMBO J *23*, 3375-3385.
Pai, R.D., Zhang, W., Schuwirth, B.S., Hirokawa, G., Kaji, H., Kaji, A., and Cate, J.H.D. (2008). Structural insights into ribosome recycling factor interactions with the 70S ribosome. J Mol Biol *376*, 1334-1347.
Pape, T., Wintermeyer, W., and Rodnina, M.V. (1998). Complete kinetic mechanism of elongation factor Tu-dependent binding of aminacyl-tRNA to the A-site of the *E. coli* ribosome. EMBO J *17*, 7490-7497.
Pavlov, M.Y., Antoun, A., Lovmar, M., and Ehrenberg, M. (2008). Complementary roles of initiation factor 1 and ribosome recycling factor in 70S ribosome splitting. EMBO J *27*, 1706-1717.
Peitsch, M.C. (1995). Protein modeling by E-mail. Bio/Technology *13*, 658-660.
Peluso, P., Shan, S., Nock, S., Herschlag, D., and Walter, P. (2001). Role of SRP RNA in the GTPase cycles of Ffh and FtsY. Biochemistry *40*, 15224-15233.
Peske, F., Rodnina, M.V., and Wintermeyer, W. (2005). Sequence of steps in ribosome recycling as defined by kinetic analysis. Mol Cell *18*, 403-412.
Peske, F.S., A., Katunin, V.I., Rodnina, M.V., and Wintermeyer, W. (2004). Conformational changes of the small ribosomal subunit during elongation factor G-dependent tRNA-mRNA translocation. J Mol Biol *343*, 1183-1194.
Peterson, H.U., Roll, T., Grunberg-Managom, M., and Clark, B.F. (1979). Specific interaction of initiation factor IF2 of *E. coli* with formylmethionyl-tRNAfMet. Biochem Biophys Res Commun *91*, 1068-1074.
Petropoulos, A.D., Kouvela, E.C., Dinos, G.P., and Kalpaxis, D.L. (2008). Stepwise binding of tylosin and erythromycin to *Escherichia coli* ribosomes, characterized by kinetic and footprinting analysis. J Biol Chem *283*, 4756-4765.
Petropoulos, A.D., Kouvela, E.C., Starosta, A.L., Wilson, D.N., Dinos, G.P., and Kalpaxis, D.L. (2009). Time-resolved binding of azithromycin to *Escherichia coli* ribosomes. J Mol Biol *385*, 1179-1192.
Pingoud, A., Urbank, C., Krauss, G., Peters, F., and Maass, G. (1977). Ternary complex formation between elongation factor Tu, GTP, and aminoacyl-tRNA: an equilibrium study. Eur J Biochem *78*, 403-409.
Pioletti, M., Schlunzen, F., Harms, J., Zarivach, R., Gluhmann, M., Avila, H., Bashan, A., Bartels, H., Auerbach, T., Jacobi, C., *et al.* (2001). Crystal structures of complexes of the small ribosomal subunit with tetracycline, edeine and IF-3. EMBO J *20*, 1829-1839.
Pisareva, V.P., Pisarev, A.V., Hellen, C.U.T., Rodnina, M.V., and Pestova, T.V. (2006). Kinetic analysis of interaction of eukaryotic release factor 3 with guanine nucleotides. J Biol Chem *281*, 40224-40235.
Polekhina, G., Thirup, S., Kjeldgaard, M., Nissen, P., Lippmann, C., and Nyborg, J. (1996). Helix unwinding in the effector region of elongation factor EF-Tu-GDP. Structure *4*, 1141-1151.

Polkinghorne, A., Hogan, R.J., Vaughn, L., Summersgill, J.T., and Timms, P. (2006). Differential expression of chlamydial signal transduction genes in normal and interferon gamma-induced persistent *Chlamydophila pneumoniae* infections. Microbes Infect *8*, 61-72.
Polkinghorne, A., Ziegler, U., Gonzalez-Hernandez, Y., Pospischil, A., Timms, P., and Vaughn, L. (2008). *Chlamydophila pneumoniae* HflX belongs to an uncharacterized family of conserved GTPases and associates with the *Escherichia coli* 50S large ribosomal subunit. Microbiology *154*, 3537-3546.
Pon, C., Paci, M., Pawlik, R., and Gualerzi, C. (1985). Structure-function relationship in *Escherichia coli* initiation factors. J Biol Chem *260*, 8918-8924.
Rasmussen, L.C.V., Oliveira, C.L.P., Jensen, J.M., Pedersen, J.S., Sperling-Petersen, H.U., and Mortensen, K.K. (2008). Solution structure of C-terminal *Escherichia coli* translation initiation factor IF2 by small-angle X-ray scattering. Biochemistry *47*, 5590-5598.
Rippa, V., Cirulli, C., Di Palo, B., Doti, N., Amoresano, A., and Duilio, A. (2010). The ribosomal protein L2 interacts with the RNA polymerase alpha subunit and acts as a transcription modulator in *Escherichia coli*. J Bacteriol *192*, 1882-1889.
Rodnina, M.V., Fricke, R., and Wintermeyer, W. (1994). Transient conformational states of aminoacyl-tRNA during ribosome binding catalyzed by elongation factor Tu. Biochemistry *33*, 12267-12275.
Rodnina, M.V., Gromadski, K.B., Kothe, U., and Wieden, H.J. (2005). Recognition and selection of tRNA in translation. FEBS Lett *579*, 938-942.
Rodnina, M.V., Stark, H., Savelsbergh, A., Wieden, H.J., Mohr, D., Matassova, N.B., Peske, F., Daviter, T., Gualerzi, C.O., and Wintermeyer, W. (2000). GTPase mechanisms and functions of translation factors on the ribosome. J Biol Chem *381*, 377-387.
Ruzheinikov, S.N., Das, S.K., Sedelnikova, S.E., Baker, P.J., Artymiuk, P.J., Garcia-Lara, J., Foster, S.J., and Rice, D.W. (2004). Analysis of the open and closed conformations of the GTP-binding protein YsxC from *Bacillus subtilis*. J Mol Biol *339*, 265-278.
Sanchez-Pescador, R., Brown, J.T., Roberts, M., and Urdea, M.S. (1998). Homology of the TetM with translational elongation factors: implications for potential modes of tetM-conferred tetracycline resistance. Nucleic Acids Res *16*, 1218.
Savelsbergh, A., Katunin, V.I., Mohr, D., Peske, F., Rodnina, M.V., and Wintermeyer, W. (2003). An elongation factor G-induced ribosome rearrangement precedes tRNA-mRNA translocation. Mol Cell *11*, 1517-1523.
Savelsbergh, A., Mohr, D., Kothe, U., Wintermeyer, W., and Rodnina, M.V. (2005). Control of phosphate release from elongation factor G by ribosomal protein L7/L12. EMBO J *24*, 4316-4323.
Savelsbergh, A., Mohr, D., Wilden, B., Wintermeyer, W., and Rodnina, M.V. (2000). Stimulation of the GTPase activity of translation factor G by ribosomal protein L7/L12. J Biol Chem *275*, 890-894.
Savelsbergh, A., Rodnina, M.V., and Wintermeyer, W. (2009). Distinct functions of elongation factor G in ribosome recycling and translocation. RNA *15*, 772-780.
Schaefer, L., Uicker, W.C., Wicker-Planquart, C., Foucher, A.-E., Jault, J.-M., and Britton, R.A. (2006). Multiple GTPases participate in the assembly of the large ribosomal subunit in *Bacillus subtilis*. J Bacteriol *188*, 8252-8258.

Schlünzen, F., Harms, J.M., Franceschi, F., Hansen, H.A., Bartels, H., Zarivach, R., and Yonath, A. (2003). Structural basis for the antibiotic activity of ketolides and azalides. Structure *11*, 329-338.
Schlunzen, F., Zarivach, R., Harms, J., Bashan, A., Tocilj, A., Albrecht, R., Yonath, A., and Franceschi, F. (2001). Structural basis for the interaction of antibiotics with the peptidyl transferase centre in eubacteria. Nature *413*, 814-821.
Schmeing, T.M., and Ramakrishnan, V. (2009). What recent ribosome structures have revealed about the mechanism of translation. Nature *461*, 1234-1242.
Schmeing, T.M., Voorhees, R.M., Kelley, A.C., Gao, Y.-G., Murphy, F.V.t., Wier, J.R., and Ramakrishnan, V. (2009). The crystal structure of the ribosome bound to EF-Tu and aminoacyl-tRNA. Science *326*, 688-694.
Schwede, T., Kopp, J., Guex, N., and Peitsch, M.C. (2003). SWISS-MODEL: an automated protein homology-modeling server. Nucleic Acids Res *31*, 3381-3385.
Seabra, M.C., and Wasmeier, C. (2004). Controlling the location and activation of Rab GTPases. Curr Opin Cell Biol *16*, 451-457.
Selmer, M., Dunham, C.M., Murphy, F.V., Weixlbaumer, A., Petry, S., Kelley, A.C., Weir, J.R., and Ramakrishnan, V. (2006). Structure of the 70S ribosome complexed with mRNA and tRNA. Science *313*, 1935-1942.
Shields, M.J., Fischer, J.J., and Wieden, H.J. (2009). Toward understanding the mechanism of the universally conserved GTPase HflX: A kinetic approach. Biochemistry *48*, 10793-10802.
Shoji, S., Walker, A., and Frederick, K. (2009). Ribosomal translocation: one step closer to the molecular mechanism. ACS Chem Biol *4*, 93-107.
Siderovski, D.P., and Willard, F.S. (2005). The GAPs, GEFs, and GDIs of heterotrimeric G-protein alpha subunits. Int J Biol Sci *1*, 51-66.
Sikora, A.E., Zielke, R., Datta, K., and Maddock, J.R. (2006). The *Vibrio harveyi* GTPase $CgtA_V$ is essential and is associated with the 50S ribosomal subunit. J Bacteriol *188*, 1205-1210.
Simonetti, A., Marzi, S., Myasnikov, A.G., Fabbretti, A., Yusupov, M., Gualerzi, C.O., and Klaholz, B.P. (2008). Structure of the 30S translation initiation complex. Nature *455*, 416-421.
Singh, N.S., Das, G., Seshadri, A., Sangeetha, R., and Varshney, U. (2005). Evidence for a role of initiation factor 3 in recycling of ribosomal complexes stalled on mRNAs in *Escherichia coli*. Nucleic Acids Res *33*, 5591-5601.
Sohmen, D., Harms, J.M., Schlünzen, F., and Wilson, D.N. (2009). Snapshot: antibiotic inhibition of protein synthesis I. Cell *138*, 1248.
Song, H., Parsons, M.R., Rowsell, S., Leonard, G., and Phillips, S.E. (1999). Crystal structure of intact elongation factor Tu from Escherichia coli in GDP conformation at 2.05 Å resolution. J Mol Biol *285*, 1245-1256.
Stark, H., Rodnina, M.V., Wieden, H.J., van Heel, M., and Wintermeyer, W. (2000). Large-scale movement of elongation factor G and extensive conformational change of the ribosome during translocation. Cell *100*, 301-309.
Sun, Q., Vila-Sanjurjo, A., and O'Connor, M. (2011). Mutations in the intersubunit bridge regions of 16S rRNA affect decoding and subunit-subunit interactions on the 70S ribosome. Nucleic Acids Res *39*, 3321-3330.
Taylor, D.E., and Chau, A. (1996). Tetracycline resistance mediated by ribosomal protection. Antimicrob Agents Chemother *40*, 1-5.

Teplyakov, A., Obmolova, G., Chu, S.Y., Toedt, J., Eisenstein, E., Howard, A.J., and Gilliland, G.L. (2003). Crystal structure of the YchF protein reveals binding sites for GTP and nucleic acid. J Bacteriol *185*, 4031-4037.
Thakor, N.S., Nechifor, R., Scott, P.G., Keelan, M., Taylor, D.E., and Wilson, K.S. (2008). Chimeras of bacterial translation factors Tet(O) and EF-G. FEBS Lett *582*, 1386-1390.
Ticu, C., Nechifor, R., Nguyen, B., Desrosiers, M., and Wilson, K.S. (2009). Conformational changes in switch I of EF-G drive its directional cycling on and off the ribosome. EMBO J *28*, 2053-2065.
Tomar, S.K., Kumar, P., and Prakash, B. (2011). Deciphering the catalytic machinery in a universally conserved ribosome binding ATPase YchF. Biochem Biophys Res Commun, doi:10.1016/j.bbrc.2011.1004.1052.
Umekage, S., and Ueda, T. (2006). Spermidine inhibits transient and stable ribosome subunit dissociation. FEBS Lett *580*, 1222-1226.
Vannuffel, P., and Cocito, C. (1996). Mechanism of action of streptogramins and macrolides. Drugs *51*, 20-30.
Varshney, U., and Seshadri, A. (2006). Mechanism of recycling of post-termination ribosomal complexes in eubacteria: a new role of initiation factor 3. J. Biosci. *31*, 281-289.
Voorhees, R.M., Schmeing, T.M., Kelley, A.C., and Ramakrishnan, V. (2010). The mechanism for activation of GTP hydrolysis on the ribosome. Science *330*, 835-838.
Walter, P., and Johnson, A.E. (19964). Signal sequence recogntion and protein targeting to the endoplasmic reticulum membrane. Annu Rev Cell Biol *10*, 87-119.
Watanabe, S. (1972). Interaction of siomycin with the acceptor site of *Escherichia coli* ribosomes. J Mol Biol *67*, 443-457.
Werner, R.G., Teraoka, H., and Nierhaus, K.H. (1978). Inhibition of protein synthesis by three erythromycin-derivatives. Biochem Biophys Res Commun *83*, 1147-1156.
Wicker-Planquart, C., Foucher, A.-E., Louwagie, M., Britton, R.A., and Jault, J.-M. (2008). Interactions of an essential *Bacillus subtilis* GTPase, YsxC, with ribosomes. J Bacteriol *190*, 681-690.
Wieden, H.J., Gromadski, K., Rodnin, D., and Rodnina, M.V. (2002). Mechanism of elongation factor (EF)-Ts-catalyzed nucleotide exchange in EF-Tu. J Biol Chem *277*, 6032-6036.
Wieden, H.J., Mercier, E., Gray, J., Steed, B., and Yawney, D. (2010). A combined molecular dynamics and rapid kinetics approach to identify conserved three-dimensional communication networks in elongation factor Tu. Biophys J *99*, 3735-3743.
Wienk, H., Tomaselli, S., Bernard, C., Spurio, R., Picone, D., Gualerzi, C.O., and Boelens, R. (2005). Solution structure of the C1-subdomain of *Bacillus stearothermophilus* translation initiation factor IF2. Prot. Sci. *14*, 2461-2468.
Wilden, B., Savelsbergh, A., Rodnina, M.V., and Wintermeyer, W. (2006). Role and timing of GTP binding and hydrolysis during EF-G-dependent tRNA translocation on the ribosome. Proc Natl Acad Sci U S A *103*, 13670-13675.
Wilson, G.J., Shull, S.E., and Cooke, R. (1995). Inhibition of muscle force by vanadate. Biophys J *68*, 216-226.
Woodcock, J., Moazed, D., Cannon, M., Davies, J., and Noller, H.F. (1991). Interaction of antibiotics with A- and P-site-specific bases in 16S ribosomal RNA. EMBO J *10*, 3099-3103.

Wout, P., Pu, K., Sullivan, S.M., Reese, V., Zhou, S., Lin, B., and Maddock, J.R. (2004). The *Escherichia coli* GTPase $CgtA_E$ cofractionates with the 50S ribosomal subunit and interacts with SpoT, a ppGpp synthetase/hydrolase. J Bacteriol *186*, 5249-5257.
Wu, H., Sun, L., Blombach, F., Brouns, S.J.J., Snijders, A.P.L., Lorenzen, K., van den Heuvel, R.H.H., Heck, A.J.R., Fu, S., Li, X., *et al.* (2010). Structure of the ribosome associating GTPase HflX. Proteins *78*, 705-713.
Yokosawa, H., Kawakita, M., Arai, K., Inoue-Yokosawa, N., and Kaziro, Y. (1975). Binding of aminoacyl-tRNA to ribosomes promoted by elongation factor Tu. Studies on the role of GTP hydrolysis. J Biochem *77*, 719-728.
Youngman, E.M., Brunelle, J.L., Kochaniak, A.B., and Green, R. (2004). The active site of the ribosome is composed of two layers of conserved nucleotides with distinct roles in peptide bond formation and peptide release. Cell *117*, 589-599.
Youngman, E.M., He, S.L., Nikstad, L.J., and Green, R. (2007). Stop codon recognition by release factors induces structural rearragement of the ribosomal decoding center that is productive for peptide release. Mol Cell *28*, 533-543.
Zheng, N., and Gierasch, L. (1996). Signal sequences: The same yet different. Cell, 849-852.